4-30-2019

Environmental Risks and Benefits of Nano-Enabled Clean Energy Technologies

Elizabeth A. Moore

Environmental Risks and Benefits of Nano-Enabled Clean Energy Technologies

by

Elizabeth A. Moore

A DISSERTATION

Submitted in Partial Fulfillment of the Requirements for the Degree of Doctor of Philosophy in Sustainability

Department of Sustainability

Golisano Institute of Sustainability

Rochester Institute of Technology

April 30, 2019

Certificate of Approval

Golisano Institute for Sustainability

Rochester Institute of Technology

Rochester, New York

Ph.D. DEGREE DISSERTATION

The Ph.D. Degree Dissertation of Elizabeth A. Moore has been examined and approved by the dissertation committee as satisfactory for the dissertation requirement for the Ph.D. degree in Sustainability.

Dr. Thomas Trabold, Director of Ph.D. program and Department Chair

Dr. Todd Pagano, Dissertation External Chairperson

Dr. Callie Babbitt, Advisor & Committee Chairperson

Dr. Anna C. Tyler, Committee Member

Dr. Gabrielle Gaustad, Committee Member

Date _____

ABSTRACT

Engineered nanomaterials (ENMs) are increasingly incorporated into clean energy technologies due to observed improvement in technological and system performance. Though these materials could revolutionize many products and technologies, increased use of ENMs can also introduce uncertainty and risks that are difficult to predict. Increase in ENM use could significantly increase ENM releases to the environment across their life cycle, from material synthesis to end-of-life. To address knowledge gaps and uncertainties, this work assesses a portfolio of ENMs from a systems perspective. First, characterization and quantification methods were developed for three carbonaceous ENMs, fullerenes (C_{60}, C_{70}, and derivative PCBM), which have promising application in solar technologies. Empirical ecotoxicity assays and predation studies were performed to determine ecotoxicity and predation effects. Next, an integrated model predicted potential risks of ENM accumulation by estimating potential manufacturing locations, spatial concentrations, and potential ecological risks. This was followed by an adaption of portfolio optimization, a model traditionally used to optimize investment performance, to model potential environmental and economic risks and simultaneous performance benefits and inform safe nano-enabled design.

Ecotoxicity findings demonstrate differences among fullerenes where organisms exposed to fullerenes also experienced significantly increased predation risk, underscoring the need to consider potential system-level effects. Based on manufacturing locations, potential ENM exposure may be within buffer distances of sensitive ecosystems. However, modeled ENM accumulation would only reach levels associated with ecotoxicity risk under extreme scenarios. Future ENM use-patterns can be informed by the portfolio optimization approach, where optimal portfolios are determined by the materials-mix that yielded the greatest overall performance

return while minimizing the portfolio risks. These novel methods and tools contribute to the knowledge of the benefits and risks of ENMs, which will help to guide more responsible and proactive policy and planning around ENM development and use.

ACKNOWLEDGEMENT

I am eternally grateful to Dr. Callie Babbitt, my PhD and Master's degree advisor. Without her help, support, and encouragement, I wouldn't be where I am today. She has gifted me with every opportunity possible to help me grow as a researcher, teacher, writer, and mentor. Thanks to Callie's support, I have traveled and presented at a number of conferences, have taught five classes at RIT, have actively participated in outreach throughout Rochester, and have researched at the United Nations University in Bonn, Germany. Callie has helped me feel confident on days when I didn't believe in myself and continues to inspire me to challenge myself and strive for more. Thank you, Callie, for helping me to achieve my goals. I can't wait to see how our relationship will continue to grow!

Thank you to my husband for supporting me for the past five years in my PhD program as well as all 11 years of our relationship. Sean—I can't thank you enough for doing most of the long driving during the years you lived in DC, for moving up to Rochester despite your resistance to the cold, and for believing in me and giving me pep talks when I didn't believe I could finish. Thank you for listening to me practice my presentations at nauseum, helping to proofread my work, for being a co-author on a publication, and for coming to feed the *Daphnia* and fish with me on the weekends. You push me to be better every single day and are the most supportive husband and best friend I could ever ask for. I hope you are as excited as I am to move to Boston and start a new journey together!

I would like to express my very great appreciation to my committee members, Dr. Christy Tyler and Gabrielle Gaustad. Christy—you are the most patient advisor I have ever met! Thank you for taking the time to teach me more about statistics, for giving me field experience and teaching me lab skills, and for helping me to be a better writer. It was always nice to talk

about life and get career advice from you during our meetings. I enjoyed getting to know you and working with your students to figure out these fullerenes! Gabby—thank you for teaching me about optimization, helping to guide my dissertation chapters, and for all of the career advice you have given me over the past year. I appreciate all of the knowledge you have shared about modeling and accounting for uncertainty and am so proud of you for becoming a dean! Thank you both for your support, guidance, suggestions, and questions to help make me better!

I greatly acknowledge my funding sources for this research: The National Science Foundation and the Golisano Institute for Sustainability. Further, the GIS community has provided me with so much support and many opportunities over the past five years. These students, faculty, and staff were my family in Rochester and looked after me when I needed help or a friendly smile. Thank you to my very best friend, roommate, wife, confidant, and favorite study buddy, Dr. Jennifer Russell. In addition to being my best friend, you are also one of the best mentors I have ever had in my life. You are selfless and are never too busy to help answer a question or to listen to problems that I am having in my personal and work life. I have learned so much from you and honestly do not think I would have finished this degree without your never-ending support. You are one of a kind—the kindest heart, a brilliant mind, and a beautiful soul. I am grateful every day for your friendship and can't wait to live closer to you again. I am so proud of you and all of your hard work at GIS. I only wish I had you for this fifth year!

I would like to express my gratitude to Dr. Tom Trabold for the opportunity to help as a GIS ambassador, for always lending advice for my dissertation and job applications, and for including me in the faculty search process so I could learn more about being a professor one day. Thank you, Dr. Todd Pagano, for being my external committee chair and for providing critical feedback for Chapter 2's revisions. Thank you to Dr. Nabil Nasr for always saying hello in the

hallway and for all of the career advice. A special thanks to Dr. Carli Flynn for her advice, friendship, and for teaching me about the application process for post-docs and professor jobs. A shout out to Lisa Dammeyer and Donna Podeszek for being my GIS moms and helping me with everything and anything I ask for, you both truly have beautiful souls and deserve all the golden bricks RIT has to offer. Lisa Templar and Carrie Deglans—thank you both for helping me to schedule tours, book rooms, and give suggestions of the best restaurants, doctors, etc. in Rochester! Finally, I couldn't have made it through each day without the banter and support from my fellow GIS students. A special thanks to Dr. Michele Bustamante, Alex Leader, Ranjit Desai, JT Coneybeer and Charlsey Coneybeer, Will Armington, Berlyn Hubler, and many, many more.

Thanks to the interdisciplinary nature of my dissertation, I have been fortunate to work with a number of professors outside of my department. Dr. Brian Tomaszewski—thank you for expanding my knowledge of GIS and for giving me opportunities to explore new research areas, travel to Germany and learn from leading researchers, travel to Texas to gain mentoring experience and learn how GIS can support the disaster cycle, and the opportunity to teach a GIS course at the undergraduate and graduate level. Dr. Sandi Connelly—thank you for your patience with me while learning about *Daphnia*, learning to design experiments, and understanding my results. I also enjoyed hearing your advice about my career path and for the opportunities to help with outreach. I am particularly grateful for the assistance given by Dr. Mike Haselkorn, Professor Rich Hailstone, Dr. Anju Gupta, and Dr. George Thurston in teaching me more about material characterization and for helping me to complete the characterization of the fullerene materials. Thank you also to the COLA and GCCIS departments for giving me the chance to teach as an adjunct and to all of my students for inspiring me to work harder and achieve my goals.

A great big thank you and shout out to my family members who support me no matter what and believe in me, even on days when I don't believe in myself. To Mema and Pop-Pop, thank you for helping me finish my undergraduate degree so I could get this far. Thank you for the visits and frequent phone calls. To my amazing aunts—thank you for always calling and checking in. A special thank you to Amy and Jay for helping me to apply to graduate school and giving me advice throughout my program. Madison and Jake: Thank you for coming to visit and for putting up with my phone calls to check in during the week. To my Moore family—I appreciate your support and encouragement, and for raising Sean to be the amazing man that he is today. And to Anne Henriksen, who I consider to be family, thank you for suggesting that I switch to a science degree in the first place. Your love and support throughout my undergraduate program helped me to have the courage to apply for a PhD program. You helped me gain teaching and research skills from the beginning and I cannot thank you enough for it.

I dedicate this dissertation to my mom. Despite the hardships that my mother has faced, she has supported me through thick and thin. She encouraged me to challenge myself in school from a young age and has always been my biggest fan. Even though she would not let me join the chemistry team in high school, she wouldn't let me quit the chemistry honors course because she believed I could do it. In college, she supported my decision to switch majors and watched with pride as I accepted the outstanding student award at my undergraduate graduation. My mom answers her phone every time I call, she makes me laugh and listens to me when I cry, and she yells at me to get back on the horse every time I feel less than because she believes I am strong and a hard worker. My mom is my rock and I am proud to share this work with her. Thank you for your sacrifices and for your support so that I could be where I am today. I love you with all my heart.

TABLE OF CONTENTS

Table of Tables

Table of Figures

GLOSSARY OF TERMS

ENM	Engineered nanomaterial
CNM	Carbon nanomaterial
C60	Fullerene
C70	Fullerene
PCBM	Phenyl C61 Butyric Acid Methyl Ester
SWCNT	Single-walled carbon nanotube
MWCNT	Multi-walled carbon nanotube
LC50	Concentration that is lethal to 50% of a population
SFW	Synthetic freshwater
OPV	Organic photovoltaic cell
LIB	Lithium-ion Battery
EV	Electric Vehicle
GIS	Geographic Information Systems
BAU	Business-as-usual
Hydrologic Unit	HUC

CHAPTER 1: INTRODUCTION TO EMERGING CONTAMINANTS: ENGINEERED NANOMATERIALS (ENMS)

Chemical release and exposure have historically led to unintended consequences such as threats to human fertility, intelligence, and survival (Colburn et al. 1996). Some of these instances include heavy metal poisoning in Japan, Minamata disease from Chisso Corporation's mercury discharge, open-air testing of nuclear weapons in New Mexico, nuclear bombs in Hiroshima and Nagasaki, Project Bravo Bomb in Bikini Atoll, and ecosystem destruction from DDT and DDD pesticide accumulation (Newman 2009). Because of these alarming epidemics, the idea of pollution dilution (disposing and dispersing contaminants to large bodies of water) was replaced by the boomerang paradigm (Newman 2009), where environmental activists brought awareness to the unintended toxic and ecotoxic consequences from chemical exposure in the environment.

Public, regulatory, and voluntary chemical testing practices have been used to varying degrees of success. In response to rising concerns about chemical exposure impacts, the U.S. Environmental Protection Agency (EPA) formed the Toxic Substance Control Act (TSCA) in 1976 to regulate the production, importation, use, and disposal of chemical substances and mixtures. One goal of TSCA was to also develop an inventory of health and environmental impact data to inform risk assessment of chemicals (Schmidt 2016). TSCA requires the tracking of chemical records (production, use, disposal) by any entity that is involved throughout the life cycle of a chemical. There is currently an inventory of over 83,000 known substances being released, which increases regularly, with up to 50 substances recommended for testing each year (Schmidt 2016). If a substance is not recommended for testing, the consequences of exposure to that chemical are relatively unknown. On the other hand, exhaustive chemical testing cannot

keep pace with the vast number of new chemicals introduced each year and is viewed as a potential disruption to innovation (Newman 2009).

These challenges are only expected to grow as technological progress allows for an almost limitless creation of new chemicals. While these chemicals are being synthesized to help solve challenges, their introduction rarely considers the potential for unintended consequences. Take for example the case of plastic microbeads, which were introduced as an innovative part of personal care products such as toothpastes, hand sanitizer, and soaps for exfoliation purposes. However, the ultimate release of these microplastics was not adequately controlled by wastewater treatment infrastructure (Driedger et al. 2015), leading to increasing plastic pollution in oceans and freshwater ecosystems such as the Laurentian Great Lakes (Eriksen et al. 2013). Exposure to these microbeads led to lethal and sublethal impacts in organisms that consumed them (Cole et al. 2011), including growth inhibition and internal abrasions in fish (Mendoza et al. 2014). The policy reaction to these concerns was the Microbead-Free Waters Act of 2015 that banned the use of microbeads by July 2017 (FDA 2015). This example underscores the need for more proactive approaches to evaluating chemical risk, as opposed to traditional command and control strategies implemented only after such risks are realized.

Emerging Contaminants of Concern: Engineered Nanomaterials (ENMs)

As demand for new and improved products and technologies increases, it is reasonable to expect a commensurate expansion of novel materials. Nanotechnology is a clear example of this expansion, as nano-scale materials and nano-enabled products have been touted as breakthroughs for commercial, medical, energy, and environmental applications described as a hotbed for an industrial revolution. Due to their unique properties and capabilities, a key emerging area for

ENMs is in clean energy technologies (Figure 1), including lithium-ion batteries, solar cells, fuel cells, and wind turbines (Hussein et al. 2015).

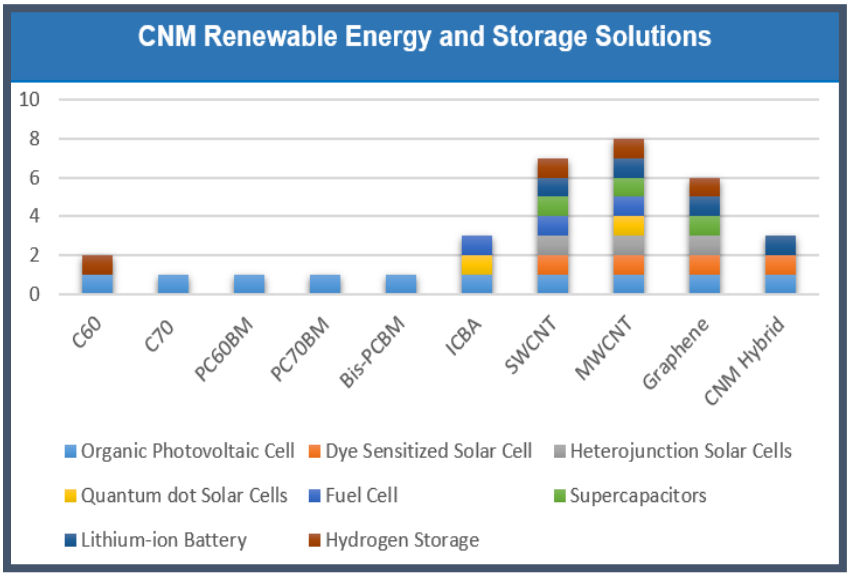

Figure 1. Literature results for carbon-based nanomaterials used in clean energy generation and storage solutions.

An increase in clean energy technologies could help to displace fossil fuel use and the resulting greenhouse gas emissions. Further, research has shown that ENMs, such as carbon nanotubes (CNTs), can have net energy benefits despite the high amount of energy needed for purification and processing steps by minimizing energy and material requirements for products (Zhai et al. 2016). ENMs are also commonly used in cosmetics, electronics, optics, and medicine (Keller et al. 2014; Woodrow Wilson Center 2009), to improve the performance and increase the benefits of the products. However, the increased use in products and technologies could significantly increase the potential for ENM releases to the environment.

The case of microbeads highlights the cause for concern: ENMs are even smaller than microbeads (with at least one dimension <100 nm) (Borm et al. 2006) and will face the similar large-scale release risks as their use in products continues to grow. Despite their potential to increase the efficiency of energy conversion and storage devices, it has yet to be fully determined

if the potential risks of ENM production and release outweigh the benefits they convey. In the literature, toxic and ecosystem-level impacts of ENM exposure have been reported (Salieri et al. 2015; Jahan et al. 2017). There are also indirect environmental impacts associated with upstream energy and material consumption (Anctil et al. 2011; Eckelman et al. 2012). For instance, Eckelman et al. (2012) found that production impacts for CNTs upstream are often greater than direct impacts such as release in aquatic ecosystems. Similarly, the embodied energy for manufacturing larger fullerenes such as C70 is even greater, due to their energy-intensive purification processes and small production volumes (Anctil et al. 2011). Because the use of clean energy technologies will only continue to increase in response to climate change, fossil fuel depletion, and increasing renewable energy adoption, it is imperative for public, regulatory, and voluntary practices to effectively and proactively consider the potential for attendant ENM releases and environmental impacts.

New guidelines for the development and commercialization of ENMs, including incentivizing sustainable nanotechnology development and adoption (Wiek et al. 2016), are needed to help ensure safe widespread nanotechnology adoption. Improvements to risk assessment can help to inform the magnitude of risk and identify ways to minimize unintended consequences.

DISSERTATION MOTIVATION AND OBJECTIVE

Problem Statement, Research Questions, and Novel Contribution

Though these materials could revolutionize many products and technologies, ENMs can also create new risks that are difficult to predict proactively. ENMs may enter the environment at any point in their life cycle, creating *direct* release risks and *indirect* impacts from upstream energy and material consumption. These risks could be defined at the material level with the potential

for ultimate toxicity to aquatic organisms in freshwater ecosystems. There could be economic risks with a large investment of capital in commercialization of ENMs and an uncertain return on investment. Energy risks are also possible due to the high amount of energy required to produce ENMs and an uncertain return on energy performance. Finally, there is a likelihood of environmental risks from the consumption of energy and release of emissions, which can ultimately cause depletion of resources and can contribute to climate change and environmental degradation. To better understand these risks, it is important to consider the ecotoxicity of the materials, the magnitude and location of future accumulation, and the extent that the materials will be adopted for various technologies. Three research questions have been developed to address these emerging challenges:

1. Could ENM life cycle releases significantly impact freshwater organisms?

A specific class of carbon-based ENMs (CNMs), fullerenes (C60, C70, and PCBM), have been chosen due to their potential for use in a variety of product categories to inform potential impacts on freshwater organisms. While the potential risks of fullerene, C60 have been studied widely throughout the literature (Lovern et al. 2007; Baun et al. 2008; Bouchard et al. 2009; Benn et al. 2011; Arndt et al. 2014), impact studies on ENM structure changes such as the addition of atoms (C_{70}) or of functional groups (PCBM) remain scarce (Lovern et al. 2007; Bouchard et al. 2008; Bouchard et al. 2009; Benn et al. 2011). To understand the tradeoffs of altering the structure of fullerene for increased performance benefits, methods were first developed to quantify and characterize all three forms of fullerenes (Chapter 2). Direct ecotoxicity was then evaluated to inform an environmental impact assessment of different ENM forms and susceptibility to predation was assessed experimentally. These ecotoxicity studies are the first to evaluate

different functional forms of fullerenes, chronic fullerene exposures over multiple generations of a model freshwater organism, and predation risk from exposed *Daphnia* spp. (Chapter 3).

2. **What are predicted regional volumes of ENM releases and where might they be released into freshwater ecosystems?**

Because direct data on nanomaterial production and release are scarce, a spatially explicit risk assessment model utilizes the predictive capacity of ArcGIS to estimate likely ENM release patterns, predicted environmental concentrations, and potential ecological risks. The model first identifies likely manufacturing sites on a regional basis. The proximity of the predicted likely locations to existing sensitive ecosystems and freshwater ecosystems are assessed to help inform spatial risks. Next, a material flow analysis (MFA) was used to predict regional volume of ENMs. Finally, predicted concentrations were then compared to known lethal dose concentrations for model organisms in order to assess the magnitude of risk and impact created upon release. The use of this combined methodology identifies pathways and potential sustainability impacts of ENMs and can also be used to predict spatially explicit risks for other emerging contaminants.

3. **How are ENMs likely to be adopted in renewable energy technologies given environmental and economic considerations?**

The use of ENMs in emerging products and technologies has inherent uncertainty that must be addressed to fully understand the tradeoffs of increased use. Current risk assessment and decision-making tools for these emerging materials cannot adequately account for uncertainty because of varying functional forms, unique environmental behavior, diverse economic costs, unknown supply and demand interactions, upstream emissions implications, and increasing use of these materials in diverse product applications (Som et al. 2010). In response to these

challenges, this work uses a novel adaptation of portfolio optimization, a model traditionally used to optimize financial investment portfolio performance. The results of this model inform the likely portfolio of ENM use in a range of products, while accounting for tradeoffs, uncertainty (numerical simulation and Monte Carlo analysis), and constraints. The utility of the model is in evaluating the cumulative impact of multiple materials, demonstrated via two case study applications that consider performance, environmental, and economic trade-offs. The trade-offs that may exist between investment of capital and environmental resources can inform the ultimate profitability and energy performance of products utilizing ENMs.

The cumulative approaches and insights of this dissertation contribute to the literature and body of knowledge through the creation of *novel methodologies and experiments* that examine the *tradeoffs* of integrating ENMs in clean energy applications (Figure 2).

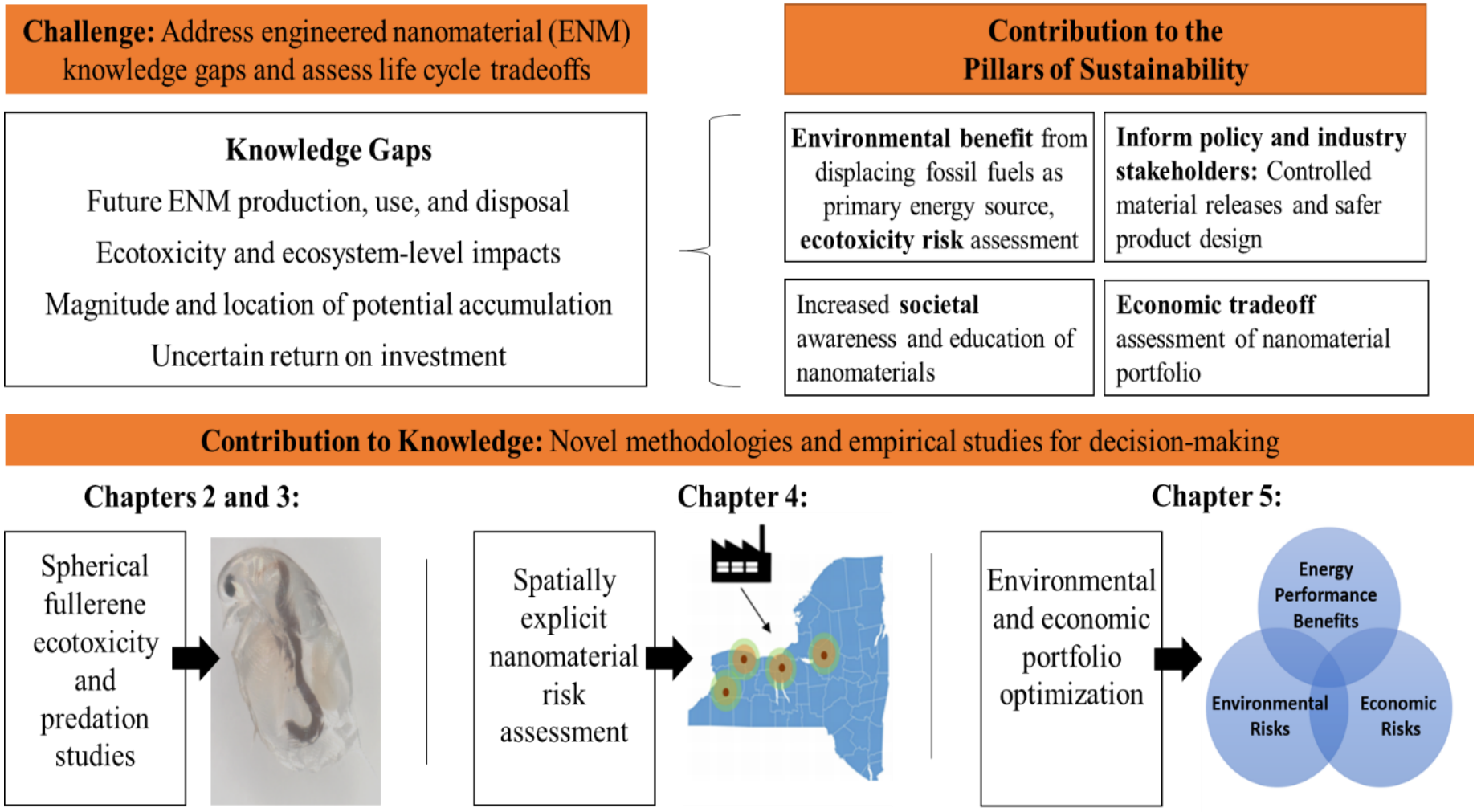

Figure 2. Overview of the challenges identified in the ENM literature and the novel methods and tools developed to assess the risks and benefits of ENMs.

CHAPTER 2:
ENM CHARACTERIZATION AND METHODS DEVELOPMENT: A CASE STUDY OF SPHERICAL FULLERENES

Introduction

In order to assess the potential for ecotoxicity and ecosystem-level impacts from ENM exposure, a specific group of carbon-based ENMs, spherical fullerenes (C60, C70) and a functionalized form (PCBM), were chosen due to their potential to improve the performance of clean energy technologies such as organic photovoltaic cells (OPVs) (Anctil et al. 2011). The first step in testing for ecotoxicity is to prepare the material samples for analysis. While the preparation methods are not necessarily novel, particularly for C60 (Fortner et al. 2005; Lovern et al. 2007; Baun et al. 2008; Bouchard et al. 2009; Benn et al. 2011; Arndt et al. 2014), the methods are inconsistent throughout the literature (Kennedy et al. 2009) and have never been tested for C70 and PCBM. For instance, variations in the solvent type, temperature, light exposure, concentration, and/or preparation method can have a meaningful impact on size, structure, behavior, and ultimate toxicity of ENMs (Petersen et al. 2015). In this chapter, methods for material solubilization, preparation of standards, initial size verification, extraction of materials, and concentration calculations were developed for C60 as well as two additional forms of C60, C70 and PCBM.

Methods Development

Fullerene (C60) Solubilization

To perform ecotoxicity testing of fullerenes, the materials first have to be solubilized in an aqueous solution to make the analysis more environmentally relevant and less likely to be influenced by residual solvent contamination (Kennedy et al. 2009). For instance, the use of solvents like tetrahydrofuran (THF) and sonication methods can contribute to toxicity effects of carbon nanotubes (Kennedy et al. 2009). C60 acute toxicity is also dependent on preparation

methods: juvenile largemouth bass assays with THF-prepared C60 resulted in 100% mortality whereas water-stirred C60 did not render acute lethal or sublethal effects (Zhu et al. 2006). Fullerenes are insoluble in water but can form agglomerates commonly known as n-C60 when stirred with water for extended periods of time. A literature review was performed to find the most environmentally relevant fullerene solubilization methods such as magnetic stirring and naphthalene adsorption, artificial seawater magnetic stirring, and various magnetic stirring and filtering methods (Appendix A). Ultimately, a standard protocol was developed where only deionized water or synthetic freshwater was used for stirring to simulate freshwater ecosystems in a controlled environment, extended magnetic stirring for a minimum of six weeks was used so additional solvents were not needed that could contribute to toxicity, and filtering methods were not used to simulate a sample taken from the environment. The standardized protocol developed for C60 was later used with different structures and functionalized forms of fullerene (C70 and PCBM).

Magnetic Stirring Method

Solubilization via magnetic stirring over a 28-day period was based on the methods by Pakarinen et al., where 100 mg of fullerene were measured into 500 mL of DI water (Pakarinen et al. 2011; Pakarinen et al. 2013). A butyl rubber stopper was used to plug the flask and Parafilm was used to secure the stopper to avoid evaporation. The flask was covered in aluminum foil to prevent exposure to light. The stir plate was set to the lowest stirring rate (150 rpm) so there was sufficient mixing without air bubbles. The solution was monitored throughout the experimental period to make sure that the fullerenes were solubilizing into the DI water. The set-up for the magnetic stirring of C60 is showing below in Figure 1.

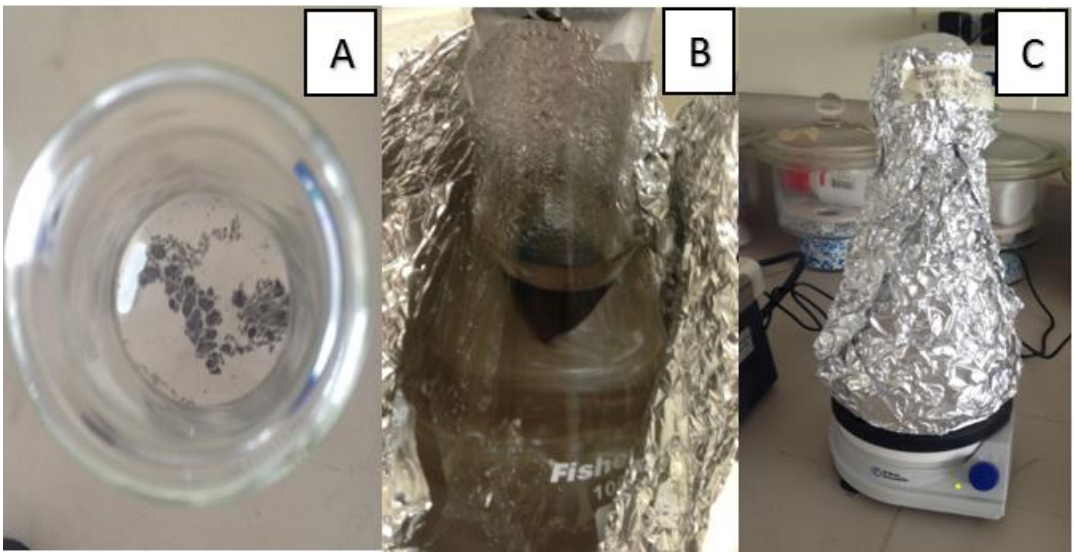

Figure 1. Pictures A-C above depict the set-up for the solubilization of fullerene using the magnetic stirring method. A) Fullerene powder added to the flask, B) fullerene powder beginning to stir in DI water, and C) Aluminum foil cover on the flask that was stirred for 28 days.

Rotary Agitator Method

To simulate a stream-like flow, rotary agitation over a 28-day period was also attempted, based on the methods by Pakarinen et al. Here, 100 mg of fullerene was measured into 500 mL of DI water (Pakarinen et al. 2011; Pakarinen et al. 2013). Parafilm was used to secure the top of the 2 L Plastic Extraction Bottle to avoid evaporation. The bottle was covered in aluminum foil to prevent exposure to light. The bottle was placed in a DC-20 8-Place Rotary Agitator and was left stirring 24 hours a day, 7 days a week for the remainder of the experiment.

Solubilization Results

After 28 days, the magnetic stir plate method proved to be the best method for fullerene solubilization. The solution turned a light brown color after 28 days, which was similar to the results reported in the literature. The solution was then kept on the magnetic stir plate to find the optimal stirring length of time. After six weeks, the solution turned the dark brown color that was described in literature. The changes in color with varying stirring times can be seen in Figure 2.

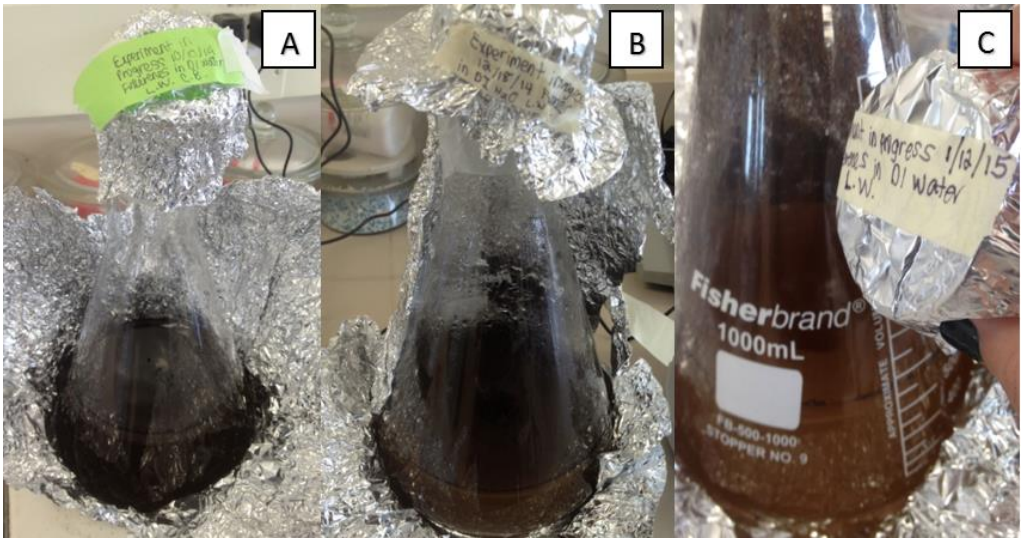

Figure 2. After several weeks of stirring, the fullerene became soluble in the DI water to create an n-C60 solution. A) 200 mg/L n-C60 solution after five months of stirring, B) 200 mg/L n-C60 solution after three months of stirring, and C) shows the 200 mg/L n-C60 solution after six weeks of stirring.

The rotary agitator method did not result in a solubilized solution, even after five months of stirring, as shown in Figure 3. Thus, the magnetic stir plate method for solubilization was used for all future experiments.

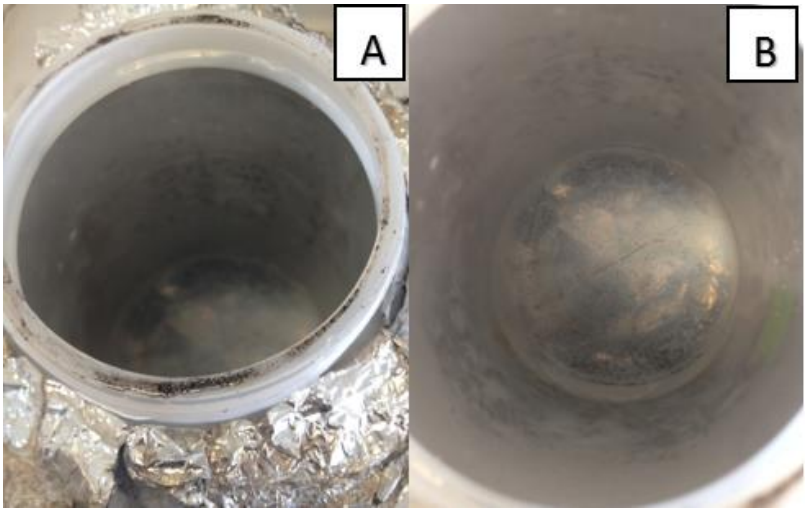

Figure 3. The results of the rotary agitator method are shown (A and B). In both pictures, the water is clear and the fullerene did not solubilize to form a brown n-C60 solution. The fullerenes were stirred in the rotary agitator for five months.

The first fullerene solubilization experiment was started on 10/10/14 (200 mg/L). The subsequent solubilization experiments were on 12/18/14 (200 mg/L), 1/15/15 (200 mg/L), 2/19/15 (50 mg/L), 6/22/15 (200 mg/L), and 6/23/15 (200 mg/L). The other materials (PCBM and C70) were purchased from SES Research and 200 mg/L solutions were created using the same protocol.

Verified Fullerene Agglomerate Size: TEM

Initial characterization of n-C60 was performed using transmission electron microscopy (TEM) and the concentrations of fullerene were estimated using spectrophotometry. Preliminary characterization analysis can be seen below in Figures 4 and 5, where the size of the fullerene agglomerates from the magnetic stirring method are shown. The images were taken using a JEOL 100CX TEM operated at 320 kV for Figure 4 and 19 kV for Figure 5. The fullerene sample was taken from a 200 mg/L sample of fullerene and DI water that had been stirring for three months. 10 microliters of the aqueous fullerene solution were added directly to the slide and was allowed to dry for one hour before viewing under the TEM.

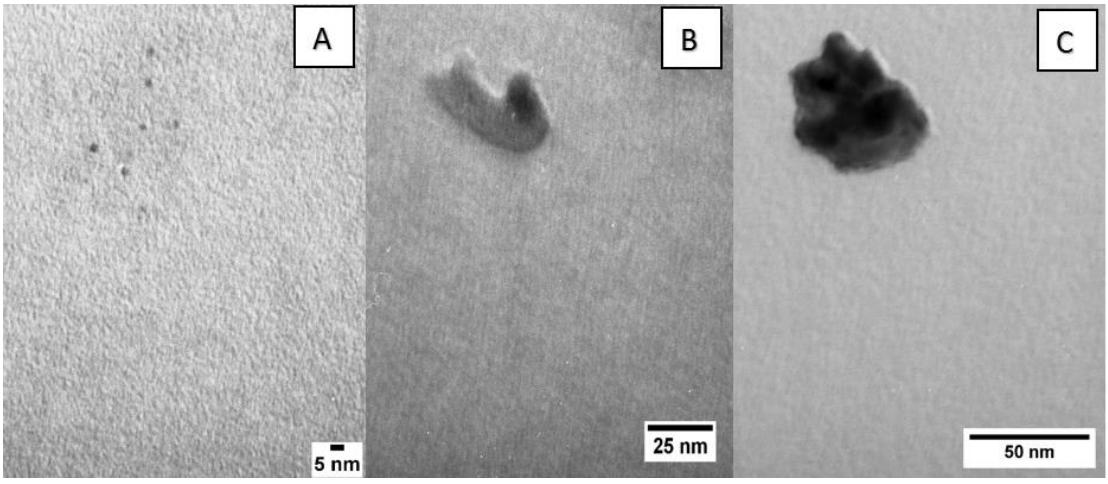

Figure 4. TEM images of fullerene (200 mg/L) at 320 kV at various sizes of n-C60 agglomerates formed during extended magnetic stirring.

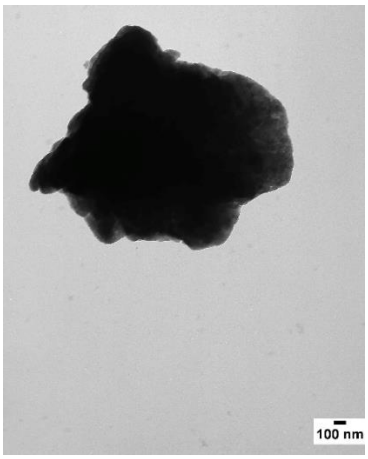

Figure 5. TEM image of fullerene (200 mg/L) at 19 kV. Toluene Extraction with n-C60

Toluene Extraction Methods

Fullerene concentration in aqueous samples could not be measured directly, and therefore samples had to be extracted into a toluene matrix for analyzing concentration via standard spectroscopic methods. This extraction protocol was developed based on extensive literature review (Appendix A, Table 3). One challenge during the extraction process is the problem of emulsion during the mixing of the solution. Various chemical solutions were found to reduce this problem (e.g. NaCl, glacial acetic acid, and calcium chloride) (Appendix A, Table 3). However, NaCl was ultimately chosen because it had the highest extraction efficiency when compared to the other chemicals. Following the methods described by Fortner et al., the amount of n-C60, toluene, and 2% NaCl added to each vial were chosen (Fortner et al. 2005). 3 mL of n-C60 (from the solubilization experiments), 3 mL of toluene, and 1.5 mL of 2% NaCl were added to each sample. The n-C60 sample was filtered with 0.45-micrometer Millipore 13 mm filters. The n-C60 was then added to the vial and 1.5 mL 2% NaCl was added as the next layer. Three mL of toluene was added to the top layer and the vials were vortexed for 5 minutes. Once the samples were vortexed, the toluene was removed with a pipette and added to a glass cuvette to measure the absorbance of the sample using UV-Vis spectrophotometry (Shimadzu 1800 UV-Vis Dual

Beam Spectrophotometer). Extractions were performed sequentially until absorbance was less than 0.02. Additionally, the extraction process was compared for filtered and unfiltered samples. Unfiltered C60 samples (Figure 6) were ultimately selected for our methods, which are more representative of an environmental sample that would be collected from the field (Bouchard and Ma 2008). The difference in color change for all three fullerenes can be observed in Figure 7.

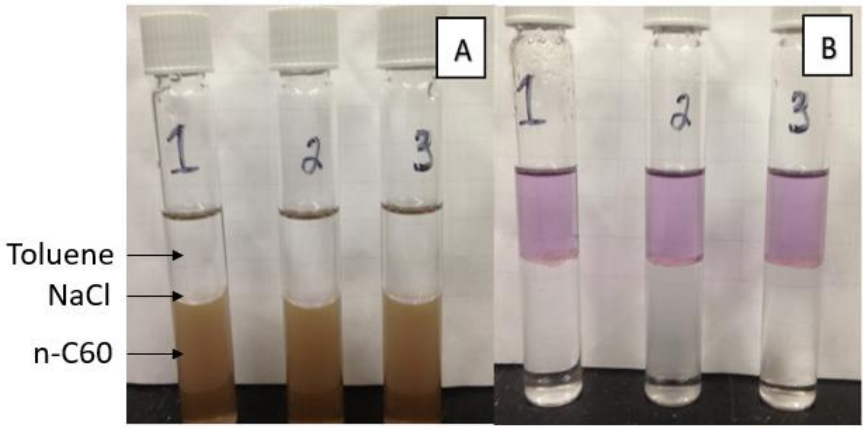

Figure 6. The glass exetainer vials with the unfiltered n-C60 before vortexing (A). The brown layer is the n-C60, the NaCl is the next layer, and the top layer is the toluene. The color change of the unfiltered n-C60 sample after vortexing the samples where the fullerene has moved from the water to the toluene layer where the fullerene is soluble and can be tested (B).

Figure 7. PCBM 25 mg/L standard (a light red color) and C70 25 mg/L standard (bright orange color) both dissolved in toluene.

In order to find the detection wavelength specific to the brand of fullerenes used, a UV-Vis absorption spectrum on the Shimadzu 1800 UV-Vis spectrophotometer analyzed the peak wavelength for all three fullerenes (C60, C70, and PCBM) (Figure 8A-C) The wavelength with the highest peak was found to be 332 nm for C60, 334 nm for C70, and 331 nm for PCBM. These wavelengths were the standard absorbances used for all subsequent experiments.

To correct for any small particles that may be in the solution, a turbidity blank was created to make sure all the fullerene was dissolved. If the absorbance at the turbidity blank was above 0.010, the sample was vortexed again. To find a wavelength that is not influenced by fullerene, the UV-Vis absorbance spectra of the toluene/fullerene solution at multiple concentrations was compared to a toluene blank, yielding a suitable turbidity wavelength at 700 nm. The standard curves for all three fullerenes were linear within a 1-25 mg/L concentration range (Figure 9A-C). Above 25 mg/L, we performed a ten-fold dilution.

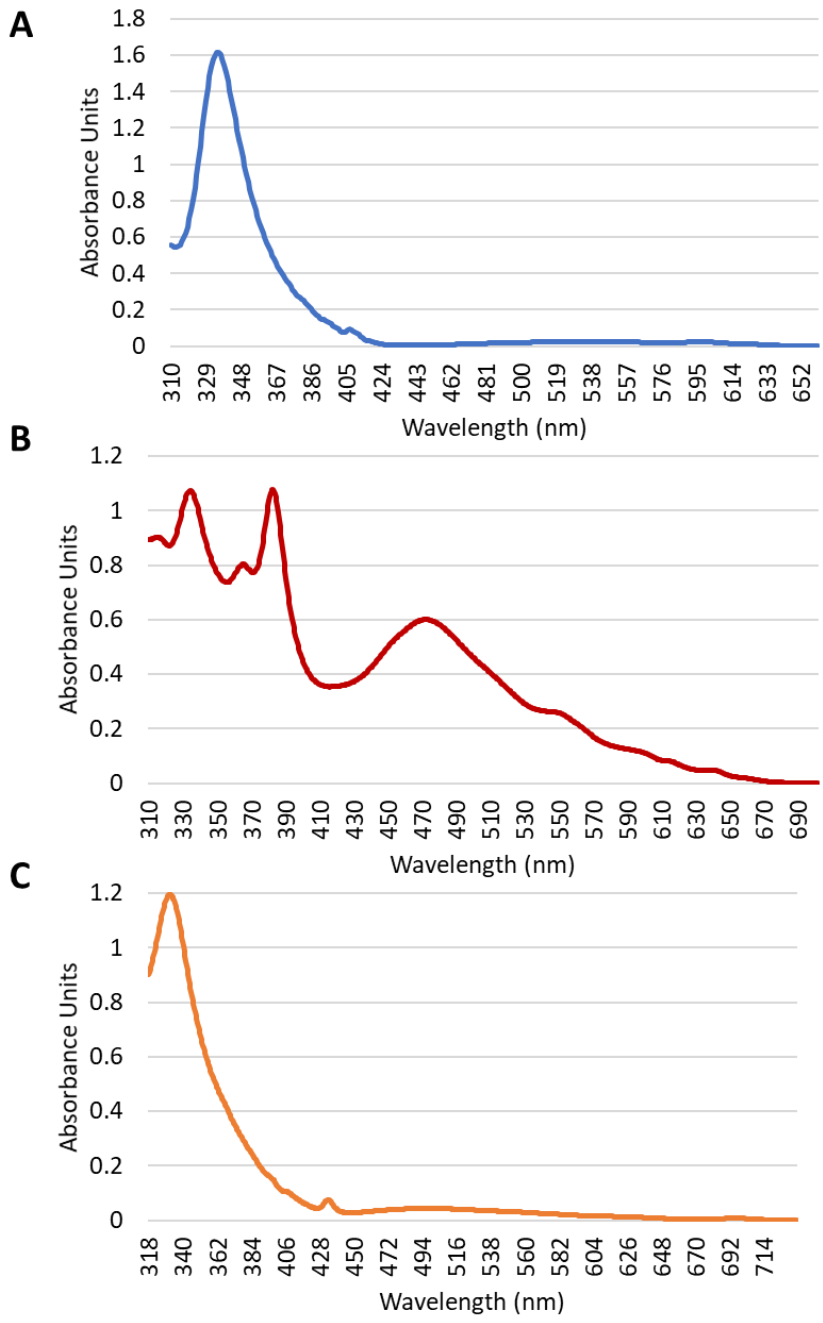

Figure 8. UV-Vis absorbance spectrum for the SES brand of C60 (A), C70 (B), and PCBM (C). The maximum absorbance peaks were 332 nm, 334 nm, and 331 nm, respectively.

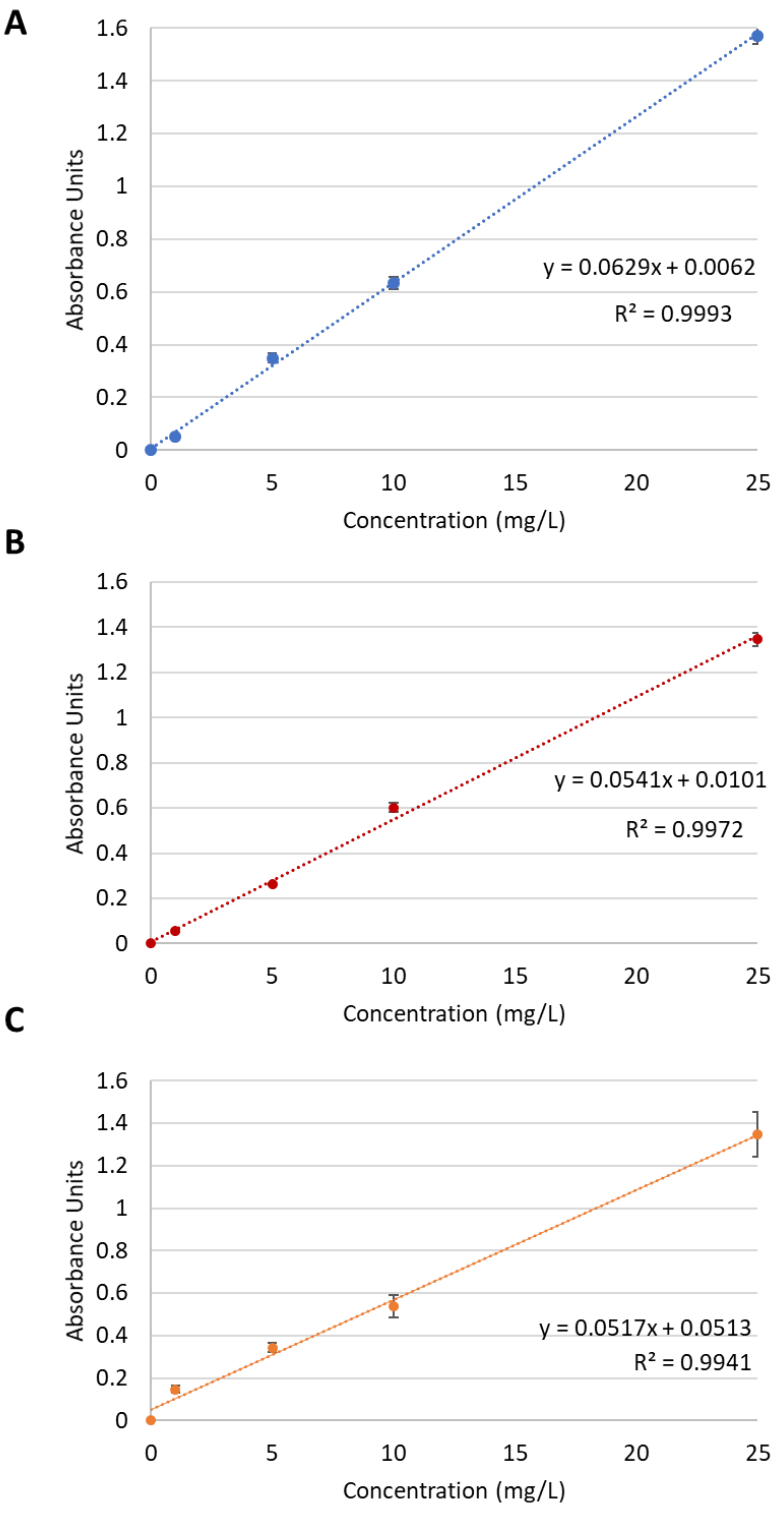

Figure 9. Standard curves (0-25 mg/L) for A) C60, B) C70, and C) PCBM in toluene. Error bars indicate standard error of the mean. The number of replicates for the fullerenes were the following: C60 (n=12), C70 (n=7), and PCBM (n=6).

An extraction blank was found by using synthetic freshwater (SFW), NaCl, and toluene to run several toluene extractions without fullerene to ensure that all the elements necessary for the extraction were present minus the fullerene. The limit of the detection (LOD) was calculated following methods by Shrivastava and Gupta (2011). The LOD was found to be 0.0009 mg/L and the LOQ was found to be 0.003 mg/L. The mean absorbance of the blanks was 0.007, which was subtracted from all sample absorbance values prior to calculating the concentration using the standard curve. The total concentration in the original sample was calculated based on the total of all extractions for each sample. The extraction efficiency was calculated for all three fullerenes from multiple extraction experiments, where most of the sample was extracted during the first extraction (Table 1).

Table 1. Fullerene and toluene extraction efficiencies (%), standard deviation of the extraction percent, and standard error of the extraction percent for C60 (n=16), C70 (n=8), and PCBM (n=13) across a range of concentrations (~111-227 mg/L).

	Extraction Efficiency		
Fullerene	**1**	**2**	**3**
C60	83%	14%	3%
Std Dev	0.10	0.08	0.02
Std Error	0.02	0.02	0.01
C70	91%	8%	1%
Std Dev	0.08	0.07	0.01
Std Error	0.03	0.02	0.01
PCBM	91%	8%	1%
Std Dev	0.05	0.05	0.01
Std Error	0.01	0.01	0.00

Settling Effects: Time Series Experiment

The fullerene suspension was observed to settle rapidly from solution. To test the impact of this settling, fullerene concentration was measured at various time points over a 5-day period. 10 mL of the solution were placed into a labeled scintillation vial and was used for only one time point. 3 mL of the settled solution was pipetted from the center and 1 cm from the top. This sample was added to an exetainer and put on a rotary shaker for ten minutes before performing the toluene extraction protocol as shown in Figure 10. The samples were placed on the rotary shaker in order to resuspend the sample prior to analysis. The toluene extraction protocol was followed for each sample and the absorbance was read for the three extractions in order to calculate the concentrations at each time point.

Figure 10. The n-C60 samples taken after different settling times were placed on the rotary shaker for ten minutes prior to the toluene extraction.

The results for the settling experiment from March 5, 2015 to April 2, 2015 using 200 mg/L n-C60 solutions can be seen below in Table 4. A scatter plot with error bars can be seen in Figure 11 for the different time points tested (n=3). The largest drop in concentration was seen after 1 hr of settling. The concentration at zero min of settling is over the 200 mg/L initial concentration, which could be explained from sampling an area from the flask with large, concentrated agglomerates.

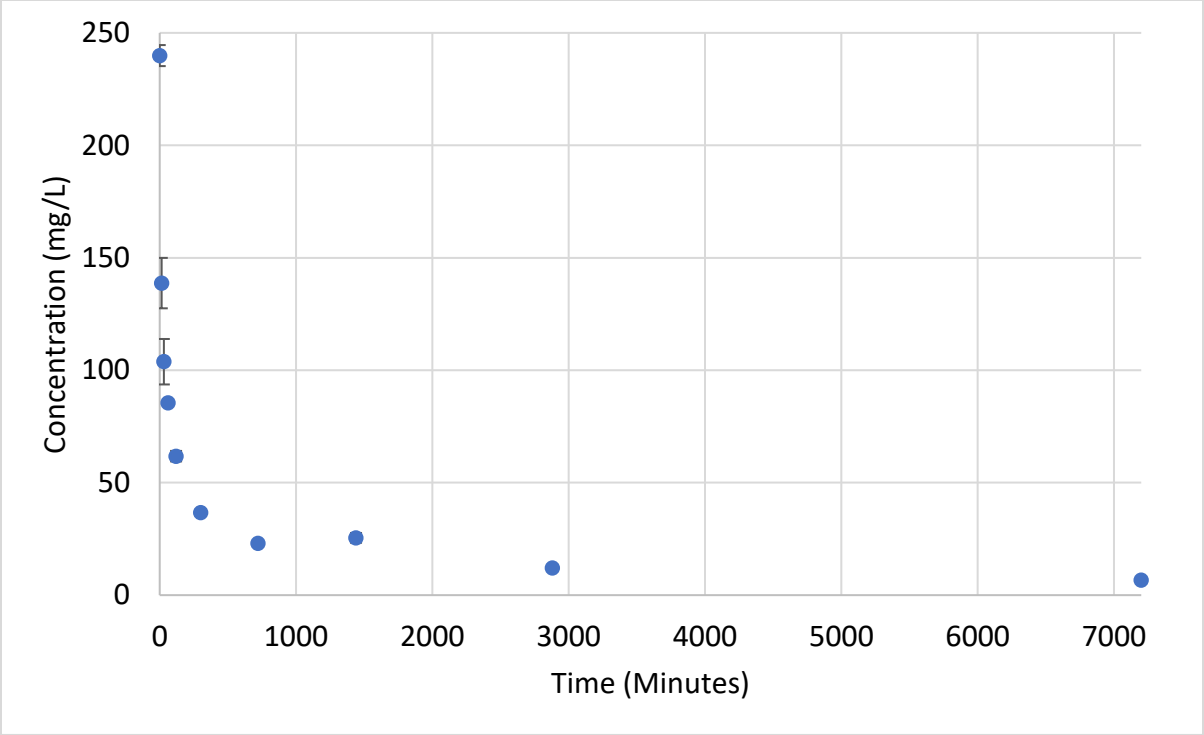

Figure 11. Graph of fullerene concentration at different settling times with error bars calculated using standard error. The largest drop in concentration is after 1 hour of settling with a starting concentration of 200 mg/L.

Based on these results, future experiments were designed to minimize the time in which fullerenes were handled or sampled after removing the mixture from the stir plate. For future experiments, all samples were taken from the stirred solution within five minutes after stopping stirring.

Fullerene Use-Phase Releases: Organic Photovoltaic Cells (OPVs)

Much of the methods development focused on the pristine and functionalized forms of fullerene. However, there are also potential risks of material exposure during the use phase of nano-enabled products and technologies. To begin to develop methods to assess the ecotoxicity impacts from use-phase exposures, OPVs were created by colleagues at Michigan State University to test the impact of fullerene released from a clean energy application. The ecotoxicity of photovoltaic panels are scarce in the literature (Tammaro et al. 2016) and those

that exist are mainly for thin-film photovoltaics such as CdTe cells. It has been found that regulated handling of CdTe cells at end-of-life will not endanger the environment (Jäger-Waldau 2009), but uncontrolled disposal could create environmental risks. Furthermore, leaching data exists for new solar cells but there are limited studies on leachates from broken, weathered, or aged cells (Zimmermann et al. 2012). OPV leaching studies were performed using a long-term perspective of 123 days for various release pathways including those that reflected mishandling of OPVs during dismantling and disposal (Zimmermann et al. 2013). To understand the potential environmental impact under different use-phase and disposal scenarios, methodology for OPV leaching was adapted from Zimmermann et al. and Brun et al. (Zimmermann et al. 2013; Brun et al. 2016) (Figure 12).

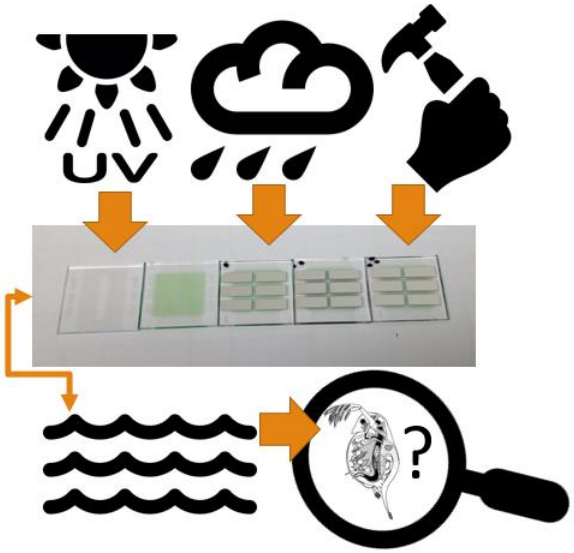

Figure 12. Schematic of weathered and aged OPV cells as a representation of OPV end-of-life scenarios to be tested on *Daphnia* species for ecotoxicity effects.

OPVs were placed into glass vials with SFW and were placed on shaker tables underneath UV-A light for three months to simulate weathering of the cells over time in the environment. The

treatments were the following: AFW control (A), C60 on a glass slide (C60), ClAlPc dye on a glass slide (Cl), glass slide with the solvent (GS), TPFB dye on a glass slide (TP), TPFB dye and C60 on a glass slide (TPC60). Each of the dye treatments were just the dye film deposited over glass. The control glass slides were sonicated in soap, DI water, and acetone followed by rinsing in boiling isopropanol and then exposure to O2 plasma. Once weathered, preliminary chronic ecotoxicity *Daphnia* studies were performed to look at both the long-term effects of weathered and aged OPV cells (Figures 13 and 14).

Figure 13. The set-up for the weathering of OPV cells from the University of Michigan is shown where the cells were placed into a vial with artificial freshwater (SFW) and are shaking on a shaker table at a constant speed of 1 under UV-A lighting. This experiment was started on 7/6/17 and continued for three months before adding *Daphnia* to test the toxicity of the weathered cells. Vials were placed randomly to eliminate bias and were randomly moved to different locations throughout the experiment to ensure all sides had exposure to UV-A light.

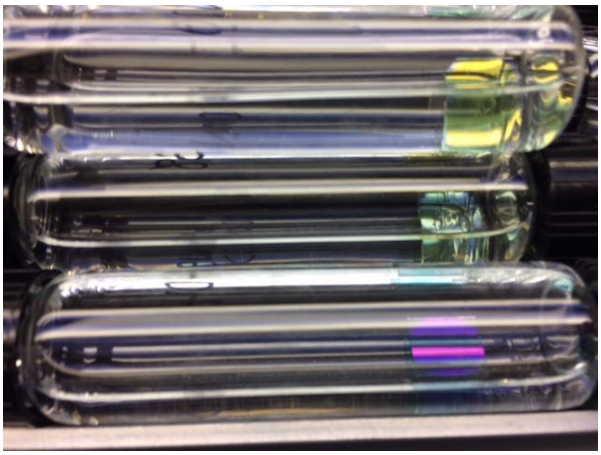

Figure 14. A close-up photograph of the OPV cells. The blue cell is representative of an OPV cell with just the dye (CIAIPc) and the green/yellow cell is a replicate of the dye and C60 combination. The changes in color were noted over time and documented with photographs.

Conclusion

Methods for preparation and quantification (via toluene extraction) of fullerene (C60, C70) and a functional form of fullerene (PCBM) were reported here. Additionally, preliminary methods were developed for potential use-phase release of fullerene from OPV cells based on previous studies of solar cell leaching. Due to the challenge of finding and replicating preparation methods from the literature for C60, these detailed methods are included for the benefit of other researchers to refer to the methods for future fullerene research. Because methods did not previously exist for the two other fullerene forms, C70 and PCBM, researchers can now refer to this chapter to find the relevant wavelength for absorbance and preparation methods for ecotoxicity. All the methods described in this chapter were used in Chapter 3, wherein the samples were prepared as described and were used for ecological impact testing for all three fullerene forms.

CHAPTER 3:
CASCADING ECOLOGICAL IMPACTS OF FULLERENES IN FRESHWATER ECOSYSTEMS[1]

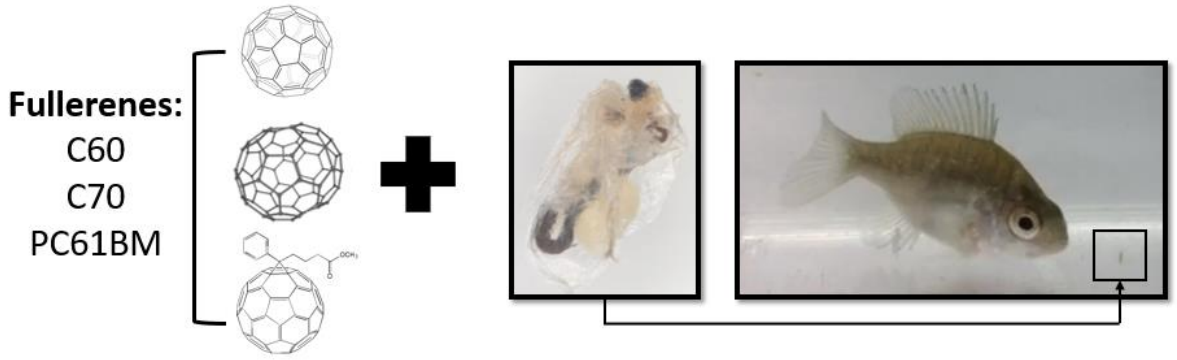

Figure A. Overview of empirical studies: Fullerene exposure can create cascading ecological impacts that are not captured through acute toxicity assays alone.

Introduction

Evidence from the literature suggests that once ENMs are released into the environment they may also pose direct risks to natural ecosystems (Jahan et al. 2017), which are often assessed by methods such as freshwater ecotoxicity assays on model organisms (Cunningham et al. 2013). In Chapter 2, methods were developed to characterize and solubilize the three types of fullerenes (C60, C70, and PCBM) to calculate concentrations for ecotoxicity assay preparation. Utilizing these methods, C60, C70, and PCBM were prepared in synthetic freshwater (SFW) to assess the risk of exposure in the environment and to identify differences among the fullerene forms. A large share of the literature on ENM ecotoxicity is focused on the most commonly utilized ENMs (i.e. TiO2, nano-Ag, C60, and carbon nanotubes) at the acute level. However, many of these studies have been critiqued for the variability of approach, scope, and results, even for the

[1] This chapter is adapted from a forthcoming publication in Environmental Toxicology and Chemistry. To avoid repetitive citations, a blanket reference to the original manuscript is provided here: (Moore et al. 2019a)

same ENM (Juganson et al. 2015). Insights offered by the C60 ecotoxicity literature are often highly variable due to lack of uniform preparation and dispersal methods. In addition, while studies on pristine C60 are widely available in the literature, studies on other functional forms within this material class remain scarce. Life cycle analysis has shown that energy impacts of fullerene production increase with size (number of carbons) and additional purification and functionalization steps (Anctil et al. 2011), but no study has yet been carried out to determine if ecotoxicity impacts change across this suite of materials. This knowledge gap is particularly relevant given findings by Arndt et al. (2013a), who studied the generational effects of various fullerene and carbon nanotube (CNT) derivatives in *D. magna* and found that the toxicity of a nanomaterial is highly dependent on surface chemistry. Thus, different structures and functionalized forms could have varying fate, transport, and toxicity effects (Juganson et al. 2015), parameters that are critical for carrying out proactive ENM risk assessment (Petersen et al. 2015).

By focusing on acute toxicity alone, chronic impacts, exposure across multiple species and generations, and trophic interactions cannot be predicted (Arndt et al. 2013a), limiting the ability to assess ecosystem level impacts (Bour et al. 2015). Intergenerational impacts of ENM exposure in model organisms may include decreased growth rate, maternal transfer of ENMs in the brood chamber, and lipid accumulation of ENMs over time (Arndt et al. 2013b). As reported for carbon nanotubes, ENMs can have sublethal chronic implications in which the material blocks the digestive tract or agglomerates on the surface of an exposed organism (Revel et al. 2015). At the ecosystem level, these outcomes could influence predation and/or trophic interactions. For example, decreased translucency of the zooplankton's skeleton can increase selective predation by visual predators (Branstrator and Holl 2000) with potential for cascading trophic outcomes

(Mitra and Flynn 2006). These effects have not yet been assessed for ENM contaminants. Uncertainty surrounding direct and ecosystem-level impacts may be amplified by variability in material form as it enters the natural environment. Through a life cycle lens, fullerenes can be released into the environment during the production stage (accidental release or process emissions), the product use phase (washing cosmetic products into the waste water), or at a product's end-of-life (disposal of fullerene-containing products into landfills) (Eckelman et al. 2012). Understanding the impact associated with the forms expected in realistic material release scenarios is therefore critical to holistic analysis of environmental risks.

The study reported herein is the first to evaluate C60, C70, and PCBM at the organismal and community levels to determine how variability in material form may impact ecotoxicity analysis and, more broadly, potential for cascading effects on ecosystems from changes in key species interactions. *Daphnia* spp. are a model aquatic invertebrate for toxicity assessment and bioindicators that play a significant role in the food chain of freshwater ecosystems. As such, a decline in the *Daphnia* populations over several generations may have trophic-level impacts that disrupt community dynamics (Zöllner et al. 2003). Prior studies suggest that ENMs such as fullerenes may negatively affect the feeding rate and/or mobility of *D. magna* (Lovern et al. 2007). We conducted acute fullerene assays to assess lethal and sub-lethal effects, such as heart rate, and chronic exposure assessments to understand longer-term and intergenerational effects. To assess potential impacts of fullerene bioaccumulation on species interactions, predation was evaluated on control and fullerene-exposed *D. pulex* to test the hypothesis that the carapace-darkening effect of fullerene exposure increases susceptibility to predation by the visual predator *Lepomis macrochirus* (bluegill).

MATERIALS AND METHODS

Preparation of fullerenes

Fullerenes – C60 (99.5%), C70 (99.0%) and PCBM (99.0%) – were purchased from SES Research in 2014 (Houston, Texas, USA). The fullerenes were maintained in synthetic freshwater (SFW; moderately hard, pH 7.4-7.8; EPA 2002). Because fullerenes are hydrophobic, 200 mg/L solutions of C60, C70, and PCBM were prepared following Pakarinen et al. (2011, 2013) to mimic mixing in natural freshwater systems. Concentration of each fullerene form in their stock solutions were verified using an adaptation of Fortner et al. (2005). Briefly, a 2:2:1 mixture of unfiltered CNM solution, toluene, and 2% NaCl were vortexed and then allowed to settle to aqueous and toluene layers, which were separated by pipette. This process was repeated three times with fresh toluene to ensure complete transfer to the organic fraction. The concentration of fullerenes extracted to the toluene fractions was estimated via absorbance at the peak absorbance value for each material on a Shimadzu 1800 UV-Vis spectrophotometer at 331 nm (PCBM), 332 nm (C60), and 334 nm (C70) using standard suspensions prepared via serial dilution.

Fullerene characterization

The morphology of the three fullerene suspensions was analyzed via transmission electron microscopy (TEM) while the chemical composition and size distribution was characterized using three optical-analytical methods: Fourier transform infrared, Zeta potential analysis, and thermogravimetric analysis.

Characterization of fullerene suspensions in SFW was performed using a JEOL 2010 transmission electron microscope (TEM) operated at 15 kV. All three materials demonstrated

substantial agglomeration in TEM images (Figure 1A-C), reflecting the form in which the *Daphnia* were exposed. The fullerenes were also characterized at higher magnifications (150 kV and 200 kV) to view the size range of nanoscale fractions (≤ 20 nm) (Figure 1D-F).

Fourier transform infrared (FTIR) was also performed for each fullerene. Each sample (~2 μL) was deposited with a Pasteur pipette between two KBr disks. Spectra were measured twice per sample using a FTIR spectroscopy (Shimadzu, IR Prestige 21, Kyoto, Japan) in the range of 4000-600 cm^{-1}, 40 scans, and a 4 cm^{-1} resolution (Gupta et al. 2018).

phase analysis light scattering were used to estimate Zeta potential over three cycles.

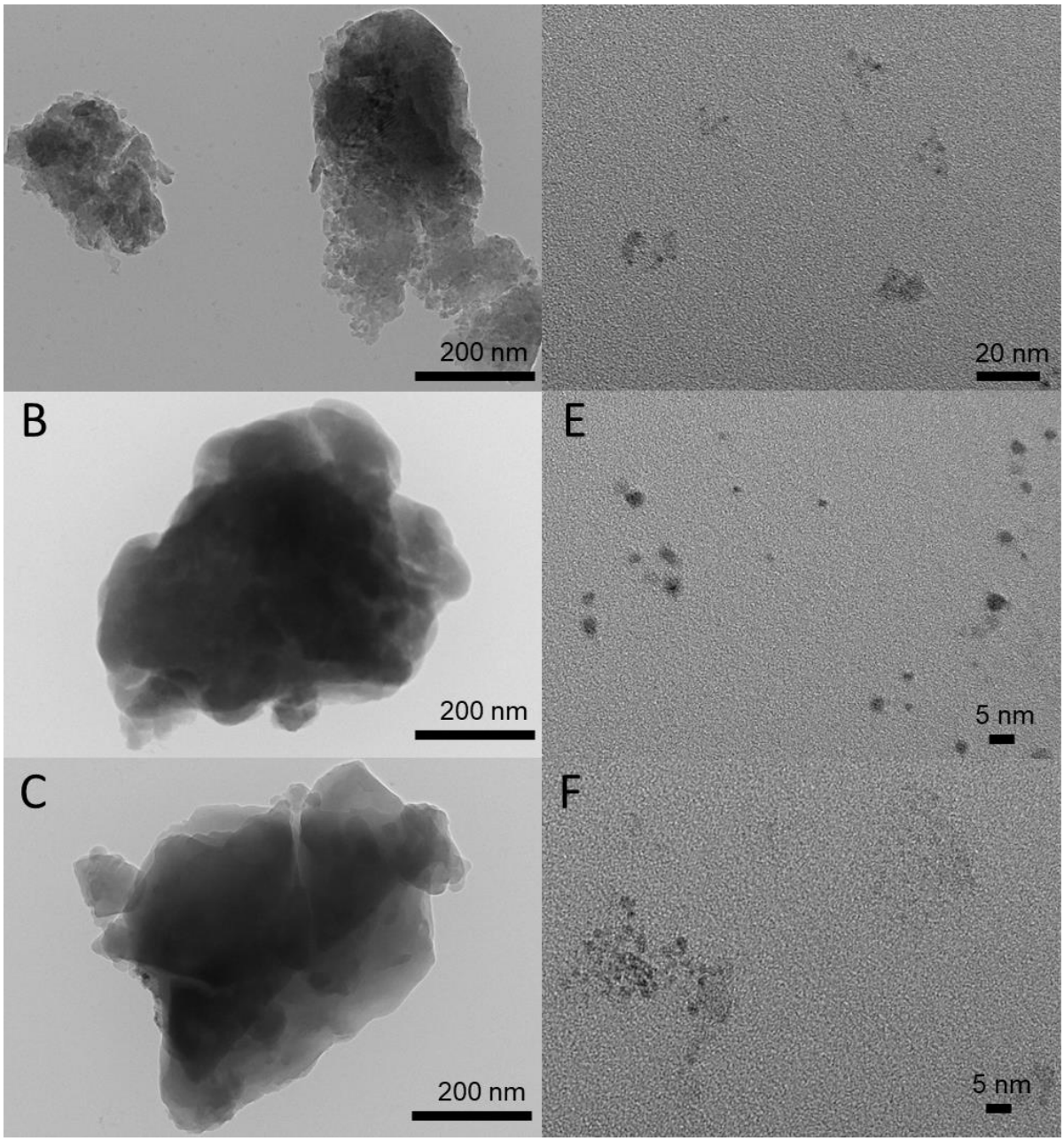

Figure 1. TEM characterization of C60 (A, D), C70 (B, E), and PCBM (C, F) agglomerates at 15 kV (A, B, C) kV, 150 kV (D), and 200 kV (E and F) in SFW.

The zeta potential was estimated for each suspension (1 mL in quartz cuvettes 10 x 10 x 45 mm) on a Malvern Instrments Zeta-sizer Nano ZS equipped with a backscattering detector angle of 173° and a 4 mW, 633 nm He-Ne laster at 25° C. Deionized water and SFW mediums were both tested since the zeta potential measurement is sensitive to changes in pH and the presence of

monovalent and polyvalent ions (Lowry et al. 2016). The hydrodynamic diameters, polydispersity index (PDI), and zeta potential were determined following methods by Gupta et al., (2018) where combined Doppler electrophoretic mobility of the fullerene particles in the solvents and phase analysis light scattering were used to estimate Zeta potential over three cycles.

The composition profile of each fullerene suspension in SFW was measured on a TA Instruments Q500 Thermogravimetric analyzer (TGA) and the data were analyzed with the TA Instruments Universal Analysis 2000 software following methods by Gupta et al., where the sample was heated from 25°C to 950°C at 5°C/min under nitrogen atmosphere (Gupta et al. 2018).

Daphnia *rearing conditions with C60, C70, and PCBM*

D. magna and *D. pulex* were purchased from Aquatic BioSystems, Inc. (Fort Collins, Colorado, USA) in 2009 and maintained in standard conditions (16:8 hr light: dark, 20° C, fed 3.75E6 cells *Pseudokirchneriella subcapitata* per 250 mL culture every three days; Connelly 2015). The cultures were maintained in synthetic freshwater (SFW; moderately hard, pH 7.4-7.8; EPA 2002). Individual *Daphnia* were isolated from the stock culture and maintained as subsample clone lines for six generations prior to initiation of fullerene exposure experiments.

Acute and chronic exposures of Daphnia *to fullerenes*

The 72-hr acute fullerene toxicity assays were performed following U.S. EPA 2002 Acute Toxicity Methods (EPA 2002) based on published work on C60 (Pakarinen et al. 2013). Both species, *Daphnia magna* (n = 10) and *Daphnia pulex* (n = 20), were exposed to 5, 10, 25, and 50 mg/L of the solubilized solutions. Since acute results do not necessarily predict chronic effects, 21-day exposure assays were performed for various life stages to determine longer-term

exposure effects, following U.S. EPA Ecological Effects Guidelines for Daphniid Chronic Toxicity Tests (EPA 1996), except where noted. Each life stage (neonate, juvenile, and egg-stage) of *D. pulex* (n=10) was exposed to a measured concentration of 7 mg/L, which was calculated based on a predicted exposure scenario (see SD for details).

Daphnia *experimental set-up*

For both acute and chronic exposures, SFW and the requisite volume of fullerene solution were added to 30 mL glass scintillation vials with one juvenile (2-7 d old) *Daphnia* spp. added randomly to each vial. The *Daphnia* spp. were fed 1 mL *P. subcapitata* (1.5E7 cells / mL) at the start of the experiment and not fed again during the acute experiments. For chronic exposures, *D. pulex* were fed 1 mL *P. subcapitata* (1.5E7 cells / mL) every 72 hr. Survival and reproductive output were measured at 72 hr for acute assays and daily for chronic assays. Surviving *D. pulex* were stored for use in the predation assays and deceased individuals fixed in 85% ethanol for light microscopy.

Measurement of sublethal effects: Daphnia *heart rates*

To determine potential sublethal effects of the fullerenes, an acute (48-hr) heart rate experiment was conducted following methods adapted from Dzialowski et al. (2006). Changes in heart rate were studied because they are linked with both behavior and population dynamics (Lovern et al. 2007; Pan et al. 2017). A single individual juvenile *D. pulex* was added to 30 mL glass scintillation vials containing either SFW (control) or a fullerene treatment (SFW with 7 mg/L fullerene; n=10). At 0-h, 24-h, and 48-h, each *D. pulex* was moved from the vial to a depression slide to view heart rates using a 40X compound microscope. Within 30 sec of placement on the slide, contractions of the heart were counted for three - 15 sec intervals and recorded using a

handheld tally counter. Reported rates represent the average beats per minute (BPM) of the three measurements. When heart rates were observed that were diminished to below one standard deviation of the mean heart rate for each treatment at 48-h, we hypothesized that the lower heart rate would ultimately lead to a fatal response. To test the hypothesis, we observed mortality of all samples within 12 hr of the final measurement.

Use-Phase Exposure to Daphnia

OPV cells (n = 10) were weathered following methods described in Chapter 2. Once weathered, preliminary chronic ecotoxicity *Daphnia pulex* studies were performed to look at both the long-term effects of weathered and aged OPV cells. The OPV cells were removed from the vial after the weathering period. *D. pulex* were added directly to the vials with the leachate to assess the chronic lifespan and fecundity.

Predation experiment

Juvenile *L. macrochirus* were obtained from Carolina Biological Supply Co. (Burlington, North Carolina, USA) in 2017 and maintained in 38-liter aquaria in SFW. The tanks were maintained using standard aquarium filtration systems at room temperature (approximately 20° C) using established maintenance protocols (Nickum et al. 2004) and fed sinking shrimp pellets four times per week.

Prior to feeding trials, food was withheld for one week to encourage prey drive and simulate natural starving periods (Frommen 2017). At the beginning of each trial (n=35 trials), one *L. macrochirus* was randomly transferred to a transparent 1 L aquarium and allowed a 2-hr acclimation period prior to feeding. A transfer pipette was used to gently and simultaneously introduce five controls and five fullerene-exposed *D. pulex*. Observations of the *D. pulex* color and time of consumption were recorded using a video camera over a 10-minute period (a video

example of this predation trial is available at Moore 2017). At the end of each trial, experimental fish were transferred to a separate tank and remaining *D. pulex* discarded.

Data analysis and statistical methods

Acute effects of the increasing concentration of fullerenes on mortality of *Daphnia* spp. were compared for each material individually using a Chi-squared test of independence. When significant effects were found, post hoc analysis was conducted using Chi-squared pair-wise comparisons between the control and each concentration of fullerene, with a Bonferroni correction for multiple pairwise comparisons. The chronic endpoints of mortality and fecundity were analyzed among material types (control, C60, C70 and PCBM) for each *D. pulex* lifestage group separately using one-way analysis of variance when assumptions of normality and homogeneity of variance were met, or a Kruskall-Wallis analysis when assumptions were violated. A Kruskall-Wallis analysis was used to analyze heart rate data at each time point (0-h, 24-h, and 48-h) to determine sublethal differences among all treatments. To determine the probability of a fatal response after observing a heart rate below one standard deviation of the mean at 48-h, a Chi-squared test of independence was performed. Chronic effects of the OPV leachates on mortality of *Daphnia pulex* were compared for each treatment using one-way analysis of variance when assumptions of normality and homogeneity of variance were met, or a Kruskall-Wallis analysis when assumptions were violated. Finally, a paired t-test was performed to determine differences in the number of control vs. fullerene-exposed *D. pulex* consumed by *L. macrochirus*. Results were considered significant at $p < 0.05$.

RESULTS

C60, C70, and PCBM characterization

Characteristics of the three fullerenes provided by the manufacturer and measured from Zeta potential analysis and dynamic light scattering are summarized in Table 1. All three fullerene samples were negatively charged and polydisperse in nature. C60 was less aggregated compared with C70 and PCBM; while C60 was within the range of the nanometer scale, C70 and PCBM ranged in microns. The FTIR and TGA results can be found in Appendix B, in Figures S1-S6.

Table 1. Characteristics of the three fullerenes. The polydispersity index (PDI), size (nm), and Zeta potential (mV) are averages of three sample replicates.

Characteristic	C60	C70	PCBM
Purity[1] (%)	99.50%	99.00%	99.00%
PDI	0.5	0.9	0.7
Size (nm)*	565.4	6459.0	1602.3
Zeta of (mV)*	-18.6	-24.3	-19.0
Zeta (mV)**	-19.1	-11.9	-7.5

1. SES Research
*Fullerenes in SFW
**Fullerenes in deionized water

C60, C70, and PCBM acute, chronic, and heart rate results

The results presented here demonstrate lethal and sublethal impacts from C60, C70, and PCBM assays, with differences between species and among forms of fullerene. C70 was the only fullerene to significantly increase mortality in *D. magna*, with mortality rates 3.5-5 times greater in the presence of C70 ($p < 0.001$; Figure 2A; Table 1). C70 also contributed to a significant increase in mortality in *D. pulex* ($p = 0.003$), but C60 also exhibited a minor effect ($p = 0.045$; Figure 2B; Table 1). In post hoc analysis, only C70 at 10 and 50 mg/L significantly increased mortality relative to the control; no pairwise differences were significant for C60. Sublethal

impacts were also observed in acute testing (Figure 2C and 2D) and chronic testing for all three fullerenes with visual darkening of the carapace observed (Figure 3).

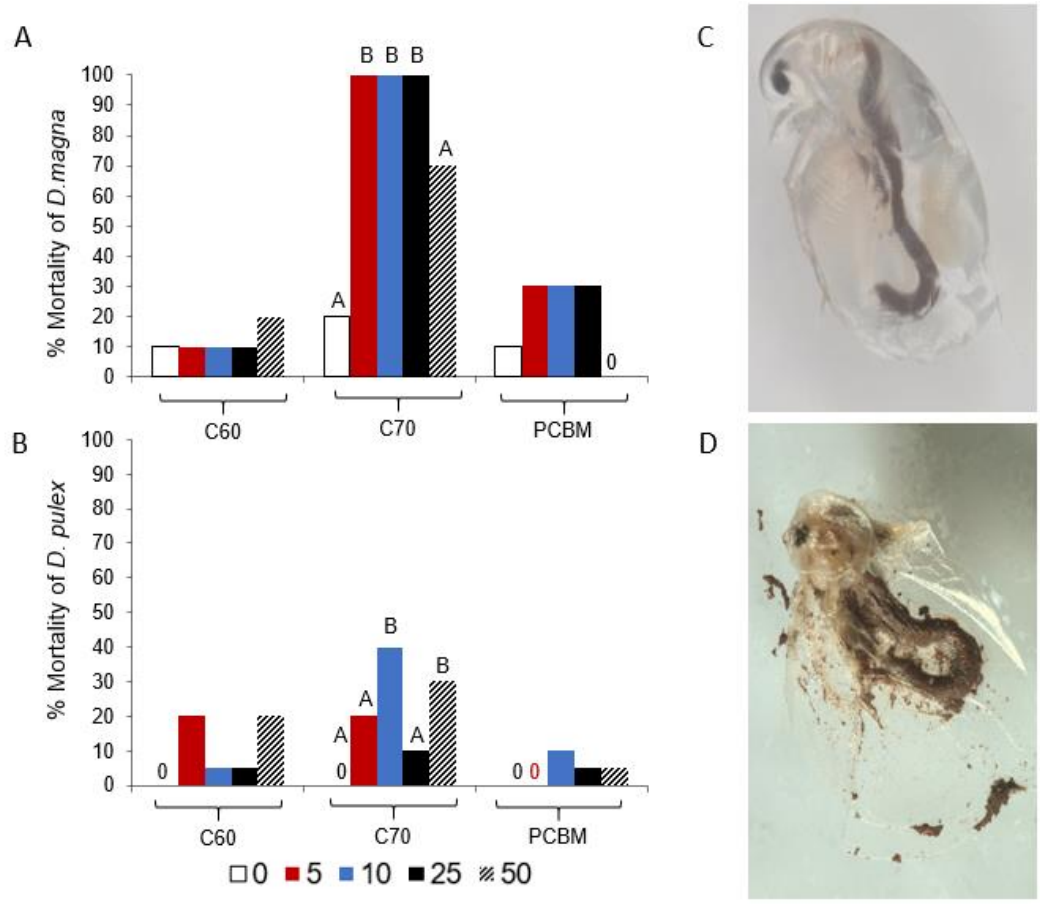

Figure 2. A) Percent mortality of D. magna (n = 10) and B) D. pulex (n = 20) for three fullerene materials at concentrations ranging from 0-50 mg/L in acute trials. Values represent the proportion of individuals that died for a given material concentration during the experiment, with each experimental unit containing a single individual. Significant differences between the control (0 mg/L results) and each concentration determined by post-hoc comparison within a material type are indicated by unique letters above each bar. C) *D. pulex* ingestion of C70 (Zeiss 56X). D) *D. magna* exhibiting PCBM agglomeration on its carapace (Zeiss 80X).

Minor chronic exposure effects for the endpoints of mortality (Figure 4A) and fecundity (Figure 4B) were observed in *D. pulex*. Neonate lifespan was marginally reduced when exposed to PCBM, suggesting PCBM exposure early in the life cycle could impact *D. pulex* population

dynamics (Figure 4A; Table 1). At the egg-stage, exposure to C70 caused a slight decrease in *D. pulex* fecundity (survival and reproduction) compared to the C60 and PCBM exposure.

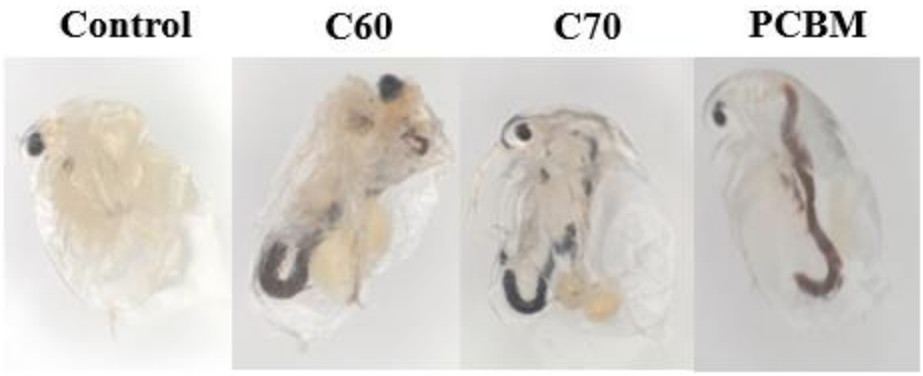

Figure 3. Light microscopy of egg-stage *D. pulex* (Zeiss 50X) post-chronic fullerene exposure.

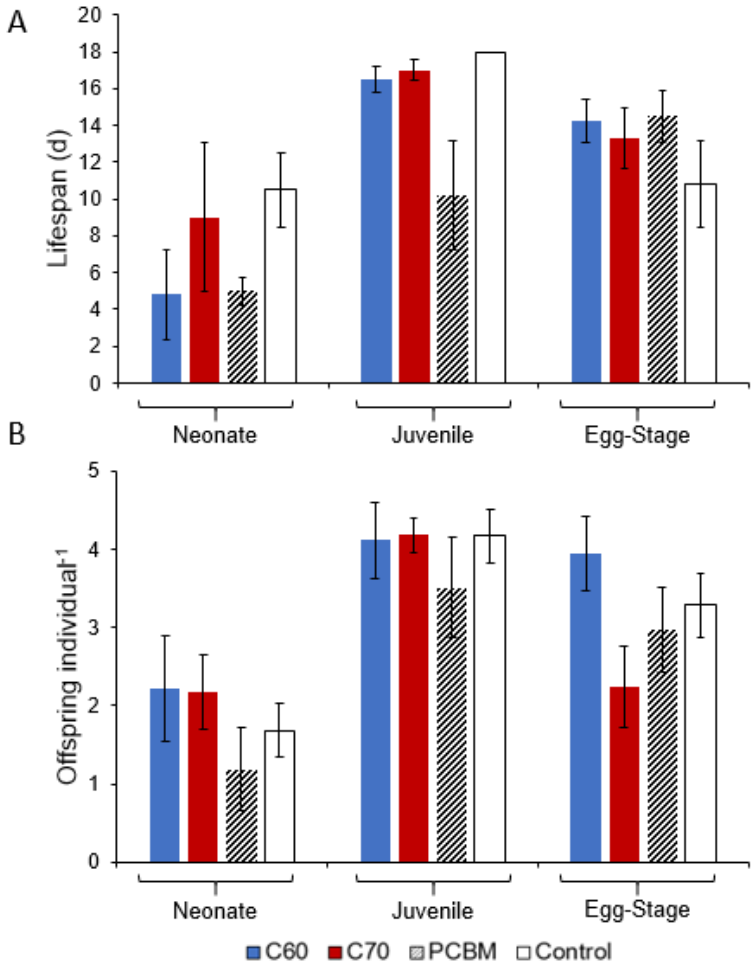

Figure 4. A) Chronic impact of fullerenes (C60, C70, PCBM) on lifespan of *D. pulex* across different lifestages at 7 mg/L exposure and controls. B) Average offspring per daphniid (fecundity) results for all three materials and the control group at 7 mg/L (B). Error bars indicate standard error of the mean.

Table 2. Results of Chi-squared analysis for mortality in acute experiments for *D. pulex* and *D. magna*, analysis of variance or Kruskall-Wallis test for toxicity evaluation across lifestages in chronic experiments with *D. pulex*, and Kruskall-Wallis test and chi-squared analysis for heart rates for *D. pulex*.

Test	Species (lifestage)	Main Effect	df	X^2	*p*
Acute	*D. magna* (juvenile)	C60	4	0.97	0.91
		C70	4	30.47	<0.001*
		PCBM	4	6.89	0.14
	D. pulex (juvenile)	C60	4	9.77	0.045*
		C70	4	15.70	0.003*
		PCBM	4	4.70	0.32
			df	F	*p*
Chronic	*D. pulex* (neonate)	Lifespan[a]	3	2.38	0.09
		Fecundity[a]	3	0.87	0.47
	D. pulex (juvenile)	Lifespan	3	1.05	0.79
		Fecundity	3	0.31	0.96
	D. pulex (egg-stage)	Lifespan	3	7.60	0.06
		Fecundity	3	0.78	0.85
			df	F	*p*
Heart rate (0-h)	*D. pulex* (juvenile)	C60	1	0.0057	0.94
		C70	1	0.052	0.82
		PCBM	1	0.24	0.65
			df	F	*p*
	D. pulex (juvenile)	C60	1	7.02	0.008*

		C70	1	8.71	0.003*
Heart rate (24-h)		PCBM	1	9.18	0.002*

			df	F	*p*
	D. pulex (juvenile)	C60	1	5.15	0.023*
		C70	1	5.15	0.023*
Heart rate (48-h)		PCBM	1	2.06	0.151

			df	X^2	*p*
	D. pulex (juvenile)	C60	1	6.19	0.013*
		C70	1	10.01	0.0016*
Probability of lethal response		PCBM	1	3.28	0.070

[a]ANOVA testing requirements were met

[*]$p < 0.05$

Initial heart rates were similar among all treatments at 0-h, but were significantly elevated relative to the control in all three fullerene treatments (Figure 5) at 24-h. After the 24-h time point, not all individuals exhibited a lethal response at the same rate. At 48-h, significant differences were observed relative to the control for C60 and C70 (Table 2). However, at this time point, a subset of individuals for each fullerene treatment had substantially diminished heart rates, leading to a lethal response within the following 12 hrs, whereas those that persisted beyond 48-h had consistently high heart rates between 24 and 48-h. A significant difference was not observed for PCBMrelative to the control at 48-h, likely because of the high variance associated with including persistent (those that lived past 60-h) and individuals closer to death. The mean for persistent individuals only in the PCBM treatment remains significantly higher

than the control (Table S1). A probability relationship between heart rates below one standard deviation of the mean heart rate at 48-h and an ultimate fatal response was tested and confirmed for C60 ($p = 0.013$) and C70 ($p = 0.0016$).

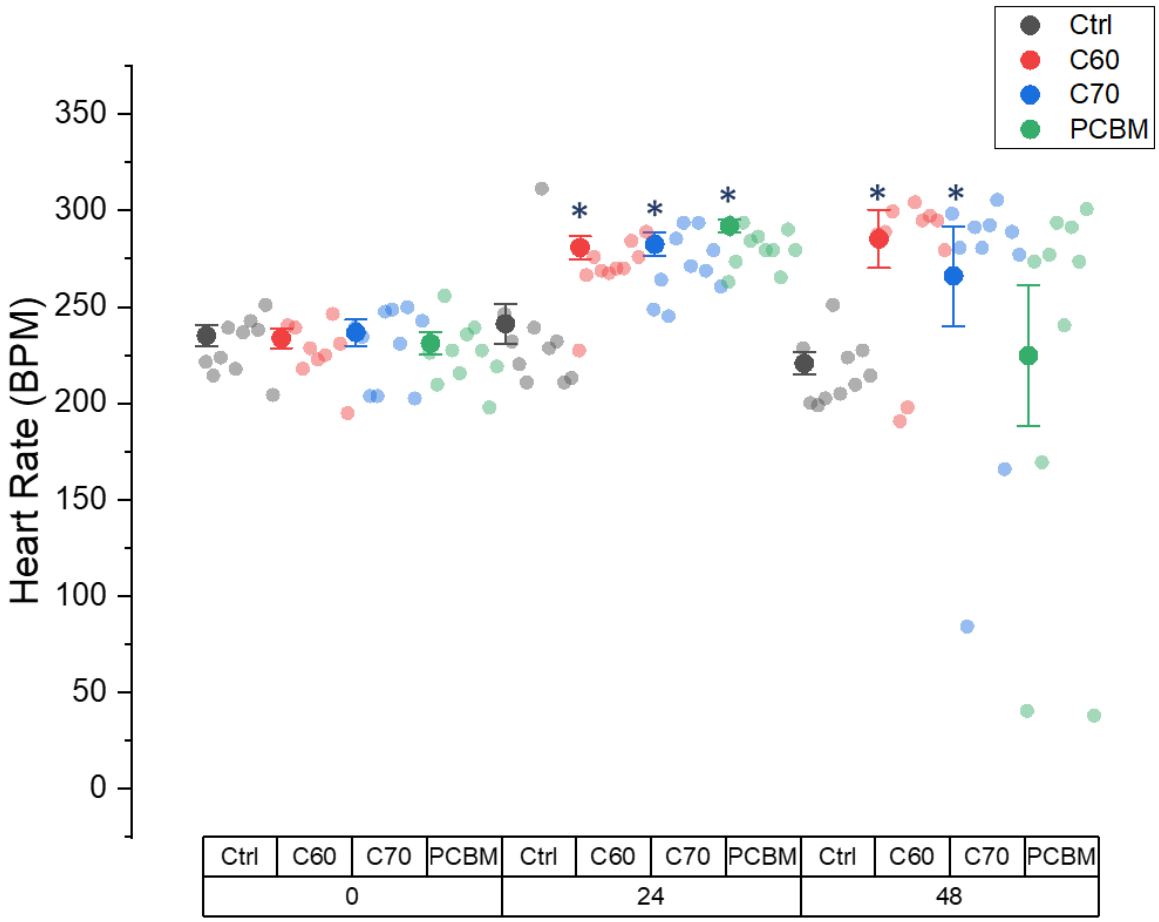

Figure 5. Average heart rates (bpm), indicated by the darker circles, for *D. pulex* (n=10) at 0-, 24-, and 48-h for all treatments. The lighter circles are representative of individual heart rates measured at each time point and asteriks indicate a statistical difference ($p < 0.05$). Error bars indicate standard error of the mean.

Preliminary Use-Phase Results

The only significant difference ($p < 0.05$) in lifespan among the D. pulex treatments was observed for the control treatment relative to all the OPV samples (Figure 6), indicating no statistical difference among the OPV treatments (dyes or C60 treatments). There were no significant differences in fecundity for any of the studied treatments (Figure 7).

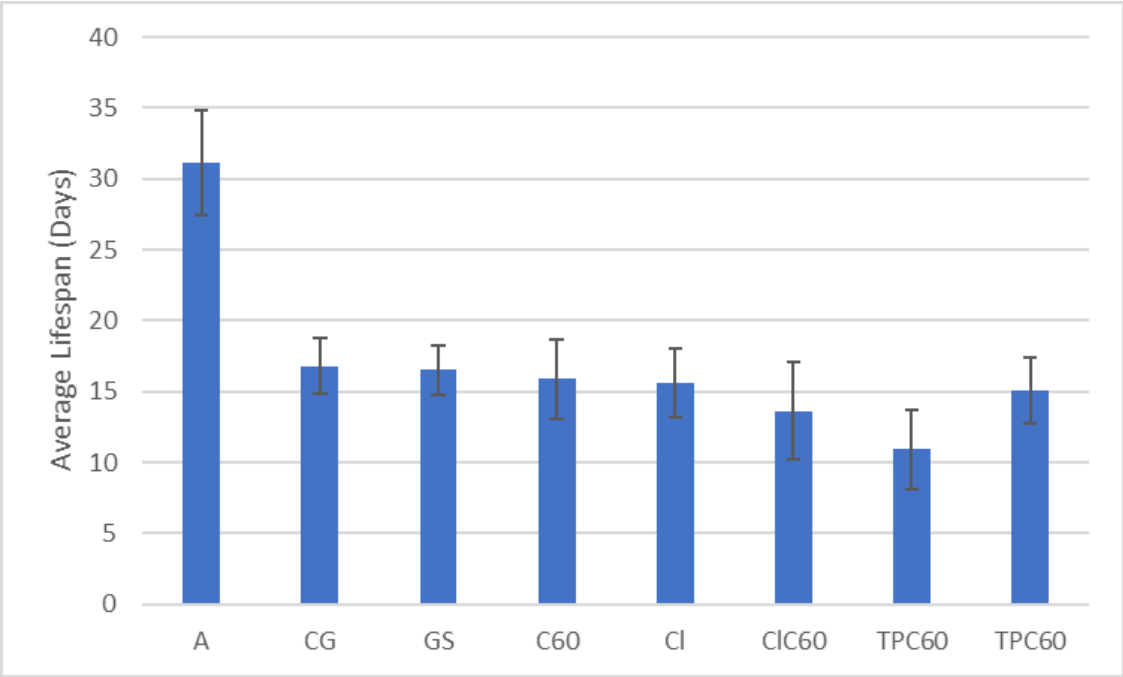

Figure 6. Preliminary one-way analysis of variance of OPV treatment and control *D. pulex* lifespan (days) results performed in the JMP statistical software. Two post-hoc tests were used to compare the means (each pair student's t and all pairs Tukey-Kramer).

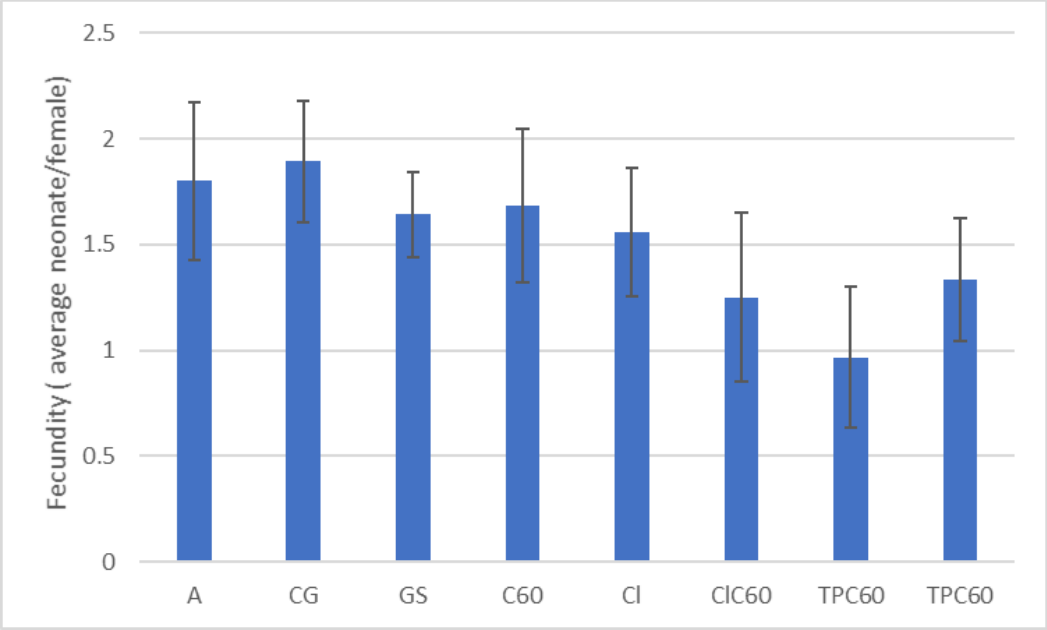

Figure 7. Preliminary one-way analysis of variance of OPV treatment and control *D. pulex* fecundity (average neonates/female) performed in the JMP statistical software. Two post-hoc tests were used to compare the means (each pair student's t and all pairs Tukey-Kramer). There was no significant difference among any of the treatments.

Because of the low concentration of C60 in the OPV samples, a visual darkening of the carapace and gut was not observed for C60 (dark brown) (Figure 8). However, the gut of the *D. pulex* TPFB dye treatment was a blue shade after exposure (Figure 9).

Figure 8. C60-exposed D. pulex after OPV cell weathering. Unlike the solubilized material studies, the carapace of the D. pulex does not show a visual darkening that could lead to predation impacts, which could be as a result of the low concentration of C60 in the cell.

Figure 9. TPFB dye-exposed *D. pulex* demonstrating the visual impact of the dye on the *D.pulex*, a blue shaded intestine.

Predation Experiment Results

L. macrochirus consumed *D. pulex* in the presence of their regular food in eight of the 35 trials; the low motivation to feed is consistent with stress observed during other feeding experiments (Schreck et al. 1997). While 23% of *L. macrochirus* involved in the trials consumed the fullerene-exposed *D. pulex*, only 11% of bluegills consumed control *D. pulex*. The fullerene-exposed *D. pulex* were consistently selected first and more quickly than unexposed daphniids (Figure 10A). A weighted rank order of consumption analysis indicated that fullerene-exposed *D. pulex* were consumed 65% faster than the controls. The effect of the darker carapace, due to material agglomeration verified by microscopy, on predation was apparent: significantly more exposed *D. pulex* were consumed (Figure 10B; $t = -1.68$, $p = 0.008$).

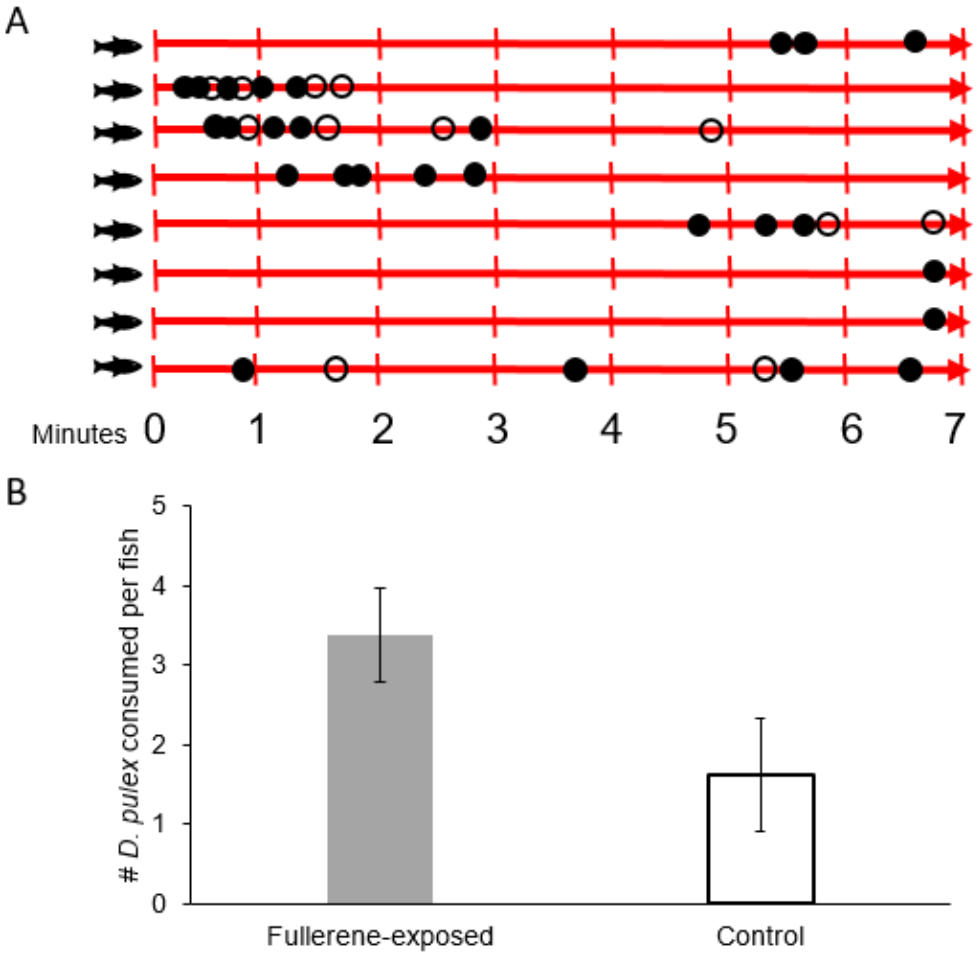

Figure 10. A) Timeline of *L. macrochirus* feeding for the eight successful trials. Each line represents a seven-minute time period over which the fish was offered *D. pulex*. Filled circles are fullerene exposed; open circles are controls B) Average fullerene-exposed (grey) and control (clear) *D. pulex* consumed per fish.

DISCUSSION

The potential for unintended consequences from ENM release must be proactively evaluated to inform the design and adoption of these emerging materials. Many ENM toxicity studies describe the potential for impacts beyond mortality, emphasizing the need for the comprehensive testing of other endpoints. While guidelines have been created for the safe handling of ENMs (OSHA 2013), most are based on conventional chemical substances and do not consider the transformations, surface chemistry, and structure unique to ENMs. As results of this study

demonstrate, varying forms and functionalization of fullerene can yield significant differences in the overall fitness of *Daphnia* spp., highlighting the importance of risk assessment and ecotoxicity assays accounting for various ENM functionalization, size, shape, purity, and other unique properties (Som et al. 2010). Current risk assessment approaches (primarily acute ecotoxicity testing) are major bottlenecks in understanding holistic, system-level impacts of emerging materials such as nanomaterials. Long-term effects at more environmentally relevant concentrations, as well as the potential for indirect impacts on ecosystem-level effects, cannot be predicted from acute studies alone.

Our results for C60 acute and chronic toxicity align with past studies where C60 was not found to be significantly toxic at environmentally relevant concentrations (Pakarinen et al. 2013). However, acute and chronic impacts were observed here for forms of fullerenes that are potentially more relevant to realistic integration of these materials in technologies like organic photovoltaics (Anctil et al. 2011). For example, C70, which can provide up to a 30% better energy efficiency performance in solar applications than C60 (Anctil et al. 2011), showed increased acute mortality in both *D. magna* and *D. pulex* at environmentally relevant concentrations. There are also impacts on fecundity and lifespan as demonstrated in chronic testing. For instance, chronic exposure to PCBM at the pre-egg stage could have implications for the reproductive cycle, and population growth and dynamics. At the egg-stage, exposure to C70 caused a decrease in *D. pulex* fecundity compared to C60 and PCBM, suggesting that populations may vary across different types of fullerene exposures, underscoring the need to characterize the associated variability in toxicity impacts.

The toxicity results observed can be interpreted considering physical and chemical characteristics of the materials. Empirical characterization demonstrated that all three fullerenes have a negative surface charge, are stable at lower temperatures, and are considered weak aggregates, which was also observed by rapid settling after material stirring ceased. In deionized water, C60 forms the most stable suspension of all three fullerenes. However, in SFW, the matrix most representative of the natural environment, C70 has the most negative zeta potential, suggesting that it is the most stable in the SFW medium, which may lead to a greater probability of C70 exposure to water column organisms. Further, the greatest lethality was associated with C70, which is the largest aggregate and may cause gut blockage if ingested by *Daphnia* species (in *D. pulex*, which are smaller than *D. magna*, the midgut cells are about 30 microns in height; Schultz and Kennedy 1976). The *D. pulex* shown in Figure 2C ingested C70 and did not clear it within the experimental duration, potentially due to blockage of the digestive tract. In the functionalized form (PCBM), the methyl ester functional group has surface properties known to increase adsorption to biological surfaces (Salciccioli et al. 2012), which is consistent with the observed material agglomeration on the outside of the organism's carapace (Figure 2D). In fact, in cases when the fullerene material aggregates reacted with the exoskeleton, immobilization was observed in both *Daphnia* species, a result observed more frequently with increasing fullerene concentration.

Additionally, our results demonstrate the importance of capturing sublethal effects across multiple species and trophic levels due to the observed physical changes due to fullerene exposure, namely carapace darkening, enhanced heart rate, and gut blockage. These findings are consistent with past C60 and C70 studies where fullerene aggregates were found in the *D. magna* gut after chronic exposure, decreasing fecundity and causing stress from the inability to

feed (Seda et al. 2012). However, because gallic acid was used to stabilize the C70, toxicity results may not be attributable to C70 alone. Nonetheless, the accumulation of fullerenes in the daphniid's gut could lead to entry into other tissues through the gut and cause oxidative stress as found with other ENMs like nano-silver (Pakrashi et al. 2017). The increased heart rate observed at 24-h for all fullerenes suggests a physiological stress response (Figure 5), that for some individuals was followed by substantially reduced heart rate at 48-h, and closely by death. While the results were significant for all three fullerenes at 24-h, a greater number of individuals succumbed more rapidly in the PCBM treatment than in the C60 or C70 treatments. This could be explained by the characteristics of PCBM, where due to the surface properties and size of the material, PCBM could adsorb to the*Daphnia* producing an earlier fatal response after exposure. This result demonstrates that fullerenes could have both a physiological and physical impact on *Daphnia* species, which could lead to population-level effects (Lovern et al. 2007).

In addition to lethal and sublethal implications of fullerene exposure for *Daphnia* spp., the darkening of the carapace and gut also have potential cascading ecological impacts. The clear preference of the visual predator *L. macrochirus* for the darker *D. pulex* suggests an indirect ecological effect of fullerene on daphniid mortality (Branstrator and Holl 2000). Selective predation enhances mortality risks associated with fullerene exposure. In an actual freshwater environment, the interaction between predator and prey could differ depending on the location, season, legacy contaminants, and other factors (Chamberlain et al. 2014). However, this experiment clearly highlights the need for broadening impact assessment studies to include ecological scales.

To provide insights about how ENMs such as fullerenes interact with and influence the health of ecosystems, material assessment approaches must incorporate more comprehensive endpoints for

long-term, multispecies, multi-generation, and trophic level studies. The results reported herein highlight a clear need and opportunity to update risk assessment of emerging materials. Changes in the form of fullerene can increase acute and chronic impacts with this study showing C70 causing significant toxicity at the acute level. The alteration of the daphnia carapace color and resulting increase in predation risk informs the potential for cascading effects such as reduced biodiversity from species loss and the potential for bioaccumulation up the food chain. Further, there were no significant differences observed for the different OPV treatments, but additional research is needed to explore the potential impacts of use-phase exposure in clean energy technologies. With this expanded perspective on fullerenes, a more informed approach to research, decision-making, and policy can be used to help reduce negative economic, environmental, and human health implications that may result from the increasing use of emerging materials.

ENMs may present an opportunity to mitigate many existing pollution problems (Zhang and Fang 2010), and holistic analysis may ultimately find that these benefits outweigh those observed with ecotoxicity as assayed here. For example, if C70 or PCBM are integrated into solar cells, the efficiency of these renewable energy systems is expected to increase (Brabec et al. 2010), leading to potential displacement of electricity generated from coal and natural gas. Avoiding fossil fuel combustion itself has significant benefit to ecosystem health, through reduction in release of toxic heavy metals (mercury, arsenic), compounds that affect human health (SO_2, CO), and waste streams (coal ash) containing heavy metals and polycyclic aromatic hydrocarbons (Holdren et al. 2000).

However, the true costs and benefits of ENM integration cannot be fully assessed without concurrent advances in risk assessment methods and empirical studies that capture the true

variability in ENM form, ecotoxicity, and ecological impacts. Many existing risk assessment models typically treat ENM production and use as spatially implicit, without considering the specific geographic location of potential emissions. By not considering geographical context, ENM accumulation or ecotoxicity impacts may be underestimated if occurring in ecologically sensitive areas. Therefore, in the next chapter, this knowledge gap is addressed by introducing an integrated predictive model that forecasts likely ENM manufacturing locations and potential emission to critical environmental and freshwater ecosystems. The potential concentrations of these emissions are then compared to measured ecotoxicity results, like the studies in this chapter, to inform the magnitude of risk.

CHAPTER 4: SPATIAL PERSPECTIVE INFORMS POTENTIAL FOR NANOMATERIAL ACCUMULATION RISKS[2]

Introduction

With an estimated value of $11.8 billion by 2025 (Mordor Intelligence, 2016), the ENM global market is growing rapidly. With increases in their production and use, the likelihood of environmental exposure and potential for environmental risks also increases, as demonstrated by the potential for toxicity and cascading ecological impacts of fullerenes in Chapter 3. After better understanding the risk of toxicity if fullerenes were to enter the environment, the next steps in this research effort were to better understand 1) where ENMs could potentially be released during their life cycle, 2) what potential concentrations could accumulate in the environment over an extended period of time, and 3) how these concentrations relate to measured toxicity results.

ENMs can enter environmental compartments (e.g. air, water, soil, sediment) at various stages of their life cycle, including material synthesis, use, and end-of-life (Köhler et al. 2008, Klaine et al. 2008, Som et al. 2010). These emissions may result in direct aquatic ecotoxicity and trophic ecosystem impacts (Farré et al. 2009, Von der Kammer et al. 2012, Juganson et al. 2015,) as well as indirect ecotoxicity due to upstream energy and material consumption (Anctil et al. 2011, Eckelman et al. 2012). To better understand these risks, research must consider the extent to which these materials will be manufactured, the location and volume of future emissions, and the ultimate toxicity and potential for ecosystem level impacts. Because of the need for a systems perspective for ENM assessment (Babbitt and Moore 2018), Industrial Ecology methods are well-equipped to assess the benefits and risks of ENMs. Tools such as material flow analysis

[2] This chapter is adapted from a publication submitted to the Journal of Industrial Ecology. To avoid repetitive citations, a blanket reference to the original manuscript is provided here: (Moore et al. 2019b)

(MFA), life cycle assessment (LCA), multi-criteria decision analysis (MCDA), and environmental risk assessment (ERA), have been adopted to estimate ENM life cycle impacts and determine the ultimate risk of release. For instance, MFA has been applied to estimate ENM concentrations in environmental and technical compartments (Gottschalk and Nowack, 2011, Smita et al., 2012, Ging et al., 2014, Yang and Westerhoff, 2014, Song et al., 2017). LCA has been utilized to quantify the cumulative energy and ecotoxicity impacts ENMs including fullerenes, nano-silver, and carbon nanotubes (Anctil et al., 2011, Eckelman et al., 2012, Pourzahedi and Eckelman 2015, Hicks et al., 2017), demonstrating the need to account for upstream emissions from embodied energy as well as direct impacts such as release in aquatic ecosystems. Further, MCDA and ERA studies (Linkov et al., 2007, Hassellöv et al., 2008, Coll et al., 2015) have provided insights for ENM characterization and have highlighted the importance of accounting for variability and uncertainty of potential concentrations and experimental data. Much of the ENM assessment literature has applied average values to capture national and global impacts. While these data choices are necessary due to lack of more disaggregated information, they may lead to three key challenges: 1) limits to our understanding of risks for a specific area, 2) potential underestimates of life cycle release risks, and 3) lack of modeling that considers accumulation within a spatial and time boundary. Spatial tools have helped to advance various disciplines including green infrastructure design (Snäll et al. 2015), urban planning (Daniel et al. 2018), biofuels (Sharma et al. 2017), drug delivery (Winner et al. 2016), and yet have been less frequently used in Industrial Ecology (Wu et al. 2017). Broader literature has acknowledged the utility of joining traditional risk assessment tools with geospatial modeling (Guinee et al. 2011, Xu et al. 2015), as spatial tools can account for regional differences in biophysical land characteristics (Geyer et al. 2010), industrial production factors, and environmental flows (Mutel

et al. 2011). Further, emissions of ENMs can vary during different life stages, particularly at end-of-life. National or global values are too coarse of scale for potential differences in wastewater and solid waste treatment (Gottschalk et al. 2015). Regional and local analyses have been proposed (Mutel et al. 2011) where impact assessment methods are combined with life cycle inventory data to better inform LCA uncertainty at the regional and/or local level (Mutel et al. 2011). In addition, ENM time-dependent studies have been proposed that can help capture accumulation over time, though many existing analyses assume a static time scale (Sun et al. 2016). However, these concepts have not yet been widely applied to ENM assessments.

The few studies that have investigated spatial dimensions of ENMs demonstrate the utility of calculating material flows with a spatial perspective. For example, depending on the environment, there may be variable concentrations due to local dilution factors (Gottschalk et al. 2011), climate variations (Parker and Keller 2019), or a range of ENM residence times (Keller et al. 2013), which are critical factors for determining ENM exposure risk to ecosystems. In addition to physical differences among different areas, demographic factors (e.g. education level, age, and population density) can play a role in how ENMs may be released from products for a given area (Keller and Lazareva 2013), ultimately impacting the location and magnitude of potential ENM emissions. For instance, different age and education levels may influence product or technology adoption as demonstrated with electric vehicle adoption in the United States (Li et al. 2017). ENMs can accumulate in sediment and other environmental sinks over time (Sun et al. 2016) as well as in ecological organisms such as multi-walled carbon nanotubes in Zebrafish (Maes et al. 2014) and copper-based ENMs in earthworms (Tatsi et al. 2018). Regional ENM studies highlight the need to question whether current ENM emission assessment methods are able to accurately predict differences over space and time. Therefore, to address

these spatio-temporal ENM emission knowledge gaps, this analysis will contribute to the Industrial Ecology and ENM literature through the development of an integrated modeling tool that predicts future ENM production locations, assesses spatial variation in ENM concentrations, and estimates ecological risks for defined geographic locations. We also discuss how results can inform future ENM and/or other emerging contaminant emission modeling, use, regulation and policy for various regions.

Materials and Methods

2.1 Overview of Integrated Risk Assessment Model

The innovative nature of ENMs necessitates an innovative approach and a complete systems perspective. The modeling framework used here (Figure 1) is demonstrated using four case study ENMs (Section 2.2) likely to be integrated in lithium-ion batteries (LIBs), which represent a growing technology sector within the clean energy landscape. First, in the predictive capacity of the geographic information system (GIS) software, ArcGIS Pro (Skilodimou et al. 2019) was used to estimate future ENM manufacturing locations for a case study region (Section 2.3). These locations, and their proximity to critical environmental areas and water bodies, are then used to assess potential emission patterns, environmental concentrations, and ecological risks. Next, likely manufacturing locations are predicted, assuming that ENM-use will continue to grow according to best available estimates. Mass flow modeling calculates potential environmental accumulation using known release rates, subsequently informing spatial concentrations in a critical environmental area over several years (Section 2.4). When the time scale is considered, accumulation over a single year may have negligible effects. Over several years, however, the accumulation of ENMs could pose ecological risks (Geissen et al. 2015). Finally, these potential spatial concentrations are compared to established lethal dose

concentrations for relevant model organisms as one example risk metric (Section 2.5). Using readily available data, this framework can also be applied to other ENMs or emerging contaminants, manufacturing locations, and/or risk endpoints to inform spatially explicit risks as emerging materials enter the market.

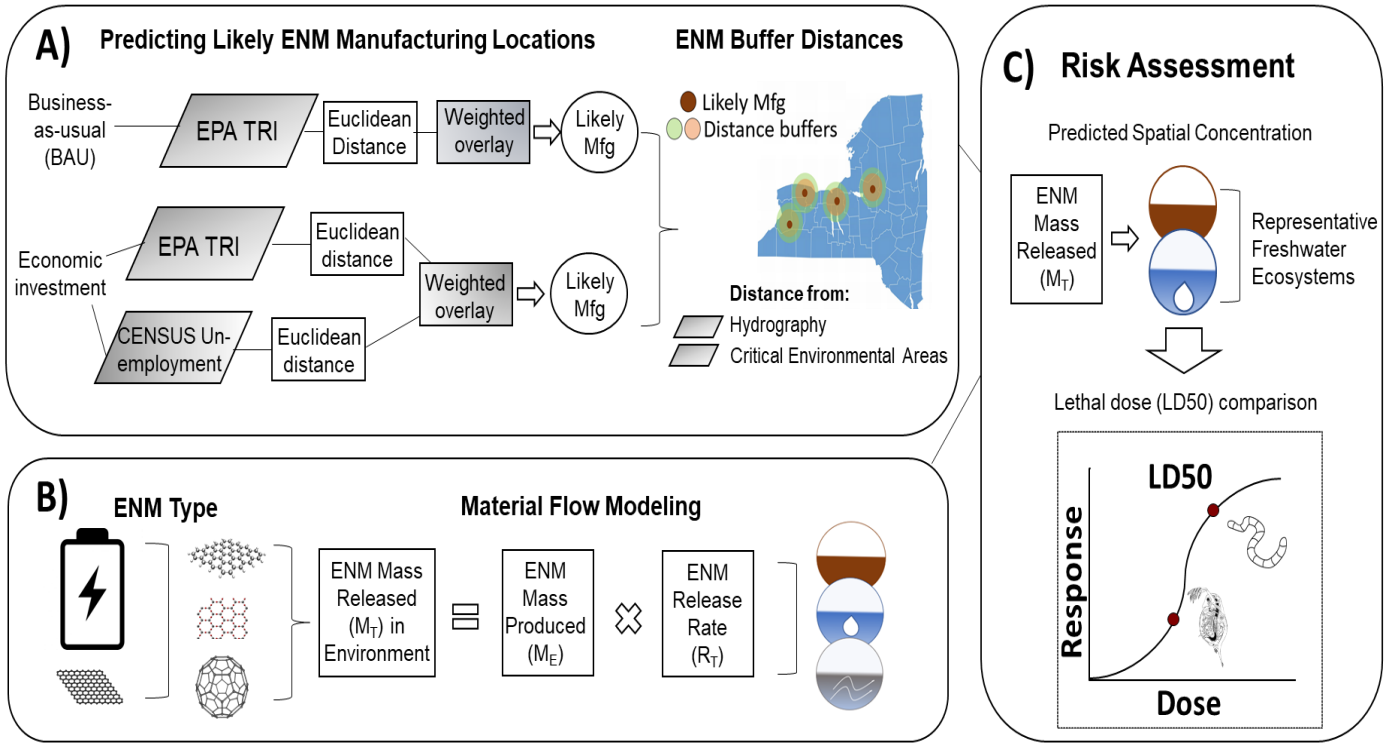

Figure 1. Spatially Explicit ENM Risk Model: Overview of the modeling framework utilized to estimate spatial risk of ENM emissions. A) Likely ENM manufacturing locations for our case study area., B) Mass flow calculations used to determine ENM emissions into environmental compartments, and C) Spatial risk assessment of potential concentrations compared to established lethal concentration values for relevant model organisms.

2.2 Case Study: ENMs for Batteries

ENMs have the potential to improve the performance of clean energy technologies, demonstrated by the increasing research and application of ENMs in lithium-ion batteries (LIBs) (Shen et al. 2017, Liu et al. 2017, Xu et al. 2018, Moore et al. 2018). As battery price falls and the demand for electric vehicle LIBs grows (Olivetti et al. 2018), it is likely that ENM demand will also rise given their promise for improving LIB performance. Further, the incumbent material for LIB

anodes (negative electrodes) is graphite, which may face increasing supply risks (Olivetti et al. 2018), leading to greater interest in ENM substitutes. Four ENM anode materials were chosen based on the frequency of their appearance in the LIB literature and the degree to which they would represent varying levels of environmental risks.

Graphene Touted as a "wonder material" (Kaplan and Woloschyn 2014), graphene is capable of advancing lithium-ion battery anode capacity, lifespan, and efficiency (Zhou et al. 2017, Raccichini et al. 2017, Ababtain et al. 2018, Zhamu et al. 2018). Graphene is not considered a new chemical substance in the Environmental Protection Agency (EPA) Toxic Substance Control Act (TSCA) (EPA TSCA Inventory, 2018) and is instead regulated as graphite, despite differences in properties, structure, and fabrication methods.

Silicon/Single-walled carbon nanotube (Si/SWNT) Another high-performance LIB anode chemistry combines Si and SWNT to increase the energy density of the cell and improve the capacity retention and cycling stability (Lin et al. 2014, Lee et al. 2016, Gattu et al. 2017). Both Si and SWNT are currently regulated under TSCA (EPA TSCA Inventory, 2018), yet in a worst-case scenario, could be accidentally released during production (Garvey et al. 2018).

SiO2 In addition to bulk Si anode chemistries, nano-SiO2 is an anode additive explored in the LIB literature. SiO2 enables increased long-term cycling stability, improved capacity and cyclability, and a higher Coulombic efficiency (Liu et al. 2014, Zhou et al. 2015, Jiang et al. 2018). Similar to graphene, nano-SiO2 is not considered a new chemical substance and is regulated under TSCA as Si (EPA TSCA Inventory, 2018). This chemistry was chosen to provide a risk comparison between Si and nano-SiO2 if released during manufacturing.

Fullerene (C60) The final high-performance anode chemistry modeled is C60, capable of improving the capacity retention, discharge capacity, and current density of a LIB cell (Hudaya

et al. 2015, Enggar et al. 2018). While fullerene is currently regulated under TSCA, this chemistry was added as a risk comparison between the varying carbonaceous ENMs.

In this study, we compare the four case study materials by assuming that the likely ENM location would produce only one type of anode, which may contain a single ENM as an additive to graphite or multiple ENMs combined as a graphite replacement (Figure 2). This approach allows for comparison of risks (e.g. toxicity and accumulation) relative to the respective material sets required to achieve the same functional performance in a LIB cell.

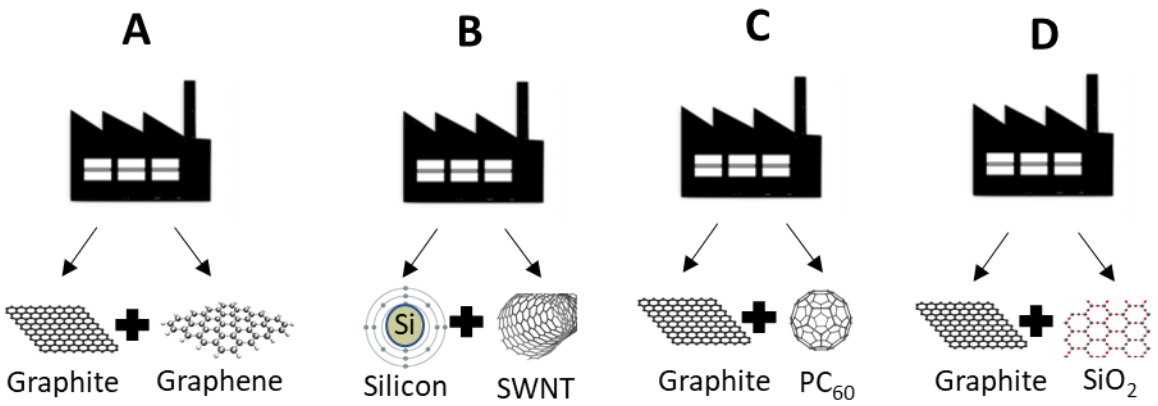

Figure 2. A comparison of potential ENM emissions is performed by assuming the ENM factory is producing a single type of anode on location (A or B or C or D), rather than all the materials at once, to calculate the potential spatial concentrations and compare the spatial risks across materials.

2.1 Targeted Study Area: Post-Rust Belt New York

As the ENM market continues to grow, it is likely that new production locations will open in the United States to meet market demand. One potential scenario is that this production activity takes place in areas with historical precedent for manufacturing (Hobor 2016). In fact, a trend towards revitalizing U.S. 'Rust Belt' cities has seen conversion of traditional manufacturing capability into new businesses and manufacturing (Tisher 2013, Wilson and Wouters 2016, Hobor 2016). The decline of US manufacturing over the past 75 years (High 2003) has led to brown fields, empty lots, and abandoned factories (Bjelland 2004, Schilling and Logan 2008),

which offer potential for redevelopment and economic revitalization. Due to the growing investment in lakeside post-rust belt cities (Schilling and Logan 2008), it is highly probable that many of these regions could revitalize manufacturing locations for new high-tech industries (e.g. LIBs, ENMs). Central and Western Upstate New York, northwest of the New York metropolitan area, was chosen because of the presence of several post-rust belt cities, existing chemical manufacturing industries, and the vast available land cover (Goe et al. 2015).

2.3 Data Collection and Geospatial Modeling

Data Collection and Transformation

To determine ENM manufacturing release locations, we first assume a business-as-usual (BAU) scenario (as shown in Figure 1, part A). As described in Section 2.2, it is likely that future manufacturing locations (e.g. ENM facilities) would be located at or near existing manufacturing locations of the same type (e.g. chemical production) for location revitalization or new construction. Thus, manufacturing location addresses were geocoded in ArcGIS Pro from the 2016 Environmental Protection Agency (EPA) Toxic Release Inventory (TRI) dataset (Appendix C, Table S1), which reports toxic chemical locations, volumes, and disposal practices for various U.S. industrial locations. To consider regions that may be prioritized for economic development, a second scenario with the objective of economic investment is also assessed, assuming that a state government is likely to invest in areas with high unemployment rates and areas historically known to have a skilled workforce for manufacturing. U.S. Census unemployment percentage data (Table S1) were collected and joined to Upstate NY county locations to determine the highest areas of unemployment for this scenario.

The ArcGIS Pro Model Builder feature and Spatial Analyst toolset was used to calculate the Euclidean distance, the straight-line distance between any two points. In the model, this distance is calculated from the center of the input data (e.g. EPA TRI and/or unemployment data) to the

center of predicted outputs (likely locations). For each predicted output, the distance to the input data is then minimized to optimally predict the location of future manufacturing locations within a source distance range of 40-km (Quik et al. 2015) based on the scenario objective (e.g. close to existing manufacturing and/or close to high unemployment areas). The range of 40-km was considered rather than a single data point to account for the uncertainty in the estimate. Then, inputs are transformed into a single output of likely locations of a manufacturing facility using the Weighted Overlay tool, which combines data inputs on a common measurement scale (ESRI 2018) and assigns weights to rank the inputs. In the BAU scenario, we assigned a 100% weighting to chemical manufacturing locations. For the economic investment scenario, we assumed equal levels of importance for both parameters: 50% weighting to chemical manufacturing locations and 50% weighting to high areas of unemployment. However, changes in weightings did not impact overall results. These location assumptions were verified by downloading and geocoding manufacturing locations listed for sale in Upstate NY from LoopNet Commercial Real Estate, one of the largest commercial real estate online marketplaces with over 500,000 listings (CoStar Group, Inc., 2018). The locations of facilities for sale were compared to existing chemical manufacturing operations and to the model-generated facility siting predictions for both scenarios. In all cases, a majority of the likely locations were within a one-mile distance of actual facilities, confirming that existing manufacturing plants could be purchased and revitalized for new industries in these areas (Figure S5).

Buffer Analysis Spatial Risk Assessment

To characterize the spatial risk of ENM release, the Buffer Analysis method in ArcGIS Pro was used to calculate the area that is likely to be affected of the likely manufacturing locations. A 2-km and 5-km buffer distance was chosen based on findings from a previous study, where Ag and

CeO_2 ENM concentrations were found close to the source (Quik et al. 2015). Data from the National Hydrography Dataset (NHD), the New York Department of Environmental Conservation (DEC) Critical Environmental Area Dataset, and the United States Geological Survey (USGS) National Land Cover Dataset (NLCD) were collected to show the proximity of potential manufacturing locations to freshwater ecosystems and existing vulnerable ecosystems (Table S2). Next, for three case study watersheds, 10-m (10-m x 10-m) digital elevation model (DEM) (USGS) data were collected and used as inputs for the ArcGIS Spatial Analyst Tool, Flow Direction, to assess where pollutants could flow if released into the watershed and if ENM emissions could potentially interact with existing vulnerable ecosystems (Baun et al. 2008).

2.4 Mass Flow Modeling

To determine the magnitude of ENM emissions from likely locations, the production amount was calculated for each case study material. Estimates were based on a known U.S. electric vehicle manufacturer's graphite plant, which produces 35,200 tons of spherical graphite for LIB anodes (USGS 2018). The ENMs proposed as anode additives were modeled as being produced in proportions relative to graphite that were determined from literature and a baseline anode (Table S3) modeled in the Argonne National Lab BatPac model (Nelson et al. 2017). Potential environmental emissions from such a facility were estimated (Equation 1), such that M_P is the total ENM mass produced at the facility (mg), M_B is the ENM mass (mg) integrated in battery production, M_R is the total mass released (mg) into different compartments according to $M_{C,i}$, where i includes releases to air (M_A), wastewater (M_{WW}), and landfill (M_L). R_T is the low or high total release rate (%), and $R_{C,i}$ is the low or high specific compartment release rate (%). A bounded uniform distribution of data (low and high) was chosen to account for the uncertainty in the underlying data. This range was assumed since there is an equal probability of the data being within the range of the lowest value (realistic scenario) and the highest value (worst-case scenario).

$$M_{C,i} = (M_P - M_B) * R_{C,i}$$ Equation 1.

We assumed all ENMs in this study not captured for battery production (M_B) were either released into a landfill (M_L) or into the environment (M_A and M_{WW}) (Figure 3), with mass percentage estimates applied from the literature (Table 1). In natural environments, ENMs could go through physical or chemical processes (e.g. dispersion, agglomeration, oxidation, dissolution, sedimentation) depending on their unique properties, the environmental conditions, and weather changes (Kidd and Westerhoff 2018). For example, some ENMs (e.g. SWNT) have poor solubility (O'Connell et al. 2001), and therefore, it is likely that they will partition into the sediment after release into freshwater. Due to lack of partitioning data from wastewater sludge and effluent to freshwater and sediment for all case study materials, we performed a worst-case scenario analysis. In the first scenario, we assumed that the percentage of the ENM mass not released to the wastewater sludge (M_S) after wastewater treatment was released completely into the effluent (M_E) and remained in the water column. Alternatively, in the second scenario, we assume 100% of the ENMs released into the effluent discharge into the sediment (M_{sd}). While we acknowledge that the ENMs will likely transform (Keller et al. 2013), material specific transformation was not addressed in this study.

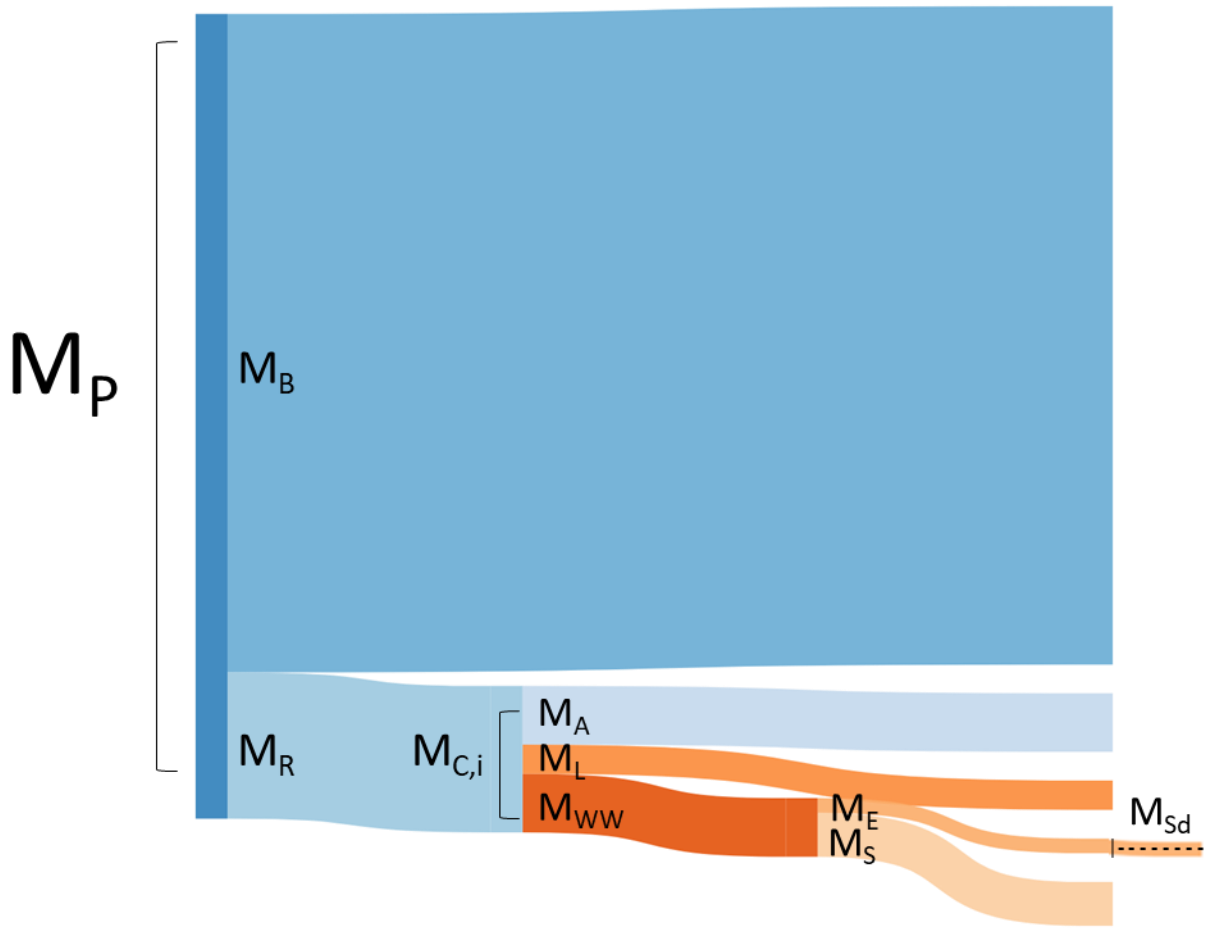

Figure 3. Mass flows from ENM total production at a single manufacturing location (M_P) to the battery application (M_B). M_R is the total mass estimated to be released into compartments, $M_{C,\,i.}$ where M_A is the air, M_L is the landfill, M_{WW} is wastewater, M_E is effluent, M_S is the sludge, and M_{sd} is the sediment compartment

Table 1. ENM mass percentage estimates used in the study to calculate the total potential ENM emissions during manufacturing. From the estimated total, potential ENM emissions were estimated for specific environmental compartments: air, landfill, and wastewater. The emissions from waste water into the water column (effluent) and sediment were also estimated.

ENM Mass Percentage Estimates	**Low (%)**	**High (%)**
% total release (R_T)*	0.1	2
% of total release to air (R_A)*	10	40
% of total release to landfill (R_L)*	80	20
% of total release to wastewater (R_w)*	10	40
% from wastewater to residue (R_S)*	97	75
% from wastewater into effluent (R_E)* or sediment (R_{Sd})	3	25
*Keller et al. 2013		

To determine the amount of ENM that may accumulate in a freshwater system over time, a median annual production growth of 5% was assumed (Giese et al. 2018) using Equation 2, where $M_{\tau,t}$ is the total mass over time (mg/year), M is the total mass released or the mass for a given compartment (mg) for a given year (i), and Y is accumulation time (years), up to 50 years in this scenario.

$$M_{\tau,t} = \sum_{i=1}^{Y} M_{i-1} \ * (1 + 0.05) \qquad \text{Equation 2.}$$

The potential spatial concentrations for freshwater ecosystem ENM emissions were calculated (Equations 6-7), where $C_{w,t}$ is the low or high ENM concentration in the water column from effluent release (mg/L) over time, M_E is the low or high ENM mass released into the water column (mg), and V is the freshwater volume for a given freshwater body (L).

$$C_{w,t} = \frac{M_E}{V} \qquad \text{Equation 3.}$$

The ENM sediment concentration was calculated (Equation 4) for the top 3 cm of the sediment layer (Gottschalk et al. 2010), where $C_{S,t}$ is the low or high ENM concentration in the sediment over time (mg/kg), M_S is the low or high ENM mass released into the sediment (mg), S_w is the surface area of the water body (m^2), , and ρ is the dry density of the sediment (kg/m^3) (Tables S12, S15, S18).

$$C_{S,t} = \frac{M_S}{S_w * 0.03} / \rho \qquad \text{Equation 4.}$$

2.5 Ecotoxicity Risk Assessment

The projected aqueous and sediment concentrations for all case study materials were compared to literature reports of concentrations at which toxicity to ecologically relevant model organisms have been observed (using the LD50, or dose that causes the death of 50% of a population) (Table S5). *Daphnia magna* are water column model organisms commonly used in ecotoxicity experiments due to their significant role in the freshwater ecosystem food chain (Zöllner et al. 2003) As filter feeders, *D. magna* have a high likelihood of ingesting pollutants in the water because they filter 16.6 mL/h of water on average (Lovern and Klaper 2006) and are considered bioindicator organisms. Thus, *D. magna* LD50 values are included in this model and compared to potential environmental concentrations of ENMs to provide insight for potential ENM exposure impacts in freshwater ecosystems. The LD50 values used for comparison were the lowest concentrations shown to be the LD50 in the literature, to assess the worst possible impacts of accumulation. While LD50 values may have shortcomings (e.g. variability and uncertainty) (Rowan 1983), this metric is still widely used in the ecotoxicity community and can provide preliminary risk assessment until more data are available. Because of the complex environmental transformations of ENMs (Dale et al. 2015), there are not enough ecotoxicity data to fully characterize the risk of emission to sediments for all case study materials. However, release to

the sediment is the most realistic exposure due to the settling properties of many of the ENMs. As an example, the risk of SWNT sediment release is considered for two sediment dwelling model organisms, *Lumbriculus variegatus* and *Hyallela Azteca* (Table S11), organisms regularly used as bioindicators of sediment health (Petersen et al. 2008, Wallis et al. 2014).

3.0 Results and Discussion

The results presented here demonstrate the added insight gained when release estimates from the manufacturing phase of the ENM life cycle are combined with spatially-explicit siting and ecosystem data. First, the potential spatial distributions of ENM manufacturing locations are presented. From these likely locations, we demonstrate the proximity of the manufacturing locations to water bodies and critical environmental areas. Next, potential environmental concentrations are calculated for three example ENM locations near significant water bodies, including a location near one of the Laurentian Great Lakes. While these examples are specific to Upstate NY, the three water bodies may be considered representative of temperate water bodies globally. The spatially-explicit concentrations are then compared to the reported concentrations at which case study materials create ecotoxicity impacts, illustrating the utility of spatial models to inform ENM risk analysis.

3.1 Likely ENM Manufacturing Locations

As ENM demand and adoption in LIBs and other applications increases, manufacturing of ENMs will also increase worldwide. The predictive capacity of this geospatial tool can determine the likely spatial distribution of future ENM manufacturing locations and thus identify potential release locations. This study identified likely manufacturing locations under two scenarios. The first objective scenario assessed the revitalization of existing manufacturing locations (BAU) and

the second scenario combined the objectives of revitalization as well as job creation (economic investment). The BAU scenario suggests ENM manufacturers will likely locate in the same locations as past chemical manufacturers (Figure 4A). Assuming Upstate NY will invest in new industries to create jobs, weighted overlay results (Figure 4B) display areas where unemployment co-occurs with the existing chemical manufacturing locations (Figure S1). In areas of high unemployment and existing manufacturing locations, the areas were classified as a "high" likelihood of a revitalized manufacturing location and areas of low unemployment and fewer manufacturing locations were classified as a "low" likelihood.

To validate these likely locations, we compared the results with industrial addresses for sale (Figure S3 and S4), demonstrating a confirmed pattern of areas likely to see new industries and investment in the coming years. For both scenarios, a spatial pattern was observed; the existing and likely locations are typically located near interstate highways (Figure S7). Manufacturing facilities are historically located close to interstate connections in rural areas to reduce transportation costs (Woodward 1992, Forkenbrock and Foster 1996). While shown here for Upstate NY, this method is adaptable for other regions, as the underlying data sources (U.S. EPA TRI database and U.S. Census unemployment data) are available for all U.S. states.

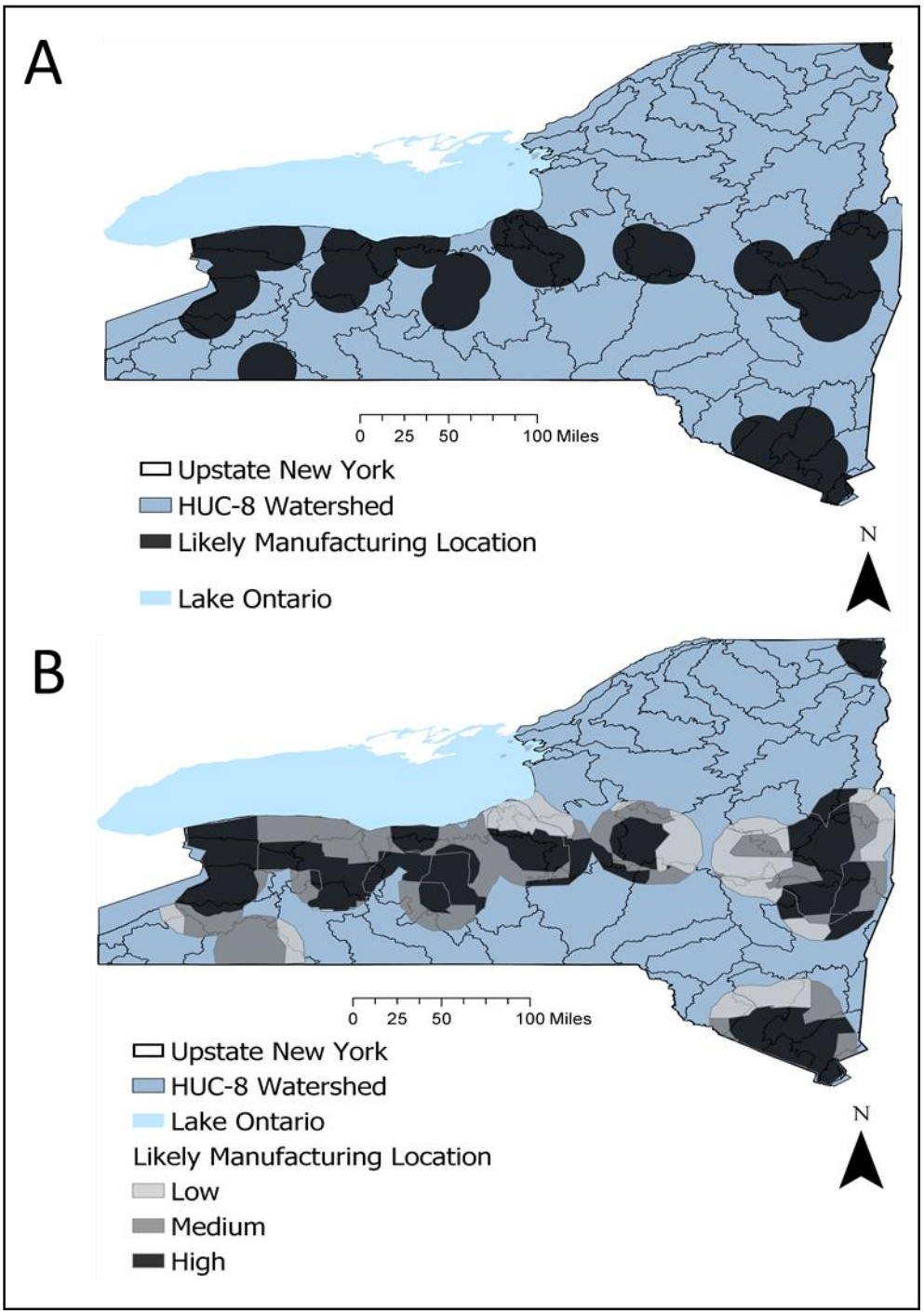

Figure 4. BAU scenario (A) and economic investment scenario (B) for likely ENM manufacturing sites relative to the hydrologic unit (HUC) 8-digit watersheds. In the economic investment scenario, the black areas indicate areas of high unemployment and existing chemical manufacturing locations, predicting potential areas for investment and revitalization and the light gray areas indicate low unemployment and fewer existing manufacturing locations.

3.2 Proximity of Likely ENM Facilities to Sensitive Ecosystems

The spatial distribution of likely ENM manufacturing locations were next layered over spatial data characterizing potentially sensitive ecosystems in the same spatial boundary: water bodies and critical environmental areas defined by New York State Department of Environmental Conservation (NYDEC) in Upstate NY. Results estimate the percentage of surface water and critical environmental areas within these distances of the ENM manufacturing locations. The potential presence of ENM facilities near sensitive ecosystems implies the need to determine the risk of release in these locations.

Buffer Distance	% of Total Hydrography Area	% of Total Critical Envt. Areas
2-km	89%	79%
5-km	90%	80%

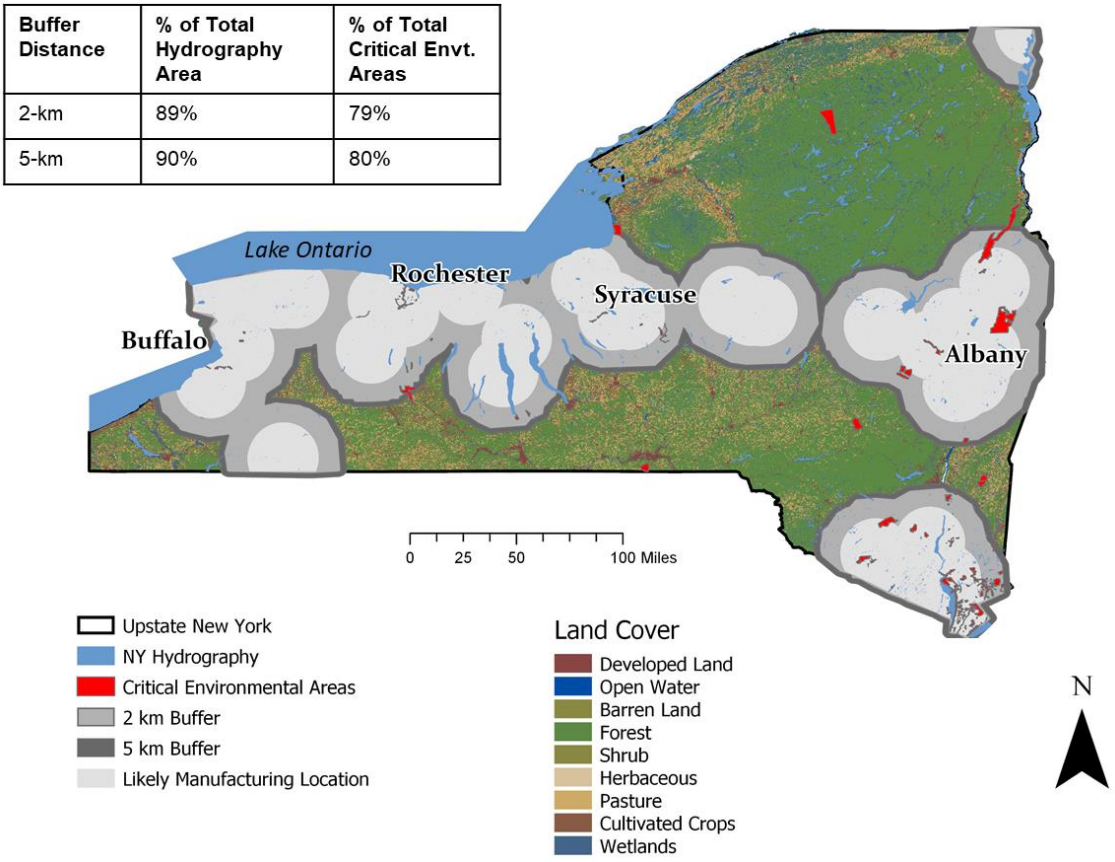

Figure 5. 2-km and 5-km buffer analysis for the BAU ENM location scenario. The buffer analysis allows the calculation of the area and distance of potentially sensitive ecosystems to potential ENM manufacturing locations, where ENMs could be released into the environment.

In addition to calculating the distance to freshwater ecosystems, we can identify the proximity of manufacturing to critical environmental areas. In the BAU scenario, 79% of total area of critical environmental areas in Upstate NY fell within the total buffer area (2-km) and 80% fell within 5-km. Different land characteristics and existing vulnerabilities can influence the overall impact of release. For instance, if ENMs are released into an already polluted area with legacy contaminants or in a threatened habitat (e.g. wetland), the combination of an existing condition and an emerging risk could result in a greater overall environmental impact (Banni et al. 2016). Thus, by using proactive decision tools that can predict potential ENM manufacturing locations, we can inform ENM location siting decisions that reduce potential release risks.

In the BAU scenario, 89% of the total surface water area in Upstate NY are within a 2-km radius buffer (excluding Lake Ontario) and 90% are within a 5-km radius buffer of a potential ENM manufacturing location (excluding Lake Ontario). The results for both the BAU and economic investment scenario were in agreement; a similar trend was observed in the percentage of critical environmental areas and freshwater ecosystems within the buffer distances of the manufacturing facilities (Figure S8). The fate of ENMs during wastewater treatment is still uncertain (Westerhoff et al. 2018). Therefore, knowledge of manufacturing locations with onsite wastewater treatment and their proximity to nearby sensitive ecosystems and watersheds can help inform ENM emission risks and regulations proactively.

3.3 ENM Release Risk Assessment: Upstate NY Lake Examples

To demonstrate the difference in the magnitude of ENM emission risk over space and accumulation time, three lakes near former Upstate NY rust-belt cities were identified based on their proximity to likely ENM manufacturing locations (under the BAU scenario). Additionally, each lake is representative of an ENM emission scenario that could occur in water bodies with

similar attributes across the U.S. For example, one likely manufacturing location is 3.8 miles from Lake Ontario, one of the Laurentian Great Lakes (Figure 6A), the largest surface freshwater system on Earth. This water body is an example of an ENM emission case wherein accidental discharge may ultimately reach a large ecosystem through the watershed. Seneca Lake spans four Upstate NY counties and is 0.1 miles from a likely manufacturing location (Figure 6B). This lake is representative of relatively deep oligotrophic water bodies (> 180 m) with a long residence time (>12 yr) and relatively undeveloped watershed (Michel and Kraemer 1995). The Seneca Lake region is well-known for its agricultural opportunities and recreational fishing as well as a salt mine on the south end of the lake (NY DEC). Finally, Onondaga Lake in Syracuse, NY (Figure 6C) is 0.3 miles from one of the likely ENM manufacturing locations. This lake is representative of water bodies with a short residence time (90-180 days), historical industrial pollution, as well as existing large industrial operations close to the lake shore (Figure S5). (Rowell 1996; Onondaga County 2013).

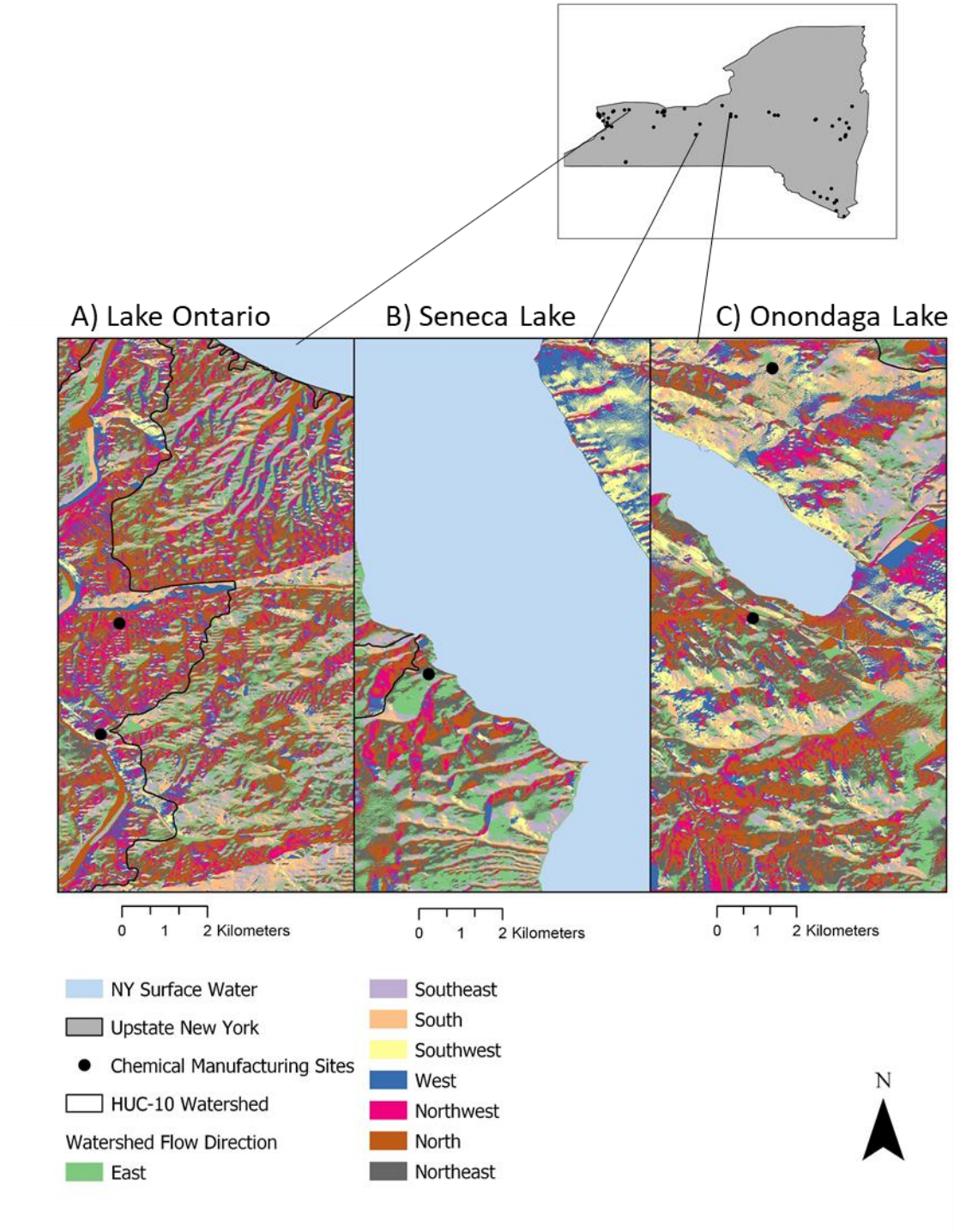

Figure 6. Distance of BAU case study locations (black) to Lake Ontario (A), Seneca Lake (B), and Onondaga Lake (C). The flow direction of water in these locations shows how ENM contaminants could flow through the watershed if accidentally released from one of these locations.

The potential ENM environmental emissions and resultant accumulation were calculated for the water column and sediment (Table S12-20) for Lake Ontario, Seneca Lake, and Onondaga Lake. We assumed that the ENMs were not reactive and therefore did not transform, but rather stayed in the environmental compartments according to the defined scenarios. The potential accumulation was calculated annually for each material, for an accumulation period of 50 years. These levels were compared to concentrations shown to have a toxic impact (LD50) for the water column organism *D. magna*. To address the risk of accumulation in the sediment, LD50 ranges for sediment dwelling organisms were calculated for SWNT. Low and high accumulation results are shown here for two of the most commonly used ENMs in batteries, SWNT (water column and sediment) and SiO2 (water column) for the Lake Onondaga emission scenario (Figure 7). For context, risk associated with accumulation of a well-known pollutant in freshwater ecosystems, methylmercury (EPA ECOTOX 2018) is also displayed. All case study material results for each scenario are included in the Supplemental Information (Figures S9-S13).

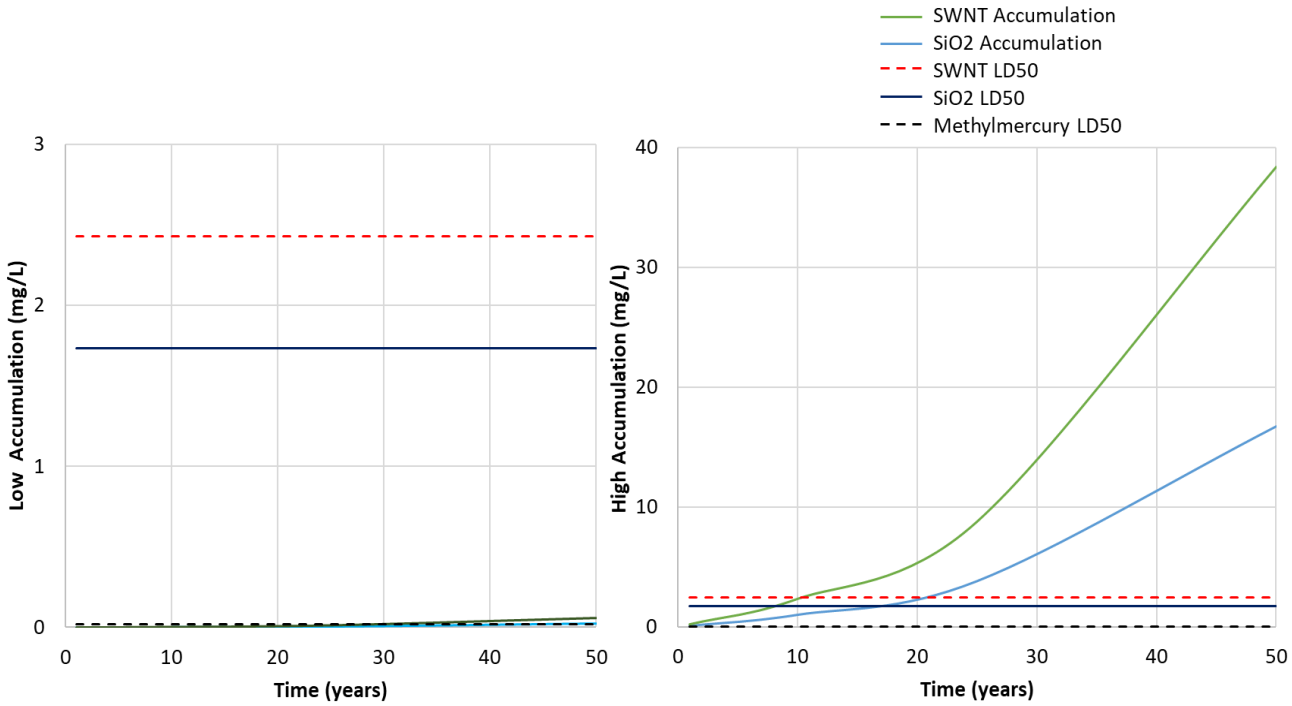

Figure 7. The low and high potential environmental accumulation (mg/L) in Onondaga Lake over time compared to the *Daphnia magna* LD50 values for SWNT, SiO2, and a reference pollutant, methylmercury. SWNT reaches the LD50 value after about 20 years of accumulation in the high scenario while SiO2 reaches the LD50 value under the high scenario at about 8 years of accumulation. However, neither of the ENMs reach their LD50 values under the low accumulation scenario, even after 50 years (note the change in scale for low accumulation).

Onondaga Lake in Syracuse, NY, flows north to Lake Ontario, has a 738-square km watershed, and is infamous for industrial pollution during the 20th century (NY DEC). It was declared an EPA Superfund site in 1994 and has since met water quality standards (NY DEC). While some manufacturing facilities in this area treat wastewater on site, the remaining facilities utilize the city's wastewater treatment plant. In either case, effluents are discharged directly into the lake. Under the high release scenario, the potential emissions for graphene and SiO2 reach their LD50 values between 5 and 10 years of ENM accumulation, and SWNT reaches its LD50 in between 10 and 25 years. However, because of the short residence time of the lake (90-180 days), the average time that water remains in the water body, it is likely that the ENMs would flow out of

Onondaga Lake if they were to remain in the water column. Thus, the more likely scenario for ENM accumulation in Onondaga Lake would be if ENMs were to settle and accumulate in the sediment, which is likely considering most of the ENMs studied here are insoluble in water (Zhao et al. 2002; Fortner et al. 2005; Tang et al. 2008). This is confirmed by past modeling studies, where predicted ENM concentrations were higher in the sediment than in the water column (Parker and Keller 2019), and deposition is rapid, particularly for water insoluble ENMs.

Seneca Lake is the largest of the Upstate New York Finger Lakes with a 1,184-square km watershed. There are point and nonpoint sources of pollution in the Seneca Lake watershed, including municipal and onsite wastewater treatment and runoff associated primarily with agriculture and CAFOs (Halfman 2011). Most of the wastewater is treated at one of the local wastewater treatment plants (Greer and Schreiber 2010) and effluent is either directly released into Seneca Lake or into Keuka Lake (NY DEC), which ultimately flows into Seneca Lake. The residence time of Seneca Lake is 12-18.1 years (NYSDEC 1996) and the lake is typically stratified because of the great depth. Based on the volume of the lake, graphene reaches its *D. magna* LD50 value in between 50 and 75 years of accumulation and SiO2 reaching the LD50 value in between 75 and 100 years. This lake has the longest residence time in this study, yet it is likely that ENMs in the water column will flow out of the lake before accumulating to a level associated with toxicity risk. However, if the ENMs were to rapidly deposit into nearshore sediment, they could accumulate and reach toxic levels for sediment dwelling organisms. The Finger Lakes are also prone to nutrient and other pollution due to the vast agriculture in the area (Halfman 2011), which could interact with ENMs and lead to unintended consequences.

The third case study is the Frank E. Vanlare wastewater treatment on the shore of Lake Ontario, that discharges effluent Lake Ontario. Lake Ontario has a watershed area of 6,371-square km and is one of the Laurentian Great Lakes, the largest surface freshwater system on Earth. Lakes in this region are vulnerable due to industrial discharge, landfill leachate, and chemical runoff

(Hallett and Brooksbank 1986). The residence time of the lake is 6 years (NOAA), which is relatively short compared to Seneca Lake. Due to the large lake volume, accumulation effects over the 50-year period were negligible; none of the ENM case study materials were close to reaching the reported LD50 values for *D. magna*.

These results suggest that the risk of ENM accumulation is dependent on a number of factors including ENM fate and behavior characteristics (e.g. solubility), lake depth, retention time, and ENM deposition in shallow or nearshore parts of the lake, as previously seen in hydrodynamic modeling of phosphorous and other nutrients (León et al. 2005). Further, the risk associated with ENM release is higher because of the historical pollution, which could lead to cascading ecosystem impacts (Fleeger et al. 2003); therefore, it may not be advisable to revitalize a location near this type of ecosystem. If ENMs were to accumulate from an accidental direct release, higher accumulation levels would be observed over time, suggesting that there are scenarios that could increase ENM accumulation risk in all three lakes, but overall the risks are relatively low because of the residence time or size of the lake in this study. Further, in this study, it was assumed that the materials are non-reactive, but transformations of the ENMs might lead to higher or lower toxicity (Wiesner et al. 2006). Results confirm that there is a need to improve assessment of ENM impacts to benthic organisms with various uptake pathways (Quik et al. 2015) to account for varying ENM properties and differences in potential release locations. Currently, there is not sufficient toxicity data to assess the risk of accumulation in the sediment and thus the risk for many ENMs is relatively unknown.

These results highlight the many challenges to the regulation of ENMs, and it remains uncertain as to whether the potential benefits outweigh the potential risks (Lai et al. 2018). For example, ENMs have different risks compared to their bulk counterparts (Keller et al. 2013, Lai et al.

2018) and therefore it is uncertain if current regulations for bulk materials are appropriate for ENMs; some studies have found that materials can be more toxic at the nano-size (Nel et al. 2006). In this study, we evaluate bulk Si and nano-SiO2. We found that nano-SiO2 has a reported LD50 value of 1.73 mg/L and can be more toxic than bulk Si, particularly in smaller freshwater ecosystems (Table S10). By using a futuristic perspective to predict where ENMs might be produced and subsequently released, this model can proactively inform future ENM release modeling, risk, use, and policy for various regions.

3.4 Sensitivity of Modeling Inputs on Evaluating Potential ENM Risks

Because of the scarcity of ENM fate and transport data as well as the uncertainty of existing data (Garvey et al. 2018), many assumptions were made throughout the modeling process. First, uncertainty was accounted for by increasing the range of possible manufacturing location distances (up to 40-km from existing address) based on previous studies. The low and high emission scenario was informed by bounded ENM release percentages, where the low scenario represented a more realistic scenario and the high scenario represented a worst-case scenario. To demonstrate the sensitivity of the input values to the output results and potential magnitude of risk, a disruptive innovation scenario was performed, assuming that ENM production increases from increased electric vehicle adoption (Moore et al. 2018). A ten-fold increase was evaluated for the low and high emission scenarios as shown in Table S21 and Figure S14, where the low scenario results still do not reach measured toxicity values. Results did show that precaution should be taken to ensure that the worst-case disruptive innovation scenario risk is minimized, since the LD50 value is reached in less than a year for SiO2 and graphene, and within 10 years for SWNT and C60. Further, the LD50 values used in this study for comparison were the most

toxic LD50 values found in the literature. If the full range of LD50 values were considered for all ENMs (Table S6) the risks would be further reduced.

Conclusion

Because of the potential risks posed by incorporating ENMs into consumer products and energy technologies, like LIBs, it is critical to take a proactive approach to analyzing risks associated with manufacture, use, and disposal of ENM-enabled technologies. In order to properly address these concerns, decision tools are needed that can account for differences in emissions over various production years and spatial boundaries. In this study, the predictive capacity of geospatial modeling has been joined with material flow modeling and ecotoxicity risk assessment. This tool has been demonstrated using a case study of ENMs well suited for LIB anodes, due to the increasing demand for battery-powered EVs. However, this tool can more generally be applied to emerging materials to proactively inform the potential risks of manufacturing in a given location.

As the use of ENMs increases over space and time, it will become increasingly difficult to thoroughly evaluate all the new ENMs coming onto the market; there is high uncertainty in much of the reported data and many knowledge gaps remain. For instance, there is a lack of monitoring and quantification tools as well as reliable data due to business privacy (Keller et al. 2013; Lai et al. 2018). Despite these limitations, predictive modeling tools can help to rank and prioritize ENMs to test (Lai et al. 2018, Falinski et al. 2018) and integrated methodology applied here addresses some of the nano-knowledge gaps and challenges. As shown throughout this analysis, the Great Lakes watershed could be impacted by nanomaterial release during the manufacturing phase. If all possibilities were considered (other uses and disposal routes), the likelihood of ENMs entering a freshwater ecosystem would increase. Further, it is important to consider releases into other types of ecosystems (e.g. terrestrial ecosystems) (Zuverza-Mena et al. 2017)

as well as potential bioaccumulation and cascading effects, which could impact many levels of the food chain. The results also underscore the importance of reliable fate and transport data, taking into account the proximity to water bodies and sensitive ecosystems, available LD50 data, and accumulation time.

The model applied here provides a starting point for predicting future locations of potential ENM emissions during manufacturing, which could be combined with other predictive modeling tools to proactively determine ecosystem risks. For instance, the predictive spatial model could also be adapted with additional Census data to determine environmental justice implications (e.g. siting and accumulation near low-income communities). The model can be applied to other emerging pollutants/applications and geographic locations using readily available national data. The use of a spatial and temporal perspective adds value to evaluating life cycle nanomaterial tradeoffs and can ultimately inform ENM siting, use, and disposal decisions.

However, there are limitations in this approach that should be highlighted relative to the findings and interpretations. For instance, the fate and transport of ENMs is still uncertain and variable due to the unknowns in the flow path from the source to the material's fate in a freshwater environment. The time scale could be long (e.g. years) if the release of the material sorbs to natural organic matter or it could be relatively short (e.g. days) if the release of the material is carried through wastewater or with another solvent. This study focuses on the utility of adding a spatial perspective, and the location of the release and resulting fate and transport is largely dependent on the landscape in which the release occurs. Therefore, future work could expand upon this initial model and also take into account vegetation cover, imperviousness, hydrodynamics of receiving waters, etc. in addition to the sensitive areas and freshwater ecosystems studied here to further improve this model.

It is important to be able to contextualize the potential ENM risks against the benefit that ENMs provide. The tool in this chapter can help to determine the potential spatial risk and proactively inform where ENM (or other emerging material) manufacturing will minimize risks while increasing the performance benefits of LIBs or other clean energy technologies. However, tools that can assess the risks as well as the benefits that the materials convey are necessary toguide safe nano-enabled product design, use, and disposal at end-of-life. Current risk assessment and decision-making tools for materials do not adequately account for these tradeoffs as well as the uncertainty of ENMs (varying functional forms, unique environmental behavior, economic costs, unknown supply and demand, upstream emissions, and increased use of ENMs in diverse applications). Thus, the complex challenges of the ENM system necessitate a novel approach. In the next chapter, the adaptation of an investment portfolio optimization model is demonstrated for environmental and economic optimization of ENM use in clean energy technologies. From a sustainability perspective, improved clean energy technologies could help extend product lifespans, reduce fossil energy consumption, and substitute ENMs for scarce incumbent materials.

CHAPTER 5: PORTFOLIO OPTIMIZATION OF NANOMATERIAL USE IN CLEAN ENERGY TECHNOLOGIES[3]

Introduction

The potential environmental risks of ENM exposure were assessed in Chapter 3 and 4, but these risks must be considered relative to the performance, energy, or environmental benefits conferred by integrating ENMs into products and technologies, particularly clean energy systems. As first-generation power plants are phased out, resilient energy generation and storage will become increasingly important to meet long-term goals like the Sustainable Development Goals, a directive led by the United Nations to address global sustainability challenges (Schwerhoff and Sy 2017; UN 2015). In this changing energy landscape, ENMs are a promising solution for cost-effective and efficient renewable energy infrastructure because of their conductive, optical, and thermal properties (Hussein 2015). In many applications, ENMs offer improved performance and competitive costs; however, they also pose unique economic and environmental risks (Savolainen et al. 2013). These risks span across ENM manufacturing, their use in products, and their ultimate disposal or release at end-of-life. For example, forecasted growth in nano-applications may increase ENM releases to the environment, where their ultimate transport, fate, and resulting ecological impacts are still poorly understood (Arndt et al. 2014; Kunhirkrishnan et al. 2015; Baalousha et al. 2016; Markus et al. 2017). Considering risk at the material level, some ENMs are believed to contribute to aquatic ecotoxicity in freshwater ecosystems (Gao et al. 2009; Eckelman et al. 2012; Kunhikrishnan et al. 2015). There are also economic risks associated with ENM manufacturing: commercialization requires a large capital investment, however there is currently significant uncertainty associated with expected return on that

[3] This chapter has been adapted from a manuscript published in Environmental Science and Technology in 2018. To avoid repetitive citations, a blanket citation is included here: Moore et al. 2018

investment (Osman et al. 2006). At a systems-level, risks also hinge on relative performance gains that ENM-enabled technologies provide, for example, the increased clean energy that can be produced (due to nano-enabled efficiency gains), compared to energy-intense manufacturing processes required to synthesize ENMs (Anctil et al. 2011; Zhai et al. 2016; Pourzahedi et al. 2017). These uncertainties are further confounded by complexity in the ENM supply chain, in that no single material is representative of all ENMs; each has different properties, performances, prices, and environmental impacts, all of which change from initial production to functionalization, incorporation into a product, and ultimate use in a final application (Anctil et al. 2011; Anctil et al. 2013).

Given the challenge of mitigating risks for a complex material portfolio, effective tools are needed for proactive environmental and economic analyses. It stands to reason that such tools may draw inspiration from other fields concerned with maximizing benefit and minimizing risk given future uncertainty. Specifically, we hypothesize that an analogous system of financial investment tools, namely, analysis of risks and returns of stock portfolios, can be adapted for analysis of risks and returns of ENM portfolios, where a choice must be made about investing in uncertain technologies with variable environmental and economic outcomes associated with changing market conditions.

Portfolio optimization models have been traditionally used to analyze financial markets and help investors assemble efficient portfolios that offer a high return objective and a small variance of historical returns given a variety of investment options (Kolm et al. 2014). ENM portfolio optimization will similarly be used to propose portfolios of ENMs for renewable energy applications that provide the highest return in terms of energy performance and smallest uncertainty in terms of economic and environmental risks. The analogy between financial stocks

and ENMs revolves around the challenge of predicting future performance, given current uncertainty. For example, future stock returns cannot be directly predicted from past performance, and are influenced by changes within a company, financial market, and the broader economic environment. Similarly, future adoption and performance of new technologies, like ENMs, can vary with application, technological progress, demand for ENM-enabled products relative to demand for competing alternatives, and the broader economic, environmental, and regulatory landscape. In the financial domain, investors seek to mitigate uncertainties by selecting a diverse portfolio of stocks, such that if some underperform, others may offset losses. Thus, it stands to reason that a similar diversification may lead to more effective "technological investments," such as research funding, basic and applied research investigations, technology commercialization, policy incentives, etc.

This adaptation builds on a limited body of literature in which portfolio-based tools (Kolm et al. 2014) have been applied in other non-financial market contexts, including optimization of fuel mix diversity (Roques et al. 2008), science policy (Wallace and Rafols 2015), renewable energy investment portfolios (Muñoz et al. 2009), and wind power deployment (Roques et al. 2010). For example, portfolio optimization demonstrated that diversification of fuels can increase resilience of an electricity system under fuel scarcity or price increases (Roques et al. 2008). In Spanish electricity markets (Muñoz et al. 2009), portfolio optimization was used to determine the optimal, normal, and pessimistic portfolios for renewable energy technologies with results highlighting the importance of subsidized tariffs. Finally, in wind power deployment, portfolio optimization's efficient frontier was critical in determining optimal geographic locations of wind farms to maximize power generation of overall European wind portfolios (Roques et al. 2010).

While portfolio optimization has rarely been merged with environmental analysis tools, other decision tools have been proposed to address ENM tradeoffs. Linkov et al. established a framework for analyzing risks and benefits of emerging ENMs through multi-criteria decision analysis (MCDA) combined with risk assessment under different stakeholder preferences (Linkov et al. 2007). This methodology has proven successful for selection of an optimal nanomaterial and has frequently been combined with LCA, e.g., Hicks' tradeoff analysis of the utility of nanosilver in textiles (Hicks 2017) and Scott et al.'s LCA-MCDA modeling of graphene for material substitution (Scott et al. 2016). Gilbertson et al. also combine LCA with impact-benefit screening to assess indirect and direct tradeoffs of a single material (CNT) used in various technologies (Gilbertson et al. 2014), proving the importance of evaluating full life cycles to realize risks avoided from incorporating ENMs. However, these methodologies consistently consider a single material or product and there is clear precedent that systems models can benefit from a more holistic approach. For example, several studies have shown the benefit of applying environmental life cycle assessment (LCA) to groups or portfolios of products. Ryen et al. performed LCA on a "community" of electronics (Ryen et al. 2015) owned in households and found apparent environmental improvements observed for a single product were offset when groups of products were considered holistically. Field et al. showed that when an entire fleet of vehicles are evaluated, the break-even time, or when upfront energy costs of manufacturing equal or exceed energy savings during the use phase, is longer than when a single vehicle is considered (Field et al. 2000). We expect that the portfolio approach could be useful for nanomaterials, since environmental impacts can vary depending on the ENM form and the product in which the ENM is contained (Gao et al. 2009; Anctil et al. 2011; Anctil et al. 2013; Gilbertson et al. 2015; Pourzahedi et al. 2017). For example, Anctil et al. demonstrated that

embodied energy could vary widely across types of fullerene derivatives, depending on how these materials were purified, functionalized, or used in renewable energy systems (Anctil et al. 2011; Anctil et al. 2013).

By understanding the optimal allocation of ENMs in clean energy applications, risk and impact reduction strategies can be prioritized, and performance can be optimized. To this end, we will demonstrate the adaptation of portfolio optimization, show its utility in the ENM case, and discuss how results can inform future research, development, and expansion of ENM use in clean energy technologies.

Materials and Methods

Portfolio Optimization Overview

In its traditional financial application, portfolio optimization modeling transforms historical stock returns (inputs) into an optimal stock portfolio (output) using an optimization that maximizes return on investment while minimizing risk of variance of returns to improve security of investment (Korn and Korn 2001; Kolm et al. 2014). Stock returns are calculated as daily change in stock price over time (Equation 1) where R is portfolio return ($), P_0 is initial stock price, P_1 is final stock price, α is portfolio share, and n is the stock in the portfolio (Korn and Korn 2001). The model constraint is the investor's available budget to purchase stocks. The overall objective is to maximize stock return ($) while minimizing variance (deviation from the mean) of those returns (Equation 2). V is overall stock portfolio variance, $\alpha_{ij}$is covariance between shares, and σ is standard deviation of the stock return (Korn and Korn 2001).

$$R = \sum \left(\frac{P_1 - P_0}{P_0}\right) * \alpha \ \forall_n \qquad \text{Equation 1.}$$

$$V = \sum_{i=1}^{n} \alpha_i^2 \, \sigma_i^2 + 2 \sum_{1 \le i < j \le n} \alpha_i \, \alpha_j \alpha_{ij} \forall_n \qquad \text{Equation 2.}$$

The model calculates portfolio weights, or in other words, the percentage of the budget to invest in each stock to compose the optimal portfolio. While a traditional optimization model may favor the portfolio with either the highest return or lowest risk, portfolio optimization considers both objectives and evaluates trade-offs to calculate the portfolio with the strongest mix of high return and low risk (Korn and Korn 2001; Roques et al. 2008). In section 2.2, we describe how the framework will be applied to ENM-enabled renewable energy applications. Section 2.3 describes specific adaptation of the model for the case studies chosen, including selection of parameters and data sources. Section 2.4 outlines scenario analysis for each case study and Section 2.5 describes sensitivity analyses used for the modeling parameters.

Novel Adaptation of Modeling Framework for ENM Portfolios

The modeling framework has been applied here to inform future-oriented decisions related to the make-up of ENM portfolios in renewable energy applications, with analogies of stocks as ENM shares and return ($) as energy performance gain. To quantify overall portfolio return, the baseline objective function was adapted from Equation 1 to maximize marginal improvement in energy performance due to adding the ENM to an application (compared to incumbent or non-nano material), simultaneously minimizing the variance of the energy gain (Equation 2 adaptation). In Equation 3, E_{gain} is the sum of energy generated from adding each ENM in the portfolio to a specific energy application where E_1 and E_0 represent the energy generated over a period of time that's held constant across all observations, α is the amount of ENM material used in the portfolio (portfolio share), and n represents all application portfolios.

$$Maximize\ E_{gain} = \sum \left(\frac{E_1 - E_0}{E_0}\right) * \alpha \quad \forall_n \qquad \text{Equation 3.}$$

Case Study: Carbonaceous ENMs and Renewable Energy Technologies

To demonstrate the utility of ENM portfolio optimization, we apply the method to a specific case of nano-enabled renewable energy technologies and carbonaceous nanomaterials (CNMs) typically contained in these technologies. Spherical fullerenes (C_{60}, C_{70}, and functionalized derivatives [6,6]-Phenyl C61 butyric acid methyl ester (PCBM) and indene-C_{60} bisadduct (ICBA) (Anctil et al. 2011; Piccino et al. 2012), carbon nanotubes (Ratier et al. 2012; Upadhyayula et al. 2012) (single-walled (SWCNT) and multi-walled (MWCNT)), and graphene (Wu et al. 2011; Ratier et al. 2012) are examples of CNMs proposed for use in renewable energy technologies (Armand and Tarascon 2008). C60 fullerene and its functionalized derivatives are shown at the lab scale to improve power conversion efficiency as electron acceptors in organic photovoltaic (OPV) cells (Anctil et al. 2011; Parish 2011; Dai et al. 2012; Piccino et al. 2012; Laird et al. 2016) and enhance lifespan, storage capacity, and efficiency of lithium-ion batteries (LIBs) (Arie et al. 2009; Dai et al. 2012). SWCNT and MWCNT are proposed as anodes for LIBs due to a ten-fold increase in power performance (Arie et al. 2009; Parish et al. 2011). Graphene and doped graphene sheets show promise for increasing power, capacity, and charging speed of LIB anodes as shown at lab-scale (Wu et al. 2011; Ratier et al. 2012).

The utility of the portfolio optimization framework enables evaluation of two fundamentally different emerging technologies. On one hand, OPVs are not currently sold at the commercial scale and therefore the model can inform future-oriented decisions concerning the acceptor material, a CNM-only case. Alternatively, LIBs are currently used in several products at commercial scale including electric vehicles. The model is also able to evaluate a non-nano anode material, graphite, which was compared with CNMs to show how emerging materials compete with incumbent options farther along the technology development spectrum. The

selected cases, and materials used therein, are non-exhaustive but useful to demonstrate the utility of the portfolio approach. The model can be easily adapted to analyze any other material and technology for which information is available to characterize its performance improvements due to use of novel materials.

When evaluating CNM tradeoffs in OPVs and LIBs, baseline objective functions maximized total power (Anctil et al. 2013) (W/g) (Equation 4) or total cell capacity (Ah/g) (Equation 5). P_{total} is total power generated for OPVs using combinations of various CNMs. P is power rating per cell area (W/m2), A is cell area per mass of the acceptor material (m2/g), and M is mass of CNMs used in the portfolio (g). C_{total} is total capacity generated for electric vehicle (EV) LIBs using combinations of CNMs and the non-nano anode, graphite. C is capacity of the anode (Ah/g), T is amount of CNMs (g) per anode (g), M is mass of CNMs used in the portfolio (g), and n represents all materials in the portfolio. These values were calculated for each CNM using values from the literature as described in Appendix D (Tables S1-S4). Portfolio Variance (Equation 6) incorporates material covariance, or the degree to which material returns move together subject to the same external influence. A and B represent different materials included in the portfolio. M% is the weight of the material in portfolio. R is an individual instance of material return. $\bar{R}$ represents the mean of returns for the specified material and n represents number of observations.

$$Max\ P_{total}(W) = P * A * M\ \forall_n \qquad \text{Equation 4.}$$

$$Max\ C_{total}(Ah) = C * T * M\ \forall_n \qquad \text{Equation 5.}$$

$$s.t.\ \ Min\ V = \sum M_A\% * M_B\% * \frac{\sum(R_A - \overline{R_A}) * (R_B - \overline{R_B}))}{n-1} \qquad \text{Equation 6.}$$

To assess potential risks of ENM use, economic and environmental aspects were also considered. Whereas the approach described above maximizes energy performance gain per amount of CNM added, it is also possible to normalize CNM usage according to environmental or economic attributes. From an economic standpoint, relative performance gain was normalized to material costs associated with incorporating potential CNMs into either OPV cells or LIBs (Ratier et al. 2012; Riesz and Elliston 2016) (Equation S3 and Tables S5-S6). To represent environmental risk, relative performance gain was normalized to cumulative energy demand (CED) (Louwen et al. 2016), the net life cycle energy invested to produce CNMs required for the portfolio, which is an indicator that typically correlates with most key life cycle environmental impacts, like acidification or ecotoxicity (Huijbregts et al. 2010). CED values used were calculated from LCA literature and the amount of CNM contained in each application (Equation S2 and Table S7). An example of the process and parameters utilized in the model are demonstrated in Figure 1 with OPV input data used shown in Table 1. The raw performance, CED, and cost data collected can be visualized in Figure S1 for each case study with the adaptation of components of a financial portfolio optimization to their ENM analogs in Table S8.

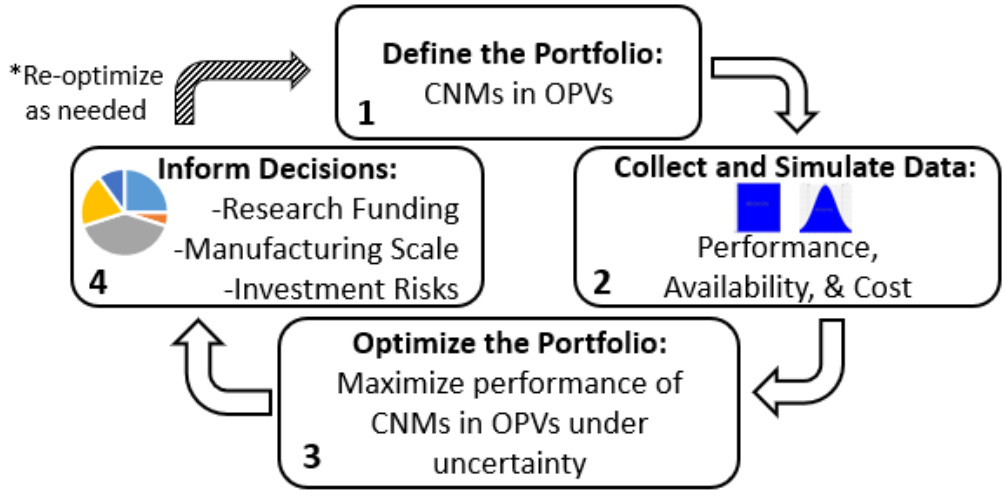

Figure 1. Portfolio optimization conceptual diagram outlining the steps taken to calculate optimal material portfolios. Example model inputs are shown for the OPV case where the data described in step 2 can be found in Table 1.

Table 1. Performance, Cost, CED, and Worldwide Production values for each of the materials used in the model were simulated using the values in this table. Materials that include low/high values in the table below were estimated using a uniform distribution. Materials that include only one value were estimated using a normal distribution.

Materials	**Performance (g/W)**		**Cost ($/g)**		**CED (GJ/kg)**		**Worldwide Production (t/year)**	
OPV Case Study	Low	High	Low	High	Low	High	Low	High
C60	0.0016	0.54	16	134	35.5		0.15-0.60	5.5-80
PC60BM	0.0038	0.038	173	475	85.7		0.15-0.60	5.5-80
PC70BM	0.0028	0.021	2080	2960	123		0.15-0.60	5.5-80
BisPCBM	0.018		1,120		87.7		0.15-0.60	5.5-80
ICBA	0.0084		1,110		55.7		0.15-0.60	5.5-80
Graphene	0.019	0.16	70		500	1,000	573	1320
SWCNT	0.01	0.048	77	849	93	328	26	359
MWCNT	0.0028		5.44	75	65	295	1,990	13,700

Scenario Development

To address emerging and uncertain demand for CNMs, scenarios were used to assess how CNM portfolios change under different market, technology, or supply conditions. For example, current CNM availability is largely goverened by demand from research and development activities, as these materials are not yet widely used in commercialized technologies. If, in the future, this demand were to vastly increase, for example, to deploy widespread solar technology to meet a climate goal, supply may respond in a perfectly elastic manner, as CNMs are typically produced from readily available precursors, like copper and nickel acetylacetonates for synthesizing CNTs from carbon monoxide (Nasibulin et al. 2003). Conversely, CNM supply could also be constrained by time delays in ramping up production infrastructure or by unexpected material

scarcity issues (potential natural graphite supply disruption from changes in government policy (Olivetti et al. 2017; Feytis 2010). Another perspective would be if CNM use continues to be completely opportunistic, wherein these materials are selected when performance, availability, and cost align with current technical needs rather than a target demand. The portfolio model should provide robust decision assistance in any of these cases. Thus, performance and risk factors were evaluated through multiple scenarios that considered impacts of monetary and energy investments from incorporating CNMs into OPVs and LIBs as well as potential considerations of CNM use: constrained vs. unconstrained supply and variable vs. fixed demand. To account for possible material supply constraints, global production quantities of each material were used (Table S1) to compare current production volumes to the optimized level of demand in the portfolio (Piccino et al. 2012). Constrained and unconstrained scenario applications are used to address varying stakeholder interests: Policy makers establishing alternative energy production strategies at a high-level may be interested in insights created through unconstrained scenarios; in contrast, an individual firm facing very specific supply-chain conditions (e.g. required, but scarce material input), and/or supply-chain risk may be interested in material implications of constrained scenarios. Because supply is currently based on limited demand, especially in the case of pre-commercial applications, and is not constrained for technical or scarcity reasons, it is conceivable that the materials could ultimately be produced at a much greater scale. Therefore, an unconstrained supply scenario was generated to represent a virtually unlimited supply of materials. The demand of the materials was also evaluted through an opportunistic use of CNMs vs. a goal-oriented demand (meeting renewable energy targets). To determine if CNM-use in OPVs could meet the U.S. Energy Information Administration's (EIA) Clean Power Plan (CPP) 2040 goal for solar, 1.5% of the 2040 Watts prediction value was set as

the target goal for the OPV demand scenario (Table S9). For the LIB case, the demand scenario was constrained to meet 2040 EIA electric vehicle predictions from the CPP (Table S10). All sixteen iterations of the model can be found in Table S12 where the case study application, availability and optimization are described for all scenarios. Equation 7 represents the model supply constraint where M is amount of material and A is material worldwide production quantity available.

$$\sum M * \alpha \leq A \qquad \text{Equation 7.}$$

Sensitivity Analysis

To understand the sensitivity of model inputs, Monte Carlo simulation was used to show different output probabilities and risks for each scenario analysis performed. Performance output ranges were simulated using uniform and normal distributions, selected based on data available in the literature, by substituting a range of values for inputs that are uncertain. @Risk was used to calculate optimization model outputs by changing the amount of each CNM used in the portfolio to find the optimal return (Palisade Corporation 2017).

In the stock market, portfolio optimization utilizes historical price data for stocks collected over time to inform investment decisions. Analysis of nano-enabled technologies do not have the advantage of a significant body of historic data, because technology is still emerging and evolving rapidly. To account for this uncertainty while also adding robustness to the model, data variability was simulated by assessing variability across literature reported performance data (often collected at lab scale). However, we anticipate that the methodology can easily be augmented as more data become available, while also informing material design and selection decisions with best currently-available information.

Results and Discussion

The results presented here suggest what optimized portfolio of CNMs will provide the greatest performance improvements to the two analyzed renewable energy technologies with least costs and/or environmental impacts (CED). The portfolios are shown for OPVs and LIBs for the constrained and unconstrained supply and fixed and variable demand scenarios.

OPV Results: Supply and Demand Scenarios

In the baseline unconstrained supply scenario (Figure 2A), the model selected three CNMs to achieve a diverse portfolio that would hypothetically minimize variance in power (W) while maximizing the possible power rating of the portfolio. C60 ICBA was selected by the model as the largest share of the OPV portfolio because it has the highest performance power rating. In the constrained supply scenario (Figure 2B), material availability was limited to the current worldwide production of each material. MWCNT was thus selected as the largest portfolio share because of its high-power rating, smaller variance, as well as its large production compared to other CNMs. While MWCNTs were selected under both supply scenarios, C60 ICBA and C60 PCBM are minimally or not at all selected. Results suggest that the portfolio could have selected more of other high performing materials (i.e. ICBA) but ran out of availability for the constrained supply scenario.

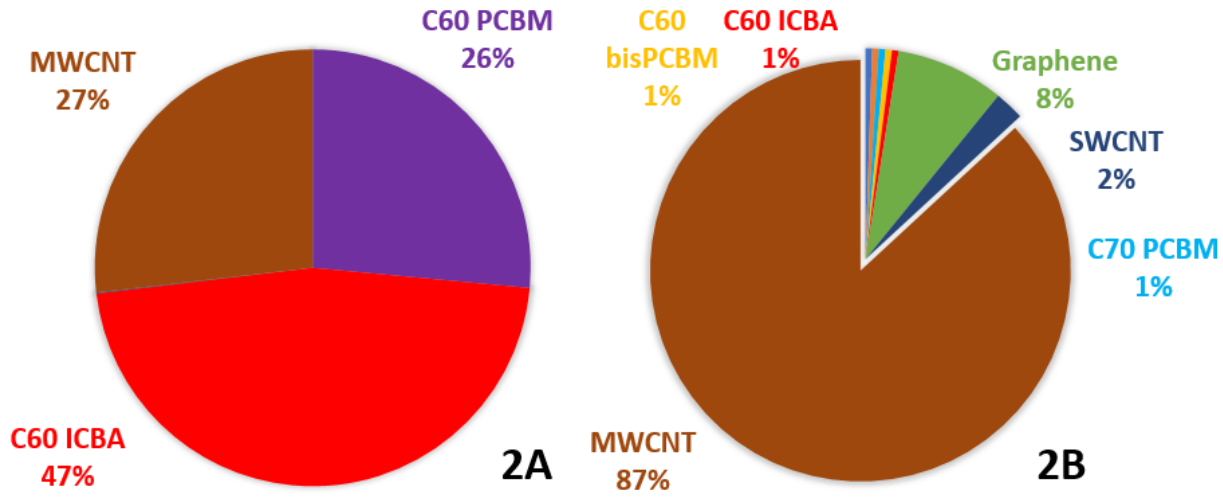

Figure 2. The OPV CNM optimal portfolios for the unconstrained supply scenario baseline case: maximizing performance while minimizing variance (2A) and the constrained supply scenario under the same optimization conditions (2B). C60 ICBA was selected as the largest portfolio share because it has the highest power rating as shown in Figure 1 for the unconstrained supply case yet MWCNT holds the largest share in 2B due to its large availability and smaller variance value.

In the remaining supply and demand scenarios (Figure 3), C60 ICBA was not selected to meet economic and environmental objectives because while there is a high-power rating, there is a premium for the high price and CED associated with its production and integration into OPV cells. The model instead selected a single material to meet the scenario objectives where MWCNT was selected when minimizing cost because it has the lowest price and C60 was selected when minimizing environmental impacts because it has the lowest CED value. While in most cases a diverse portfolio of stocks or materials will maximize return while minimizing variance, there are instances in which portfolio optimization will choose a portfolio comprised of only one material or stock. Given the variance values used as inputs for the model as well as the variability that the model builds into the optimization itself, these scenarios minimize variance and maximize output with a portfolio made up of one material because the benefit of diversification is outweighed by the relatively small variance and high output relative to the other

materials. In the goal-oriented EIA demand scenario with unconstrained supply, the model selected seven materials to meet 1.5% of the predicted EIA solar demand because they contributed to the target portfolio power goal while minimizing the variance in the overall power. In contrast, the EIA demand scenario with constrained supply was not able to meet 52% of the predicted demand given the current worldwide material availability. These results can be used as a justification to accelerate research funding and production for promising materials, like C60 ICBA, which despite being energy and cost intensive, provides high energy efficiency, and scaling up has the potential for the greatest impact on OPV energy performance.

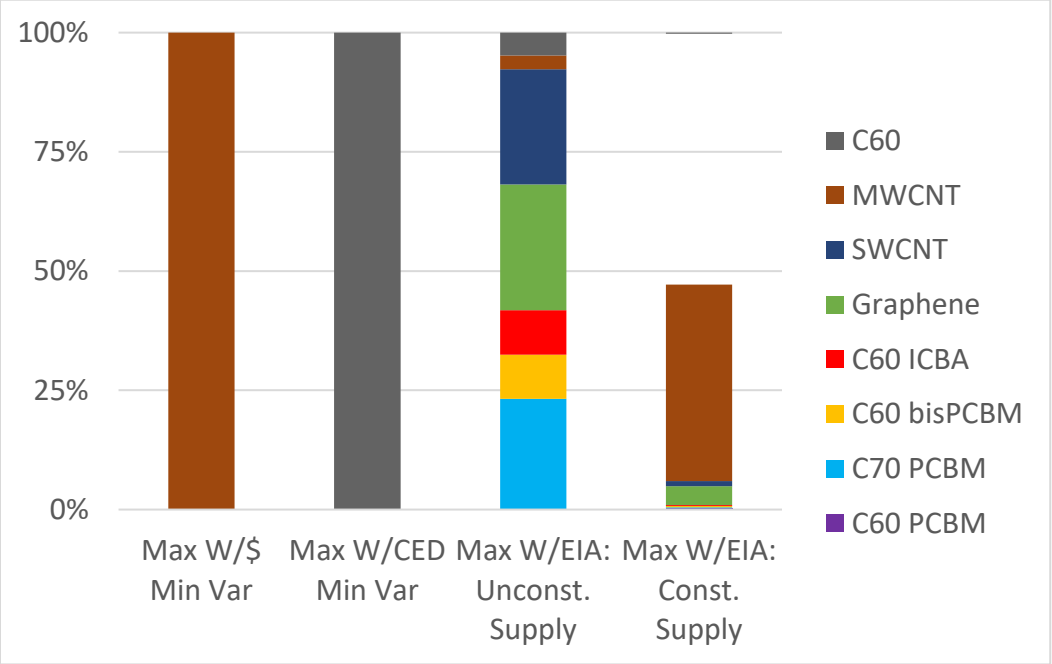

Figure 3. The OPV CNM optimal portfolios for both the supply scenarios: the economic case (Max W/$, Min Var) and environmental case (Max W/CED, Min Var) given opportunistic demand. MWCNT was selected for both supply scenarios when the performance was normalized to the dollars invested because it is the cheapest material whereas C60 was selected when the performance was normalized to the energy invested due to the lower CED value. In the goal-oriented demand case, both unconstrained and constrained supply were evaluated. The model selected seven materials under unconstrained supply to meet the projected power and since the portfolio was diverse, the variance was minimized. In the constrained supply case, 52% of the demand was not able to be met given the current material supply and therefore more material will need to be produced to meet these goals or performance will need to be improved for the applications.

LIB Results: Supply and Demand Scenarios

Similar to the OPV case, the return (capacity) of the LIB portfolio under different scenarios was optimized. For the baseline unconstrained supply scenario (Figure 4A), the model selected five CNMs with the largest share allocated to Si/SWCNT at 57%. This material has the highest performance capacity when normalized to the amount of material added to the anode. In the constrained supply scenario (Figure 4B), the material availability was limited to the current worldwide production of each material. The incumbent anode material, graphite, was selected as the highest portfolio share due to its large production capacity compared with the CNMs which currently do not have the same demand. The results suggest that the portfolio could have selected more of the higher performing, lower variance materials such as Si/SWNCT but did not have enough current availability to overcome the supply of graphite. These results can inform future investment in research, development, and infrastructure that may prioritize high-performing ENM options.

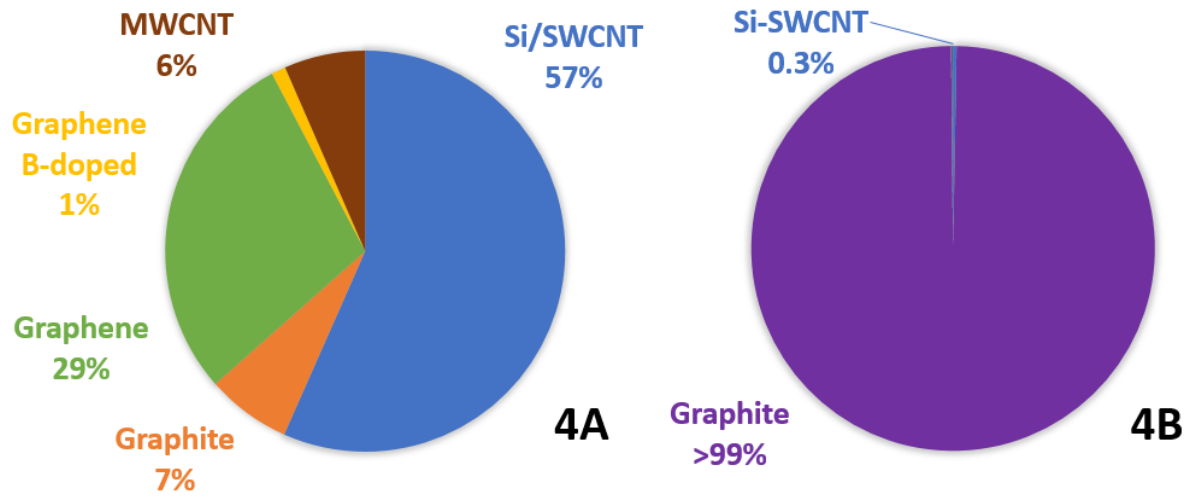

Figure 4. The LIB CNM and incumbent material portfolios for the unconstrained supply scenario baseline case: maximizing performance while minimizing variance (4A) and the constrained supply scenario under the same optimization conditions (4B). Si/SWCNT was selected as the largest portfolio share because it has the highest performance capacity when normalized to the amount of material added to the anode as shown in Figure 1 for the unconstrained supply case yet graphite holds the largest share

in 4B due to its large availability. Graphite is currently used worldwide and has a greater demand than the CNMs included in the portfolio. Over time, the demand profiles of all the materials may change which could skew the results of the constrained supply scenario.

The LIB CNM optimal portfolios for the remaining supply, demand, and risk scenarios are shown in Figure S2 in the SI file. Graphite is the optimal material selected in each of these scenarios when the capacity is normalized to cost and CED value in both the unconstrained and constrained supply scenarios. Graphite has a much lower cost currently because it is farther along the technology maturity spectrum and has had time to reach economies of scale. It also has the lowest CED value because it does not necessitate the same kind of processing steps that ENMs do. In the goal-oriented EIA demand scenario with unconstrained supply, the model selected graphite to meet the predicted EIA electric vehicle demand. Once again, even in the unconstrained supply cases, the maximized performance relative to the variance of one material outweighed a diverse portfolio with many materials. In the EIA demand scenario with constrained supply, the portfolio could meet the predicted electric vehicle demand given the current material availability of graphite and the CNMs (Figure S2). Figure 4B and Figure S2 suggest availability and criticality of these materials (e.g. long-term availability of graphite (Olivetti et al. 2017)) may play a significant role in cost-effectiveness and thereby adoption of clean energy technologies. Firms should consider this in production planning decisions and national policy makers should be aware when determining incentives.

Sensitivity and Uncertainty Analysis

If OPV and battery firms can adopt CNMs and scale-up without compromising material performance, then these innovations may catalyze more widespread adoption of solar as well as electric and hybrid vehicles. OPVs and LIBs with CNMs are currently not on the market and the model assumes that commercial-level OPV and battery production with CNMs are feasible. There is uncertainty inherent in the model due to the lab-scale performance values used from the literature, the unknown rate at which the

technologies and materials will reach economies of scale, and the lack of widespread market availability and demand at this time. To account for the possibility of disruptive material innovation, a scenario was created to evaluate the changes in the OPV portfolio from a large performance increase in a single material. In Figure S1, graphene has the lowest OPV performance relative to the other CNMs. Alcalde et al. describe graphene as an up-and-coming disruptive material due to its unique properties that enable its use in a variety of products and technologies (Alcalde et al. 2013). In the OPV literature, graphene has increased its power conversion efficiency from 0.4% (Chen et al. 2013) at its introduction to 3.57% in 2015 (Kim et al. 2015)—an improvement factor of 9. Assuming the same improvement factor, the sensitivity of the OPV unconstrained supply portfolio was evaluated. While graphene was excluded from the portfolio under the unconstrained supply baseline scenario (Figure 2A), the material comprised 17% of the portfolio when graphene performance was increased (Figure 5). These results show that the model is sensitive to large increases in performance and can account for disruptions if they occur.

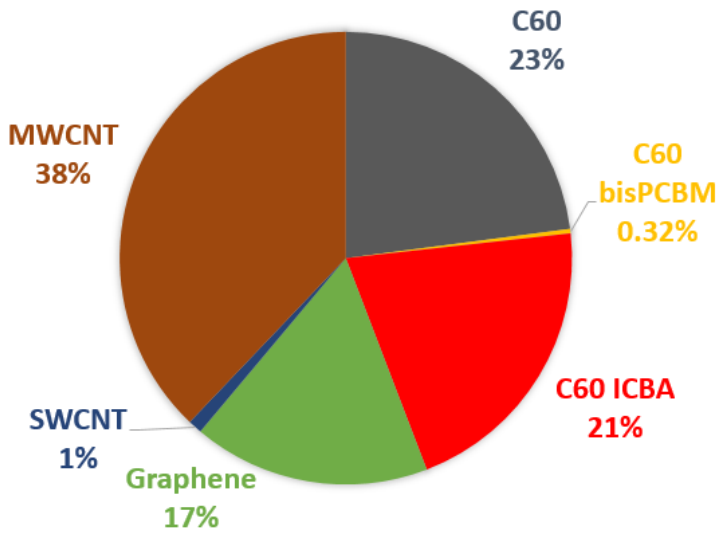

Figure 5. The OPV CNM portfolio for the unconstrained supply scenario for the baseline case: maximizing performance while minimizing variance. MWCNT and C60 ICBA once again were selected as large portfolio shares along with graphene due to the disruptive innovation in graphene's power rating performance.

Concerns over the supply of battery-grade graphite have been raised for quite some time (Gaines et al. 2009; Wadia et al. 2011), however with recent goals from companies and countries to

completely phase out internal combustion engines, the demand from the electric vehicle sector is expected to increase exponentially. Such an increase will almost certainly lead to supply constraints as competition among industries for these materials grows (Olivetti et al. 2017). This work examines this potential challenge with a scenario where graphite supply is reduced by 30% (Figure S3); in reality, market signals like price will actually increase dramatically due to a supply constraint but it is unlikely that the renewable energy sector will be able to pass on such increased costs to consumers compared to other competing sectors (Sensfuß et al. 2008). An extreme case where graphite was eliminated from the portfolio as a result of insufficient supply relative to demand was also evaluated (Figures S4 and S5), resulting in portfolios with heavy reliance on graphene and silicon/single-walled carbon nanotubes. Although these CNM-enabled technologies are not widely available currently, the information from the model can be useful in helping firms decide if they should invest in the research and development of the new technology by understanding whether or not the technology can meet demand projections, reduce costs, and withstand disruptive scenarios.

Broader Implications

While research has begun to evaluate ENM trade-offs and net benefits (Eckelman et. Al 2012; Gilbertson et al. 2015; Zhai et al. 2016), the opportunity remains for new approaches that factor in performance, environmental risks, and economic considerations, which are an important part of the material system and decision-making. A portfolio approach is needed to evaluate the tradeoffs of emerging contaminants such as ENMs because of their potential for widespread use in multiple applications. For example, this portfolio approach could be combined with research that compares net life cycle energy benefits of the same ENMs in different applications building on the approach of Zhai et al. who compared human health benefits and risks of CNTs in

different application (Zhai et al. 2016). The portfolio methodology is flexible and could also be expanded to include other environmental indicators such as freshwater ecotoxicity, building on work by Eckelman et al. and Deng et al., which have pointed out the importance of considering upstream life cycle impacts in addition to direct toxicity risks (Eckelman et al. 2012; Deng et al. 2017).

The results from the model show that the decision to adopt CNMs into the OPV or LIB product portfolio is dependent on a number of trade-off factors including the price, the environmental impact, and the overall power/capacity output of the material. The results can inform investment and design decisions when faced with emerging material uncertainty, speculation, and possible disruptive innovation. From a sustainability perspective, an improved OPV for powering electronics or LIB for an electric vehicle could help extend product lifespans, reduce fossil energy consumption, and substitute ENMs for scarce incumbent materials. Results obtained from best currently-available data suggest that MWCNT is a promising acceptor material for OPV technology and may be a good candidate for greater research and development. However, a change in the performance of one material can alter the entire portfolio, proving that a combination of nanomaterials is necessary to reduce variability in the amount of power OPVs can output for energy security.

For the LIB scenario, the incumbent material, graphite, was selected over many of the CNMs considered, due to high current availability, low costs, and smaller environmental impacts. However, graphite has increasing scarcity concerns (Feytis 2010; Olivetti et al. 2017) that could impact its use in this sector, underscoring the utility of portfolio optimization for informing potential ENMs as substitutes in battery anodes. With this new approach to guiding material use and understanding possible portfolios in a suite of technologies, portfolio optimization can help

material stakeholders to invest in materials and inform design decisions, predict unintended consequences, and support emerging contaminant policy. If the objective of the user is to scale-up manufacturer's least cost pathway, users of the model can utilize the values that show the optimal portfolio when cost is minimized. Results can also inform which materials should be prioritized for research and development to increase pace and decrease cost of full-scale deployment in the event of risks or shortages for incumbent materials, like graphite. The integrated model presented herein also has the potential to advance the modeling of material selection and tradeoffs in other emerging technologies beyond the nano-enabled systems discussed here. The portfolio perspective combines multi-objective optimization and uncertainty analysis through a holistic lens that can be used in different contexts to inform how materials should be invested considering both the risks and benefits of the material portfolio. For example, this methodology could be used to compare various blends of materials required within a system, such as the combinations of metallic cathode chemistries in a lithium-ion battery (Appiah et al. 2016), material combinations for high entropy alloys (Fu et al. 2017), or biofuel blends for transportation applications (Lin et al. 2013). The model can also be utilized to select the 'best' materials under different objective scenarios e.g. considering the criticality or scarcity in a material system (Gaustad et al. 2017), choosing the optimal material when designing electronic product communities (Ryen et al. 2015), or utilizing the model to once again to inform nano-enabled products such as in agricultural (Jain et al. 2016) applications. Furthermore, future versions of the model can be adapted to account for multiple ENM materials that may coexist in a single application if the ratio of materials is known, such as case presented here where a mix of nano-scale silicon and SWCNT are combined in a Li-ion battery (Lee et al. 2016). The resulting portfolio that the model selects can help inform future research

and development, design considerations, reduce economic and environmental risks, and ensure environmental health and safety of the products throughout their life cycle through the use of this proactive modeling tool.

CHAPTER 6: CONCLUSIONS AND RECOMMENDATIONS

In the age of sustainable development, we are faced with a growing number of global challenges; However, these challenges can also be viewed as windows of opportunity to create positive social, environmental, and economic change. The challenge of introducing novel materials and technologies without consideration of their sustainability impacts has historically led to unintended consequences. To avoid such negative outcomes, potential sources of pollution must be proactively identified and assessed to minimize risks (Persson et al. 2013). The same tools and methods that have been applied in the past to evaluate chemical pollution impacts may not always be suitable for emerging materials like ENMs. Thus, the goal of this research effort was to apply novel empirical and modeling approaches to resolve key uncertainties surrounding potential consequences of ENM use in clean energy.

Policy Implications

As demand for new and improved products and technologies increases, development of novel materials to help meet this demand also increases. Currently, TSCA's Interagency Testing Committee recommends up to 50 substances/year for testing (EPA 2016). If a substance is not recommended for testing, the consequences of exposure to that chemical are relatively unknown. Additionally, the testing that is performed has been found to "…remain biased toward single-species tests done in lab…" (Newman 2009) rather than multiple species tests. This approach is criticized, as results could easily be skewed: even if the one type of organism tested is not impacted by the exposure, another different organism may actually be more sensitive or susceptible to that same chemical. The TSCA structure, meant to advise the health and safety of chemical substances, does not currently accommodate the extensive testing that may be necessary for emerging contaminants with unique properties and capabilities. Exhaustive testing

may include long-term exposure effects, interaction with legacy pollutants, and changes in chemical behavior throughout different release media. Unfortunately, exhaustive testing is time-consuming and expensive and there are concerns that its requirement may hinder innovation and technology development (Malloy et al. 2011).

To begin to address emerging contaminant challenges proactively, there is a disconnect between decision makers and researchers that must be addressed. While countries in the European Union and North America are beginning to develop priority lists for chemical testing and regulation (Taheran et al. 2018), new substances and chemicals are still released into the marketplace via new products and production inputs at a rapid rate throughout the world, as underscored by the planetary boundary research on chemical pollution (Rockström et al. 2009). Researchers recognize that emerging contaminants all have different properties and capabilities and can also be released at low concentrations. This can make it difficult to quantify and characterize these contaminants, and to fully understand their fate and impacts over space and time (Taheran et al. 2018). Risk assessment screening tools to aid in identification and ranking are being developed for emerging contaminants, such as the Ashby charts for nanomaterials (Falinski et al. 2018). However, utilization of decision-making tools remains a challenge, due to the lack of reliable and available data on a growing list of chemicals. Even where data are available, much of the data are not considered standard; the reliability and comparability of the data is a challenge due to varying testing protocols (Ostraat et al. 2013). While many materials have standard protocols for testing, emerging substances with novel properties may not conform to the same protocols; there is a need for updated testing protocols that are better able to capture and cover the increasing range of emerging substances. Thus, research priorities that can inform policy regulations for emerging contaminants include: 1) expanded and reliable risk assessment data for emerging

substances based on standard protocols, 2) decision-making tools that can aid in the priority identification and ranking of these materials, and 3) decision-making tools to facilitate improved communication between decision-makers and researchers.

Summary and Key Takeaways

- Engineered nanomaterials can catalyze the performance of clean energy technologies, helping them to compete in a fossil-fuel dominant world.
- Whereas much of the nanomaterial research focuses on the potential ecotoxicity impacts, this dissertation emphasizes the benefit of offsetting fossil-fuel emissions and minimizing environmental impacts.
- Through novel empirical and modeling studies, this research contributed to filling knowledge gaps and addressing all four pillars of sustainability.
    - First, the impacts on the environment were assessed through ecotoxicity empirical assays, predation studies, and spatially explicit risk assessment.
        - Ecological impact results demonstrate the utility of assessing multiple ENM forms and looking beyond acute ecotoxicity studies and incorporating more chronic, multi-species, and multi-trophic level assessments to inform the magnitude of environmental risk, which can inform future research on emerging nanomaterials and other novel materials.
        - Predicted ENM emissions are within the buffer zones of sensitive ecosystems, yet only reach potential ecotoxicity levels during an accumulation period of 5-10 years under the high release scenario.

- Next, this effort evaluated ENMs that maximize performance of clean energy technologies while minimizing risks (economic and environmental), which can be used to inform policy and industry stakeholders.
    - Results suggest the decision to adopt specific ENMs into clean energy technologies is dependent on the price, environmental impact, and overall material performance, but that for most cases, a diverse material portfolio could minimize risks, similar to what is observed in the financial market.

- Chemical pollution is an important global challenge. To address this challenge, we can be proactive and minimize potential consequences while supporting technological progress and innovation with design and decision-making tools.

Future Work

Fullerene Use Phase Releases

Much of this research effort focused on the manufacturing stage of the carbon nanomaterial life cycle. However, future work should expand on these efforts to also include impacts during the use phase of clean energy technologies as well as the disposal phase. Though the ecotoxicity studies of the fullerenes alone inform potential impacts if the material were to be released at the manufacturing stage, these materials are more likely to be released during the use-phase or at a product's end-of-life. One potential fullerene release pathway during the use-phase (OPV cells) was studied in Chapter 2 to understand the impact if released into freshwater ecosystems. These results were preliminary and demonstrated a significant difference between the OPV replicates relative to the control. However, it was not clear if the toxicity was attributed to the fullerenes, the OPV dyes, or the fabrication processing steps from our results. Future experiments could improve the experimental design to isolate the various materials to better inform possible OPV

material release risks. As demonstrated in Chapters 4 and 5, fullerenes are also integrated into lithium-ion battery anodes. Future work could incorporate this clean energy technology to inform use-phase risks. End-of-life management and the associated life cycle impacts of these technologies is uncertain (Raugei and Winfield 2019) yet risks could be simulated using TCLP landfill methods (Dutta et al. 2018) to begin to quantify possible end-of-life release impacts. The preliminary methods and results for use-phase ecotoxicity can also help inform life cycle impact assessment (LCIA) for fullerenes (C60, C70) and the fullerene derivative, PCBM to quantify differences over the total life cycle. Results can be used to calculate ecotoxicity impact characterization factors that currently do not exist for these materials because of the uncertainty in the nanomaterial life cycle, especially in the use and disposal phase.

Natural vs. Engineered Fullerene Impacts

This work specifically focused on engineered nanomaterial forms, but these materials also occur naturally in the environment (e.g. soot from fires). It is also difficult to differentiate between natural fullerene soot and engineered fullerenes in the environment. The relative magnitude and impacts of potential ecotoxicity impacts of natural forms could be an interesting area to explore. However, there are methods that can aid with this identification such as fluorescence labeling of the materials (Zanker and Schierz 2012) and imaging to assess differences in shape and size as shown with nano-iron oxide particles (Von der Kammer et al. 2014). The toxicity of natural and engineered nanomaterials could vary due to the functionalization of many of the engineered forms such as C70 and PCBM (Sharma et al. 2015). Thus, empirical studies could be performed to assess the 1) direct ecotoxicity impacts of natural and engineered forms and 2) the potential fate and cascading effects of the natural and engineered nanomaterials in a freshwater ecosystem

as performed in Chapter 3. The distinction between natural and engineered forms in the environment is critical in assessing the risk of engineered fullerenes.

Conclusions and Recommendations

Emerging pollutants are human-driven challenges, but there is an opportunity for human-driven solutions (Rockström et al. 2009) to address these challenges. ENMs can catalyze the performance of clean energy technologies, helping them to compete in a fossil-fuel dominant world. Whereas much of the nanomaterial research focuses on the potential ecotoxicity impacts, this dissertation emphasizes the importance of also considering potential benefits of ENMs in clean energy that offsets fossil-fuel emissions and minimize environmental impacts.

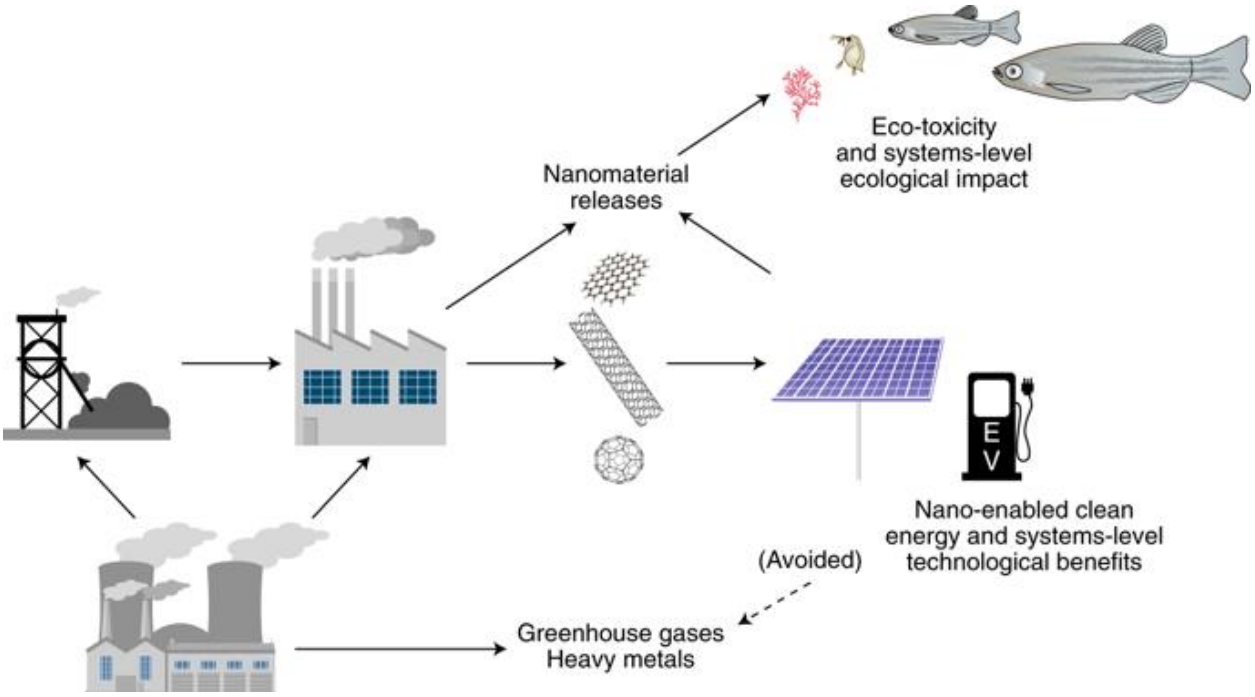

Figure 1. From improved performance of clean energy technologies, environmental impacts and emissions can be avoided by displacing fossil-fuel use (Babbitt and Moore 2018).

The results from this research can be used to inform material selection, sustainable design of products and technologies, and emphasizes the benefit of adding chronic, multi-species, and trophic-level experiments to increase the understanding of impacts. As results have shown, there

are differences in impacts with varying fullerene forms. Thus, this work also informs future academic research in life cycle assessment modeling of nanomaterials as well as nanomaterial design and risk assessment. Ultimately, the differences in fullerene forms must be accounted for in chemical testing protocols as implemented in policies such as TSCA. Much of this research effort focused on the manufacturing stage of the ENM life cycle. But, knowledge gaps remain for the ENM use and disposal phases. Preliminary results of OPV leachates demonstrate that there were not significant differences among OPV treatments for *Daphnia pulex*. However, future work should expand on these efforts and investigate other likely ENM release pathways. Additionally, while a spatial and temporal perspective predicted potential ENM emissions during the manufacturing stage, future research could identify potential locations of release from commonly used products and/or disposal sites. The results of the portfolio optimization tradeoff analysis highlighted ENMs that could optimize performance for OPVs (e.g. ICBA and MWCNT) and LIBs (Si/SWNT). It is recommended that future clean energy technology research consider these materials and increase research and development efforts. Results also emphasized scarcity implications of graphite, the incumbent anode material for LIBs, which underscores the importance of considering other anode materials as electric vehicle adoption and LIB use rises. These novel modeling efforts can support the development of future models and are tools that can help aid decision-making during the design process.

In addition to the empirical and modeling research performed in this dissertation, another goal was to increase public understanding of engineered nanomaterial use, benefits, and potential impacts. A collaboration between researchers at Golisano Institute for Sustainability, researchers in the Environmental Science program at RIT, and Rochester's World of Inquiry School No. 58 for three years resulted in nanomaterial outreach lesson modules to help teach students at the

high school level. These outreach modules were featured in the National Science Teacher Association (NSTA) Free Resources newsletter, Dec. 2018. The project, Nanomaterials: To Use or Not to Use, was designed for high school biology and AP Environmental Science students. This module presented four lessons; Exploring nanomaterials, Introduction to material flows, Effects of emerging pollutants, and Communicating results. The goal of this effort was to share nanomaterial outreach education materials with a large audience of teachers and students. These materials are freely available via the web: https://www.rit.edu/gis/nanomaterials-use-or-not-use. Community outreach efforts can help to increase societal awareness and education of nanomaterials, an emerging challenge as novel engineered nanomaterials are increasingly developed and introduced in the global market.

Despite the growing number of global challenges, novel tools and methods can be used to evaluate chemical pollution impacts, resolve uncertainties of emerging contaminants like ENMs, and inform critical knowledge gaps. Results from these tools can help to resolve the disconnect between decision-makers and researchers. Through intentional and proactive approaches, we can create, use, and manage chemical technology that provides benefits to the world while minimizing negative consequences.

REFERENCES

1. Adeleye, A. S.; Conway, J. R.; Garner, K.; Huang, Y.; Su, Y.; Keller, A. A., Engineered nanomaterials for water treatment and remediation: costs, benefits, and applicability. *Chemical Engineering Journal* **2016,** *286*, 640-662.

2. Alcalde, H.; de la Fuente, J.; Kamp, B.; Zurutuza, A., Market uptake potential of graphene as a disruptive material. *Proceedings of the IEEE* **2013,** *101* (7), 1793-1800.

3. Anctil, A.; Babbitt, C. W.; Raffaelle, R. P.; Landi, B. J., Cumulative energy demand for small molecule and polymer photovoltaics. *Progress in Photovoltaics: Research and Applications* **2013,** *21* (7), 1541-1554.

4. Appiah, W. A.; Park, J.; Van Khue, L.; Lee, Y.; Choi, J.; Ryou, M.-H.; Lee, Y. M., Comparative study on experiments and simulation of blended cathode active materials for lithium ion batteries. *Electrochimica Acta* **2016,** *187*, 422-432.

5. Biosystems, A. http://www.aquaticbiosystems.com/.

6. Armand, M.; Tarascon, J.-M., Building better batteries. *Nature* **2008,** *451* (7179), 652-657.

7. Arndt Devrah, A.; Chen, J.; Moua, M.; Klaper Rebecca, D., Multigeneration impacts on Daphnia magna of carbon nanomaterials with differing core structures and functionalizations. *Environmental Toxicology and Chemistry* **2013,** *33* (3), 541-547.

8. Arndt, D. A.; Moua, M.; Chen, J.; Klaper, R. D., Core Structure and Surface Functionalization of Carbon Nanomaterials Alter Impacts to Daphnid Mortality, Reproduction, and Growth: Acute Assays Do Not Predict Chronic Exposure Impacts. *Environmental Science & Technology* **2013,** *47* (16), 9444-9452.

9. Baalousha, M.; Cornelis, G.; Kuhlbusch, T.; Lynch, I.; Nickel, C.; Peijnenburg, W.; Van Den Brink, N., Modeling nanomaterial fate and uptake in the environment: current knowledge and future trends. *Environmental Science: Nano* **2016,** *3* (2), 323-345.

10. Babbitt, C. W.; Moore, E. A., Sustainable nanomaterials by design. *Nature nanotechnology* **2018,** *13* (8), 621.

11. Baun, A.; Hartmann, N. B.; Grieger, K.; Kusk, K. O., Ecotoxicity of engineered nanoparticles to aquatic invertebrates: a brief review and recommendations for future toxicity testing. *Ecotoxicology* **2008,** *17* (5), 387-395.

12. Bilgen, S., Structure and environmental impact of global energy consumption. *Renewable and Sustainable Energy Reviews* **2014,** *38*, 890-902.

13. Bjelland, M. D., Brownfield sites in Minneapolis-St. Paul: The interwoven geographies of industrial disinvestment and environmental contamination. *Urban Geography* **2004,** *25* (7), 631-657.

14. Brabec Christoph, J.; Gowrisanker, S.; Halls Jonathan, J. M.; Laird, D.; Jia, S.; Williams Shawn, P., Polymer–Fullerene Bulk-Heterojunction Solar Cells. *Advanced Materials* **2010,** *22* (34), 3839-3856.

15. Branstrator, D. K.; Holl, C. M., Planktivory by bluegill (Lepomis macrochirus) on Leptodora kindti in a small North American lake. *Hydrobiologia* **2000,** *437* (1), 101-106.

16. Supply, C. B., 2017.

17. Chamberlain Scott, A.; Bronstein Judith, L.; Rudgers Jennifer, A., How context dependent are species interactions? *Ecology Letters* **2014,** *17* (7), 881-890.

18. Chan, C. K.; Peng, H.; Liu, G.; McIlwrath, K.; Zhang, X. F.; Huggins, R. A.; Cui, Y., High-performance lithium battery anodes using silicon nanowires. *Nature nanotechnology* **2008,** *3* (1), 31-35.

19. Chen, D.; Zhang, H.; Liu, Y.; Li, J., Graphene and its derivatives for the development of solar cells, photoelectrochemical, and photocatalytic applications. *Energy & Environmental Science* **2013,** *6* (5), 1362-1387.

20. Chen, X.; Li, C.; Grätzel, M.; Kostecki, R.; Mao, S. S., Nanomaterials for renewable energy production and storage. *Chemical Society Reviews* **2012,** *41* (23), 7909-7937.

21. Coll, C.; Notter, D.; Gottschalk, F.; Sun, T.; Som, C.; Nowack, B., Probabilistic environmental risk assessment of five nanomaterials (nano-TiO2, nano-Ag, nano-ZnO, CNT, and fullerenes). *Nanotoxicology* **2016,** *10* (4), 436-444.

22. Connelly, S. J.; Walling, K.; Wilbert, S. A.; Catlin, D. M.; Monaghan, C. E.; Hlynchuk, S.; Meehl, P. G.; Resch, L. N.; Carrera, J. V.; Bowles, S. M.; Clark, M. D.; Tan, L. T.; Cody, J. A., UV-Stressed Daphnia pulex Increase Fitness through Uptake of Vitamin D3. *PLOS ONE* **2015,** *10* (7), e0131847.

23. Group, C., Commercial Real Estate. 2018.

24. Cunningham, S.; Brennan-Fournet, M. E.; Ledwith, D.; Byrnes, L.; Joshi, L., Effect of Nanoparticle Stabilization and Physicochemical Properties on Exposure Outcome: Acute Toxicity of Silver Nanoparticle Preparations in Zebrafish (Danio rerio). *Environmental Science & Technology* **2013,** *47* (8), 3883-3892.

25. D'Mello, S. R.; Cruz, C. N.; Chen, M.-L.; Kapoor, M.; Lee, S. L.; Tyner, K. M., The evolving landscape of drug products containing nanomaterials in the United States. *Nature nanotechnology* **2017,** *12* (6), 523.

26. Dai, L.; Chang, D. W.; Baek, J. B.; Lu, W., Carbon nanomaterials for advanced energy conversion and storage. *small* **2012,** *8* (8), 1130-1166.

27. Dale, A. L.; Casman, E. A.; Lowry, G. V.; Lead, J. R.; Viparelli, E.; Baalousha, M., Modeling nanomaterial environmental fate in aquatic systems. ACS Publications: 2015.

28. Daniel, M.; Lemonsu, A.; Déqué, M.; Somot, S.; Alias, A.; Masson, V., Benefits of explicit urban parameterization in regional climate modeling to study climate and city interactions. *Climate Dynamics* **2018**, 1-20.

29. Diamond, M. L.; de Wit, C. A.; Molander, S.; Scheringer, M.; Backhaus, T.; Lohmann, R.; Arvidsson, R.; Bergman, Å.; Hauschild, M.; Holoubek, I., Exploring the planetary boundary for chemical pollution. *Environment international* **2015,** *78*, 8-15.

30. Dzialowski, E. M.; Turner, P. K.; Brooks, B. W., Physiological and reproductive effects of beta adrenergic receptor antagonists in Daphnia magna. *Archives of environmental contamination and toxicology* **2006,** *50* (4), 503-510.

31. EPA. OPPTS 850.1300
Daphnid Chronic
Toxicity Test 1996. https://www.epa.gov/sites/production/files/2015-07/documents/850-1300.pdf.

32. EPA. Methods for Measuring the Acute
Toxicity of Effluents and Receiving
Waters to Freshwater and Marine
Organisms 2002. https://www.epa.gov/sites/production/files/2015-08/documents/acute-freshwater-and-marine-wet-manual_2002.pdf.

33. EPA, Toxics Resource Inventory. 2019.

34. EPA, TSCA Chemical Substance Inventory. 2019.

35. ESRI Weighted Overlay. http://desktop.arcgis.com/en/arcmap/10.3/tools/spatial-analyst-toolbox/weighted-overlay.htm.

36. FDA, The Microbead-Free Waters Act. 2015.

37. Feytis, A., The bright side of graphite. *Industrial Minerals* **2010,** *7*, 31-39.

38. Field, F.; Kirchain, R.; Clark, J., Life-Cycle Assessment and Temporal Distributions of Emissions: Developing a Fleet-Based Analysis. *Journal of Industrial Ecology* **2000,** *4* (2), 71-91.

39. Fleeger, J. W.; Carman, K. R.; Nisbet, R. M., Indirect effects of contaminants in aquatic ecosystems. *Science of the Total Environment* **2003,** *317* (1-3), 207-233.

40. Fleeger, J. W.; Carman, K. R.; Nisbet, R. M., Indirect effects of contaminants in aquatic ecosystems. *Science of the total environment* **2003,** *317* (1-3), 207-233.

41. Fortner, J. D.; Lyon, D. Y.; Sayes, C. M.; Boyd, A. M.; Falkner, J. C.; Hotze, E. M.; Alemany, L. B.; Tao, Y. J.; Guo, W.; Ausman, K. D.; Colvin, V. L.; Hughes, J. B., C60 in Water: Nanocrystal Formation and Microbial Response. *Environmental Science & Technology* **2005,** *39* (11), 4307-4316.

42. Fu, X.; Schuh, C. A.; Olivetti, E. A., Materials selection considerations for high entropy alloys. *Scripta Materialia* **2017,** *138* (Supplement C), 145-150.

43. Gaines, L.; Nelson, P. In *Lithium-ion batteries: possible materials issues*, 13th international battery materials recycling seminar and exhibit, Broward County Convention Center, Fort Lauderdale, Florida, 2009; p 16.

44. Garvey, T.; Moore, E. A.; Babbitt, C. W.; Gaustad, G., Comparing ecotoxicity risks for nanomaterial production and release under uncertainty. *Clean Technologies and Environmental Policy* **2018**, 1-14.

45. Gaustad, G.; Krystofik, M.; Bustamante, M.; Badami, K., Circular economy strategies for mitigating critical material supply issues. *Resources, Conservation and Recycling* **2017**.

46. Geissen, V.; Mol, H.; Klumpp, E.; Umlauf, G.; Nadal, M.; van der Ploeg, M.; van de Zee, S. E.; Ritsema, C. J., Emerging pollutants in the environment: a challenge for water resource management. *International Soil and Water Conservation Research* **2015,** *3* (1), 57-65.

47. Giese, B.; Klaessig, F.; Park, B.; Kaegi, R.; Steinfeldt, M.; Wigger, H.; Gleich, A.; Gottschalk, F., Risks, release and concentrations of engineered nanomaterial in the environment. *Scientific reports* **2018,** *8* (1), 1565.

48. Gilbertson, L. M.; Busnaina, A. A.; Isaacs, J. A.; Zimmerman, J. B.; Eckelman, M. J., Life cycle impacts and benefits of a carbon nanotube-enabled chemical gas sensor. *Environmental science & technology* **2014,** *48* (19), 11360-11368.

49. Gottschalk, F.; Lassen, C.; Kjoelholt, J.; Christensen, F.; Nowack, B., Modeling flows and concentrations of nine engineered nanomaterials in the Danish environment. *International journal of environmental research and public health* **2015,** *12* (5), 5581-5602.

50. Gottschalk, F.; Nowack, B., The release of engineered nanomaterials to the environment. *Journal of Environmental Monitoring* **2011,** *13* (5), 1145-1155.

51. Gottschalk, F.; Nowack, B., A probabilistic method for species sensitivity distributions taking into account the inherent uncertainty and variability of effects to estimate environmental risk. *Integrated environmental assessment and management* **2013,** *9* (1), 79-86.

52. Gottschalk, F.; Ort, C.; Scholz, R. W.; Nowack, B., Engineered nanomaterials in rivers–exposure scenarios for Switzerland at high spatial and temporal resolution. *Environmental Pollution* **2011,** *159* (12), 3439-3445.

53. Guinée, J. B.; Heijungs, R., Life cycle sustainability analysis. *Journal of Industrial Ecology* **2011,** *15* (5), 656-658.

54. Gupta, A.; Jaikumar, A.; Kandlikar, S. G.; Rishi, A.; Layman, A., A Multiscale Morphological Insight into Graphene Based Coatings for Pool Boiling Applications. *Heat Transfer Engineering* **2018,** *39* (15), 1331-1343.

55. Halfman, J. D. *Water quality of Seneca Lake, New York: A 2011 update*; Technical Report Hobart and William Smith Colleges, Geneva, NY, 2011 …: 2011.

56. Hallett, D.; Brooksbank, M., Trends of TCDD and related compounds in the Great Lakes: The Lake Ontario ecosystem. *Chemosphere* **1986,** *15* (9-12), 1405-1416.

57. Hassellöv, M.; Readman, J. W.; Ranville, J. F.; Tiede, K., Nanoparticle analysis and characterization methodologies in environmental risk assessment of engineered nanoparticles. *Ecotoxicology* **2008,** *17* (5), 344-361.

58. Hicks, A. L., Using multi criteria decision analysis to evaluate nanotechnology: nAg enabled textiles as a case study. *Environmental Science: Nano* **2017,** *4* (8), 1647-1655.

59. Hicks, A. L.; Theis, T. L., A comparative life cycle assessment of commercially available household silver-enabled polyester textiles. *The International Journal of Life Cycle Assessment* **2017,** *22* (2), 256-265.

60. Hobor, G., Surviving the era of deindustrialization: The new economic geography of the urban rust belt. *Journal of Urban Affairs* **2013,** *35* (4), 417-434.

61. Holdren, J. P.; Smith, K. R.; Kjellstrom, T.; Streets, D.; Wang, X.; Fischer, S., Energy, the environment and health. *New York: United Nations Development Programme* **2000**.

62. Huijbregts, M. A.; Hellweg, S.; Frischknecht, R.; Hendriks, H. W.; Hungerbühler, K.; Hendriks, A. J., Cumulative energy demand as predictor for the environmental burden of commodity production. *Environmental science & technology* **2010,** *44* (6), 2189-2196.

63. Jahan, S.; Yusoff, I. B.; Alias, Y. B.; Bakar, A. F. B. A., Reviews of the toxicity behavior of five potential engineered nanomaterials (ENMs) into the aquatic ecosystem. *Toxicology reports* **2017,** *4*, 211-220.

64. Jain, A.; Ranjan, S.; Dasgupta, N.; Ramalingam, C., Nanomaterials in food and agriculture: an overview on their safety concerns and regulatory issues. *Critical reviews in food science and nutrition* **2016,** (just-accepted), 00-00.

65. Jain, A.; Ranjan, S.; Dasgupta, N.; Ramalingam, C., Nanomaterials in food and agriculture: an overview on their safety concerns and regulatory issues. *Critical reviews in food science and nutrition* **2018,** *58* (2), 297-317.

66. Keller, A. A.; McFerran, S.; Lazareva, A.; Suh, S., Global life cycle releases of engineered nanomaterials. *Journal of nanoparticle research* **2013,** *15* (6), 1692.

67. Kennedy Alan, J.; Gunter Jonas, C.; Chappell Mark, A.; Goss Jennifer, D.; Hull Matthew, S.; Kirgan Robert, A.; Steevens Jeffery, A., Influence of nanotube preparation in Aquatic Bioassays. *Environmental Toxicology and Chemistry* **2010,** *28* (9), 1930-1938.

68. Kidd, M. J.; Westerhoff, P., Physicochemical Properties and Their Importance in the Environment: Current Trends in Nanomaterial Exposure. In *Physico-Chemical Properties of Nanomaterials*, Pan Stanford: 2018; pp 211-246.

69. Kim, N.; Xin, G.; Cho, S. M.; Pang, C.; Chae, H., Microwave-reduced graphene oxide for efficient and stable hole extraction layers of polymer solar cells. *Current Applied Physics* **2015,** *15*(9), 953-957.

70. Klaine, S. J.; Alvarez, P. J.; Batley, G. E.; Fernandes, T. F.; Handy, R. D.; Lyon, D. Y.; Mahendra, S.; McLaughlin, M. J.; Lead, J. R., Nanomaterials in the environment: behavior, fate, bioavailability, and effects. *Environmental toxicology and chemistry* **2008,** *27* (9), 1825-1851.

71. Köhler, A. R.; Som, C.; Helland, A.; Gottschalk, F., Studying the potential release of carbon nanotubes throughout the application life cycle. *Journal of Cleaner Production* **2008,** *16* (8-9), 927-937.

72. Kolm, P. N.; Tütüncü, R.; Fabozzi, F. J., 60 Years of portfolio optimization: Practical challenges and current trends. *European Journal of Operational Research* **2014,** *234* (2), 356-371.

73. Korn, R.; Korn, E., *Option pricing and portfolio optimization: modern methods of financial mathematics*. American Mathematical Soc.: 2001; Vol. 31.

74. Kunhikrishnan, A.; Shon, H. K.; Bolan, N. S.; El Saliby, I.; Vigneswaran, S., Sources, distribution, environmental fate, and ecological effects of nanomaterials in wastewater streams. *Critical Reviews in Environmental Science and Technology* **2015,** *45* (4), 277-318.

75. Lai, R. W.; Yeung, K. W.; Yung, M. M.; Djurišić, A. B.; Giesy, J. P.; Leung, K. M., Regulation of engineered nanomaterials: current challenges, insights and future directions. *Environmental Science and Pollution Research* **2018,** *25* (4), 3060-3077.

76. Lai, R. W.; Yeung, K. W.; Yung, M. M.; Djurišić, A. B.; Giesy, J. P.; Leung, K. M., Regulation of engineered nanomaterials: current challenges, insights and future directions. *Environmental Science and Pollution Research* **2018,** *25* (4), 3060-3077.

77. Laird, D. W.; Stegamat, R.; Richter, H.; Vejins, V.; Scott, L. T.; Lada, T. A., Organic photovoltaic devices comprising fullerenes and derivatives thereof. Google Patents: 2016.

78. Lee, J. H.; Yoon, C. S.; Hwang, J.-Y.; Kim, S.-J.; Maglia, F.; Lamp, P.; Myung, S.-T.; Sun, Y.-K., High-energy-density lithium-ion battery using a carbon-nanotube-Si composite anode and a compositionally graded Li[Ni0.85Co0.05Mn0.10]O2 cathode. *Energy & Environmental Science* **2016,** *9* (6), 2152-2158.

79. León, L. F.; Imberger, J.; Smith, R. E.; Hecky, R. E.; Lam, D. C.; Schertzer, W. M., Modeling as a tool for nutrient management in Lake Erie: a hydrodynamics study. *Journal of Great Lakes Research* **2005,** *31*, 309-318.

80. Lin, J.; Gaustad, G.; Trabold, T. A., Profit and policy implications of producing biodiesel–ethanol–diesel fuel blends to specification. *Applied energy* **2013,** *104*, 936-944.

81. Linkov, I.; Satterstrom, F. K.; Steevens, J.; Ferguson, E.; Pleus, R. C., Multi-criteria decision analysis and environmental risk assessment for nanomaterials. *Journal of Nanoparticle Research* **2007,** *9* (4), 543-554.

82. Liu, M.; Jin, H.; Uchaker, E.; Xie, Z.; Wang, Y.; Cao, G.; Hou, S.; Li, J., One-pot synthesis of in-situ carbon-coated Fe3O4 as a long-life lithium-ion battery anode. *Nanotechnology* **2017,***28* (15), 155603.

83. Liu, N.; Huo, K.; McDowell, M. T.; Zhao, J.; Cui, Y., Rice husks as a sustainable source of nanostructured silicon for high performance Li-ion battery anodes. *Scientific reports* **2013,** *3*, 1919.

84. Louwen, A.; Van Sark, W. G.; Faaij, A. P.; Schropp, R. E., Re-assessment of net energy production and greenhouse gas emissions avoidance after 40 years of photovoltaics development. *Nature communications* **2016,** *7*, 13728.

85. Lovern Sarah, B.; Klaper, R., Daphnia magna mortality when exposed to titanium dioxide and fullerene (C60) nanoparticles. *Environmental Toxicology and Chemistry* **2009,** *25* (4), 1132-1137.

86. Lowry, G. V.; Hill, R. J.; Harper, S.; Rawle, A. F.; Hendren, C. O.; Klaessig, F.; Nobbmann, U.; Sayre, P.; Rumble, J., Guidance to improve the scientific value of zeta-potential measurements in nanoEHS. *Environmental Science: Nano* **2016,** *3* (5), 953-965.

87. Markus, A. A.; Parsons, J. R.; Roex, E. W. M.; de Voogt, P.; Laane, R. W. P. M., Modelling the Release, Transport and Fate of Engineered Nanoparticles in the Aquatic Environment – A Review. In *Reviews of Environmental Contamination and Toxicology Volume 243*, de Voogt, P., Ed. Springer International Publishing: Cham, 2017; pp 53-87.

88. Mitra, A.; Flynn, K. J., Promotion of harmful algal blooms by zooplankton predatory activity. *Biology Letters* **2006,** *2* (2), 194.

89. Moore, E., Predation Experiment Video. 2017.

90. Moore, E. A.; Babbitt, C. W.; Gaustad, G.; Moore, S. T., Portfolio optimization of nanomaterial use in clean energy technologies. *Environmental science & technology* **2018,** *52* (7), 4440-4448.

91. Intelligence, M. *Global nanomaterials market-segmented by product type, end-user industry, and geography-trends and forecasts (2015–2020)*; 2016.

92. Muñoz, J. I.; de la Nieta, A. A. S.; Contreras, J.; Bernal-Agustín, J. L., Optimal investment portfolio in renewable energy: The Spanish case. *Energy Policy* **2009,** *37* (12), 5273-5284.

93. Mutel, C. L.; Pfister, S.; Hellweg, S., GIS-based regionalized life cycle assessment: how big is small enough? Methodology and case study of electricity generation. *Environmental science & technology* **2011,** *46* (2), 1096-1103.

94. Myers, J. P.; Dumanoski, D., *Our stolen future: are we threatening our fertility, intelligence, and survival?; a scientific detective story*. Little, Brown: 1996.

95. Nasibulin, A. G.; Moisala, A.; Brown, D. P.; Kauppinen, E. I., Carbon nanotubes and onions from carbon monoxide using Ni(acac)2 and Cu(acac)2 as catalyst precursors. *Carbon* **2003,** *41*(14), 2711-2724.

96. Nel, A.; Xia, T.; Mädler, L.; Li, N., Toxic potential of materials at the nanolevel. *science* **2006,** *311* (5761), 622-627.

97. Nel, A.; Xia, T.; Mädler, L.; Li, N., Toxic potential of materials at the nanolevel. *science* **2006,** *311* (5761), 622-627.

98. Nelson, P.; Gallagher, K.; Bloom, I., BatPaC (battery performance and cost) software, Argonne National Lab. 2017.

99. Conservation, N. Y. D. o. E. Seneca Lake. https://www.dec.ny.gov/outdoor/25574.html.

100. Newman, M. C., *Fundamentals of ecotoxicology: the science of pollution*. CRC press: 2014.

101. Nickum, J.; Bart Jr, H.; Bowser, P.; Greer, I.; Hubbs, C.; Jenkins, J.; MacMillan, J.; Rachlin, J.; Rose, J.; Sorensen, P., Guidelines for the use of fishes in research. *FISHERIES-BETHESDA-* **2004,** *29* (3), 26-26.

102. Laboratory, N.-G. L. E. R., About Our Great Lakes: Lake by Lake Profiles. 2019.

103. DEC, N., Onondaga Lake. 2019.

104. O'Connell, M. J.; Boul, P.; Ericson, L. M.; Huffman, C.; Wang, Y.; Haroz, E.; Kuper, C.; Tour, J.; Ausman, K. D.; Smalley, R. E., Reversible water-solubilization of single-walled carbon nanotubes by polymer wrapping. *Chemical physics letters* **2001,** *342* (3-4), 265-271.

105. Olivetti, E. A.; Ceder, G.; Gaustad, G. G.; Fu, X., Lithium-Ion Battery Supply Chain Considerations: Analysis of Potential Bottlenecks in Critical Metals. *Joule 1* (2), 229-243.

106. Olivetti, E. A.; Ceder, G.; Gaustad, G. G.; Fu, X., Lithium-ion battery supply chain considerations: analysis of potential bottlenecks in critical metals. *Joule* **2017,** *1* (2), 229-243.

107. County, O., Ambient Monitoring
Program: 2011. 2013.

108. OSHA. Working Safely with Nanomaterials
2013. https://www.osha.gov/Publications/OSHA_FS-3634.pdf.

109. Osman, T. M.; Rardon, D. E.; Friedman, L. B.; Vega, L. F., The commercialization of nanomaterials: Today and tomorrow. *JOM* **2006,** *58* (4), 21-24.

110. Pakarinen, K.; Petersen, E. J.; Leppänen, M. T.; Akkanen, J.; Kukkonen, J. V. K., Adverse effects of fullerenes (nC60) spiked to sediments on Lumbriculus variegatus (Oligochaeta). *Environmental Pollution* **2011,** *159* (12), 3750-3756.

111. Pakarinen, K.; Petersen Elijah, J.; Alvila, L.; Waissi-Leinonen Greta, C.; Akkanen, J.; Leppänen Matti, T.; Kukkonen Jussi, V. K., A screening study on the fate of fullerenes (nC60) and their toxic implications in natural freshwaters. *Environmental Toxicology and Chemistry* **2013,** *32* (6), 1224-1232.

112. Pakrashi, S.; Tan, C.; Wang, W. X., Bioaccumulation-based silver nanoparticle toxicity in Daphnia magna and maternal impacts. *Environmental toxicology and chemistry* **2017**.

113. Corporation, P. *@Risk for Excel*, Palisade: 2017.

114. Pan, Y.; Yan, S.-w.; Li, R.-z.; Hu, Y.-w.; Chang, X.-x., Lethal/sublethal responses of Daphnia magna to acute norfloxacin contamination and changes in phytoplankton-zooplankton interactions induced by this antibiotic. *Scientific reports* **2017,** *7*, 40385.

115. Parish, A., Production and applications of carbon nanotubes, carbon nanofibers, fullerenes, graphene and nanodiamonds: A global technology survey and market analysis. *ET-113. Stamford, CT, USA: Innovative Research and Products* **2011**.

116. Parker, N.; Keller, A. A., Variation in regional risk of engineered nanoparticles: nanoTiO 2 as a case study. *Environmental Science: Nano* **2019**.

117. Peretz, J.; Flaws, J. A., Bisphenol A down-regulates rate-limiting Cyp11a1 to acutely inhibit steroidogenesis in cultured mouse antral follicles. *Toxicology and applied pharmacology* **2013,** *271* (2), 249-256.

118. Peretz, J.; Vrooman, L.; Ricke, W. A.; Hunt, P. A.; Ehrlich, S.; Hauser, R.; Padmanabhan, V.; Taylor, H. S.; Swan, S. H.; VandeVoort, C. A., Bisphenol A and reproductive health: update of experimental and human evidence, 2007–2013. *Environmental health perspectives* **2014,** *122* (8), 775-786.

119. Persson, L. M.; Breitholtz, M.; Cousins, I. T.; de Wit, C. A.; MacLeod, M.; McLachlan, M. S., Confronting unknown planetary boundary threats from chemical pollution. ACS Publications: 2013.

120. Petersen, E. J.; Diamond, S. A.; Kennedy, A. J.; Goss, G. G.; Ho, K.; Lead, J.; Hanna, S. K.; Hartmann, N. B.; Hund-Rinke, K.; Mader, B.; Manier, N.; Pandard, P.; Salinas, E. R.; Sayre, P., Adapting OECD Aquatic Toxicity Tests for Use with Manufactured Nanomaterials: Key Issues and Consensus Recommendations. *Environmental Science & Technology* **2015,** *49* (16), 9532-9547.

121. Piccinno, F.; Gottschalk, F.; Seeger, S.; Nowack, B., Industrial production quantities and uses of ten engineered nanomaterials in Europe and the world. *Journal of Nanoparticle Research* **2012,** *14* (9), 1109.

122. Pourzahedi, L.; Zhai, P.; Isaacs, J. A.; Eckelman, M. J., Life cycle energy benefits of carbon nanotubes for electromagnetic interference (EMI) shielding applications. *Journal of Cleaner Production* **2017,** *142*, 1971-1978.

123. Quik, J. T.; de Klein, J. J.; Koelmans, A. A., Spatially explicit fate modelling of nanomaterials in natural waters. *Water research* **2015,** *80*, 200-208.

124. Quik, J. T.; Velzeboer, I.; Wouterse, M.; Koelmans, A. A.; Van de Meent, D., Heteroaggregation and sedimentation rates for nanomaterials in natural waters. *Water research* **2014,** *48*, 269-279.

125. Reap, J.; Roman, F.; Duncan, S.; Bras, B., A survey of unresolved problems in life cycle assessment. *The International Journal of Life Cycle Assessment* **2008,** *13* (5), 374.

126. Revel, M.; Fournier, M.; Robidoux, P. Y., Toxic effect of single walled carbon nanotubes combined with cadmium to the crustacean Daphnia magna. *International Letters of Natural Sciences* **2015,** *42*.

127. Riesz, J.; Elliston, B., Research and deployment priorities for renewable technologies: Quantifying the importance of various renewable technologies for low cost, high renewable electricity systems in an Australian case study. *Energy Policy* **2016,** *98*, 298-308.

128. Roques, F. A. In *Analytic Approaches to Quantify and Value Fuel Mix Diversity*, 7th Conference on Applied Infrastructure Research, Berlin, Germany, TU Berlin: Berlin, Germany, 2008.

129. Roques, F.; Hiroux, C.; Saguan, M., Optimal wind power deployment in Europe—A portfolio approach. *Energy Policy* **2010,** *38* (7), 3245-3256.

130. Rowan, A., Shortcomings of LD50-values and acute toxicity testing in animals. *Acta pharmacologica et toxicologica* **1983,** *52*, 52-64.

131. Rowell, H. C., Paleolimnology of Onondaga Lake: the history of anthropogenic impacts on water quality. *Lake and Reservoir Management* **1996,** *12* (1), 35-45.

132. Salciccioli, M.; Edie, S. M.; Vlachos, D. G., Adsorption of Acid, Ester, and Ether Functional Groups on Pt: Fast Prediction of Thermochemical Properties of Adsorbed Oxygenates via DFT-Based Group Additivity Methods. *The Journal of Physical Chemistry C* **2012,** *116* (2), 1873-1886.

133. Savolainen, K.; Backman, U.; Brouwer, D.; Fadeel, B.; Fernandes, T.; Kuhlbusch, T.; Landsiedel, R.; Lynch, I.; Pylkkänen, L., Nanosafety in Europe 2015–2025: towards safe and sustainable nanomaterials and nanotechnology innovations. *Finnish Institute of Occupational Health, Helsinki* **2013**.

134. Schilling, J.; Logan, J., Greening the rust belt: A green infrastructure model for right sizing America's shrinking cities. *Journal of the American Planning Association* **2008,** *74* (4), 451-466.

135. Schmidt, C. W., TSCA 2.0: A new era in chemical risk management. National Institute of Environmental Health Sciences: 2016.

136. Schultz, T. W.; Kennedy, J. R., The fine structure of the digestive system of Daphnia pulex (Crustacea: Cladocera). *Tissue and Cell* **1976,** *8* (3), 479-490.

137. Schwerhoff, G.; Sy, M., Financing renewable energy in Africa–Key challenge of the sustainable development goals. *Renewable and Sustainable Energy Reviews* **2017,** *75*, 393-401.

138. Scott, R. P.; Cullen, A. C.; Fox-Lent, C.; Linkov, I., Can Carbon Nanomaterials Improve CZTS Photovoltaic Devices? Evaluation of Performance and Impacts Using Integrated Life-Cycle Assessment and Decision Analysis. *Risk Analysis* **2016,** *36* (10), 1916-1935.

139. Seda, B. C.; Ke, P. C.; Mount, A. S.; Klaine, S. J., Toxicity of aqueous C70-gallic acid suspension in Daphnia magna. *Environmental toxicology and chemistry* **2012,** *31* (1), 215-220.

140. Sensfuß, F.; Ragwitz, M.; Genoese, M., The merit-order effect: A detailed analysis of the price effect of renewable electricity generation on spot market prices in Germany. *Energy policy* **2008,** *36* (8), 3086-3094.

141. Research, S. https://www.sesres.com/.

142. Sharma, B.; Birrell, S.; Miguez, F., Spatial modeling framework for bioethanol plant siting and biofuel production potential in the US. *Applied energy* **2017,** *191*, 75-86.

143. Shen, T.; Xia, X.-h.; Xie, D.; Yao, Z.-j.; Zhong, Y.; Zhan, J.-y.; Wang, D.-h.; Wu, J.-b.; Wang, X.-l.; Tu, J.-p., Encapsulating silicon nanoparticles into mesoporous carbon forming pomegranate-structured microspheres as a high-performance anode for lithium ion batteries. *Journal of Materials Chemistry A* **2017,** *5* (22), 11197-11203.

144. Shrivastava, A.; Gupta, V. B., Methods for the determination of limit of detection and limit of quantitation of the analytical methods. *Chronicles of young scientists* **2011,** *2* (1), 21.

145. Skilodimou, H. D.; Bathrellos, G. D.; Chousianitis, K.; Youssef, A. M.; Pradhan, B., Multi-hazard assessment modeling via multi-criteria analysis and GIS: a case study. *Environmental Earth Sciences* **2019,** *78* (2), 47.

146. Snäll, T.; Lehtomäki, J.; Arponen, A.; Elith, J.; Moilanen, A., Green infrastructure design based on spatial conservation prioritization and modeling of biodiversity features and ecosystem services. *Environmental management* **2016,** *57* (2), 251-256.

147. Song, R.; Qin, Y.; Suh, S.; Keller, A. A., Dynamic model for the stocks and release flows of engineered nanomaterials. *Environmental science & technology* **2017,** *51* (21), 12424-12433.

148. Souter, I.; Smith, K. W.; Dimitriadis, I.; Ehrlich, S.; Williams, P. L.; Calafat, A. M.; Hauser, R., The association of bisphenol-A urinary concentrations with antral follicle counts and other measures of ovarian reserve in women undergoing infertility treatments. *Reproductive toxicology* **2013,** *42*, 224-231.

149. Tang, B. Z.; Xu, H., Preparation, alignment, and optical properties of soluble poly (phenylacetylene)-wrapped carbon nanotubes. *Macromolecules* **1999,** *32* (8), 2569-2576.

150. Tao, X.; Fortner, J. D.; Zhang, B.; He, Y.; Chen, Y.; Hughes, J. B., Effects of aqueous stable fullerene nanocrystals (nC60) on Daphnia magna: Evaluation of sub-lethal reproductive responses and accumulation. *Chemosphere* **2009,** *77* (11), 1482-1487.

151. Tisher, E. M., Re-Stitching the Urban Fabric: Municipal-Driven Rehabilitation of Vacant and Abandoned Buildings in Ohio's Rust Belt. *Vt. J. Envtl. L.* **2013,** *15*, 173.

152. Bureau, U. S. C. Labor Force Statistics. https://www.census.gov/topics/employment/labor-force.html.

153. UN, G. A. *Transforming our world: The 2030 agenda for sustainable development*; A/RES/70/1, 21 October: 2015.

154. Information, U. M.
Graphite. https://minerals.usgs.gov/minerals/pubs/commodity/graphite/.

155. Vance, M. E.; Kuiken, T.; Vejerano, E. P.; McGinnis, S. P.; Hochella, M. F.; Rejeski, D.; Hull, M. S., Nanotechnology in the real world: Redeveloping the nanomaterial consumer products inventory. *Beilstein Journal of Nanotechnology* **2015,** *6*, 1769-1780.

156. Vázquez-Santos, M. a. B.; Morales, E.; Tartaj, P.; Amarilla, J. M., Toward a Better Understanding and Optimization of the Electrochemical Activity of Na-Ion TiO2 Anatase Anodes Using Uniform Nanostructures and Ionic Liquid Electrolytes. *ACS Omega* **2017,** *2* (7), 3647-3657.

157. Von der Kammer, F.; Ferguson, P. L.; Holden, P. A.; Masion, A.; Rogers, K. R.; Klaine, S. J.; Koelmans, A. A.; Horne, N.; Unrine, J. M., Analysis of engineered nanomaterials in complex matrices (environment and biota): general considerations and conceptual case studies. *Environmental Toxicology and Chemistry* **2012,** *31* (1), 32-49.

158. Wadia, C.; Albertus, P.; Srinivasan, V., Resource constraints on the battery energy storage potential for grid and transportation applications. *Journal of Power Sources* **2011,** *196* (3), 1593-1598.

159. Wallace, M. L.; Rafols, I., Research portfolio analysis in science policy: moving from financial returns to societal benefits. *Minerva* **2015,** *53* (2), 89-115.

160. Wang, P.; Luo, C.; Li, Q.; Chen, S.; Hu, Y., Mitochondrion-mediated apoptosis is involved in reproductive damage caused by BPA in male rats. *Environmental toxicology and pharmacology* **2014,** *38* (3), 1025-1033.

161. Wiesner, M. R.; Lowry, G. V.; Alvarez, P.; Dionysiou, D.; Biswas, P., Assessing the risks of manufactured nanomaterials. ACS Publications: 2006.

162. Winner, K. R. K.; Steinkamp, M. P.; Lee, R. J.; Swat, M.; Muller, C. Y.; Moses, M. E.; Jiang, Y.; Wilson, B. S., Spatial modeling of drug delivery routes for treatment of disseminated ovarian cancer. *Cancer research* **2016,** *76* (6), 1320-1334.

163. Center, W. W., Project on emerging nanotechnologies. *Consumer Products Inventory. Disponível em: http://www. nanotechproject. org/inventories/consumer/analysis_draft/http://www. ecosynthetix. com/BioBasedPkg. html (disponível até dia 26 de fev de* **2009**.

164. Wu, S. R.; Li, X.; Apul, D.; Breeze, V.; Tang, Y.; Fan, Y.; Chen, J., Agent-Based Modeling of Temporal and Spatial Dynamics in Life Cycle Sustainability Assessment. *Journal of Industrial Ecology* **2017,** *21* (6), 1507-1521.

165. Wu, Z.-S.; Ren, W.; Xu, L.; Li, F.; Cheng, H.-M., Doped graphene sheets as anode materials with superhigh rate and large capacity for lithium ion batteries. *ACS nano* **2011,** *5* (7), 5463-5471.

166. Xu, M.; Cai, H.; Liang, S., Big data and industrial ecology. *Journal of Industrial Ecology* **2015,** *19* (2), 205-210.

167. Yang, Y.; Westerhoff, P., Presence in, and release of, nanomaterials from consumer products. In *Nanomaterial*, Springer: 2014; pp 1-17.

168. Yoo, E.; Kim, J.; Hosono, E.; Zhou, H.-s.; Kudo, T.; Honma, I., Large reversible Li storage of graphene nanosheet families for use in rechargeable lithium ion batteries. *Nano letters* **2008,** *8* (8), 2277-2282.

169. Yu, J.; Fan, J.; Cheng, B., Dye-sensitized solar cells based on anatase TiO2 hollow spheres/carbon nanotube composite films. *Journal of Power Sources* **2011,** *196* (18), 7891-7898.

170. Zhai, P.; Isaacs, J. A.; Eckelman, M. J., Net energy benefits of carbon nanotube applications. *Applied Energy* **2016,** *173*, 624-634.

171. Zhang, L.; Fang, M., Nanomaterials in pollution trace detection and environmental improvement. *Nano Today* **2010,** *5* (2), 128-142.

172. Zhang, W.; Ravi, S.; Silva, P., Application of carbon nanotubes in polymer electrolyte based fuel cells. *Reviews on Advanced Materials Science* **2011,** *29* (1), 1-14.

173. Zhao, W.; Song, C.; Pehrsson, P. E., Water-soluble and optically pH-sensitive single-walled carbon nanotubes from surface modification. *Journal of the American Chemical Society* **2002,***124* (42), 12418-12419.

174. Zhu, S.; Oberdörster, E.; Haasch, M. L., Toxicity of an engineered nanoparticle (fullerene, C60) in two aquatic species, Daphnia and fathead minnow. *Marine Environmental Research* **2006,** *62*, S5-S9.

175. Zöllner, E.; Santer, B.; Boersma, M.; Hoppe, H. G.; Jürgens, K., Cascading predation effects of Daphnia and copepods on microbial food web components. *Freshwater Biology* **2003,** *48*(12), 2174-2193.

176. Zuverza-Mena, N.; Martinez-Fernandez, D.; Du, W.; Hernandez-Viezcas, J. A.; Bonilla-Bird, N.; Lopez-Moreno, M. L.; Komarek, M.; Peralta-Videa, J. R.; Gardea-Torresdey, J. L., Exposure of engineered nanomaterials to plants: Insights into the physiological and biochemical responses-A review. *Plant Physiology and Biochemistry* **2017,** *110*, 236-264.

APPENDIX A

Table 1. Literature review of fullerene solubilization methods used to inform methods development for ecotoxicity experiments.

Fullerene Solubilization Methods								
Title	**Amount of Fullerene**	**Dissolved in**	**Amount of Solvent/ Water**	**Type of Preparation**	**Stirring Rate**	**Time**	**Preparation for Analysis**	**Concentration Analysis**
Naphthalene Adsorption and Desorption from Acqueous C60 Fullerene Cheng et al.	mg, 21+/-0.1 and 24+/-0.1	Electrolyte solution	mL, 0.1 headspace	Magnetic stirring: Sealed with teflon-septum caps, stirred on a magnetic stirrer	rpm, 1000	days, 2	Adsorption induced by injecting naphthalene stock solution into two sample vials.	C60 was sampled after 2 days of mixing and dissolved in toluene. It was analyzed by UV-vis spectrophotometer.
Analysis of Fullerene C60 and Kinetic Measurements for its Accumulation and Depuration in Daphnia Magna Tervonen et al.	mg, 250 of crystalline fullerene	AFW	mL, 500	Magnetic stirring	rpm, 1000	days, 28	The fullerene suspension was filtered with glass fibers to remove the largest agglomerates.	Concentration was analyzed by extracting fullerenes to toluene and recording spectra from 280 to 600 nm using a spectrophotometer and recording a calibration curve at 335 nm.
Ecotoxicology of carbon-based engineered nanoparticles: Effects of fullerene (C60) on aquatic organisms Oberdorster et al.	mg, 500 fullerene	Milli-Q Water	mL, 1000	Water-stirred (better than THF which contributes to toxicity)	-	days, 56	Stirring produces water-soluble fullerene at up to 35 ppm concentrations in milliQ water. In full-strength artifical sea water, water-soluble fullerene came out of solution	Concentration is measured by first oxidizing the fullerene solution with a strong oxidant (bleach or magnesium persulfate) and extracting toluene. The absorbance of toluene is measured at 332 nm compared to a standard curve.

Distribution of Fullerenes between Sediment and Water in Freshwaters Pakarinen et al.	mg, 100+/-0.1 crystalline fullerene	AFW	mL, 500	Magnetic stirring	rpm, 1000	days, 28	Sediment (5 g ww) and AFW sample placed in 10 cm long, 50 mL capped glass tube. Fullerene added to produce 8 concentrations with the final volume at 30mL. Tubes then placed vertically in rotary mixer around horizontal axis at 6 rpm for six days.	Sampling with centrifuging so that overlying water could be replaced with clean water after six days. Water samples of 1.5 mL were analyzed with the help of toluene extraction and absorbance measurements at 335 nm to record amount of fullerenes. Clean AFW added to test tubes and mixing/sampling procedures were repeated on the 1st, 2nd, 4th, and 8th day after the starting day.
Extraction and high-performance liquid chromatographic analysis of C60, C70, and [6,6]-phenyl C61-butyric acid methyl ester in synthetic and natural waters Bouchard et al.	mg, 100 of fullerene	Appropriate aqueous medium	mL, 400	Extended stirring technique, magnetic stirring	-	days, 13	Stirring was terminated and the suspension sat for an hour before sampling. Several aliquots were collected, specifically a 1-mL aliquot that was placed in a 4-mL extraction vessel containing 100 micro Liters of 1 M Mg(ClO4)2. A 1-mL volume of toluene was added and it was vortexed and placed horizontally on an orbital shaker at 200 rpms for 30 minutes. 800-mL of the sample was removed after 15 minutes from the toluene supernatant layer for analysis by HPLC-UV. The samples were then frozen and three sequential extractions were taken. The fullerene mass extracted each time was determined by the HPLC.	Fullerene calibration standards were prepared by dissolution in toluene and sonication. A Dionex Ultimate 3000 HPLC system with UV/vis-DAD was used to perform quantitative analyses. PALS was used to estimate the electrical potential of the fullerene particles in suspension.

Table 2. Literature review of fullerene concentrations used in past fullerene experiments.

Literature Review of Fullerene Concentrations Used in Experiments				
Literature Source	**Concentration Added**	**Medium Used**	**Method**	**Results & Observations**
Pakarinen et al. 2011	10-50 mg/kg	Sediment	L. variegatus were exposed to 10 and 50 mg fullerenes/kg sediment dry mass for 28 days. Stock solutions made by mixing 100 mg fullerene in 500 mL AFW. Concentration was found by extracting fullerenes to toluene and measuring absorbance. After the fullerene suspension was spiked to 1000 g wet Lake sediment, it was mixed for 4 hours by vigorous stirring using a rotating metal blade.	To quantify fullerene, sediments were dried overnight in an oven at 105 degrees C and pulverized in a mortar. Test sediments (60 g ww per container) were mixed, weighed, and added to 300 mL glass jars. 15 replicates were prepared at nominal dry mass concentrations and 15 control jars were also prepared. 100 mL of AFW gently added to sediments to minimize re-suspension. Sediments settled for 1 day and a few millimeter layer of quartz sand was deposited onto the sediment. Fullerenes did not affect the burrowing behavior of the worms and only minimal effects such as decreased depuration efficiency and pellet production, smaller masses, and damaged cuticle fibers were shown.
Wang et al. 2014	0.05-11.33 mg/kg	Sediment	Toxicity screening test and 28-day bioaccumulation test for L. variegatus were performed.	No mortality observed and the BSAF was relatively low. An oxidative stress indicator (CAT) showed elevation on day 14, which was the highest observed body residues in the study (199+/80 micrograms C60/kg dry weight sediment).
Li and Alvarez 2011	2,000 mg/kg and 10,000 mg/kg; 5,000 mg/kg, 10,000 mg/kg, and 50,000 mg/kg	Sediment	Soil mixtures were tumbled and mixed overnight to achieve homogenous mixing. Phenanthrene was added to separate treatments as a positive control.	Earthworms did not significantly avoid soil amended with C60 powder during 48 hours. Worms lost weight during 28 day incubation because they were not provided food. At higher concentrations, the earthworm cocoon production was decreased.
Van der Ploeg et al. 2013	0, 15, 154 mg/kg	Sediment	Containers with soil and earthworms maintained under constant conditions (24 h light, 15 degrees C, 61% humidity). C60 was dissolved in an aqueous soil extract by stirring control soil in Milli-Q water (0.4 g soil/mL) for one hour. It was then filtered and C60 was added to a part of the extract to a final nominal concentration of 2 g/L.	First experiment had healthy adult earthworms exposed to the different concentrations for four weeks. 8 replicates and 40 earthworms per treatment. The second experiment had offspring from parent earthworms exposed to the same C60 treatment for 350 days. For the adult earthworms exposed to C60 for only four weeks, only one of the genes showed a clear concentration-dependent change of expression in tissue homogenates. The study shows that earthworms exposed to C60 in soil can suffer adverse sub-lethal effects, which include loss of protective cuticle and altered gene expression of the whole organism.

Pakarinen et al 2014	1-70 mg/L sediment	Sediment/AFW Mixture	C60 solution added to sediment/AFW mixture, and mixed on a horizontal rotary mixer for 6 days	c60 resolubilized slowly from the sediment, eventually reaching a steady state
Oberdorster et al. 2006	Daphnid: 35 and 30 mg/L Copepod: 0 mg/L, 3.75 mg/L, 7.5 mg/L, 15 mg/L, and 22.5 mg/L	Water	10 neonatal daphnids per exposure group individually exposed to 40 mL water-soluble fullerene in RHW in 50 mL glass beakers. Initial results taken after 48 h and then life-cycle assays performed for 21 days. Uptake study also performed exposing daphnid to 30 ppm fullerene for up to 5 days. Copepods were also looked at and were observed in a 96-well plate at different concentrations.	Daphnia reduced offspring production at 2.5 and 5 ppm. At the end of 21 days, fewer and smaller broods produced but surviving daphnids adapted to the nC60 exposure. In copecods, the high salt content of the seawater caused precipitation of fullerene and the max concentration that was seen was 22.5 ppm.
Spohn et al. 2009	6 mg/L, 12 mg/L, and 24 mg/L	Water	10 Daphnia offspring were exposed to the different concentrations and survival numbers were recorded after 0, 18, 24, and 48 hours to calculate the EC50 value and compared to untreated controls. SEM was used to analyze the morphological appearance.	The lack of mortality did not exclude any other subtoxic effects like behavioral changes or light exposure effects. THF suspended nC60 didn't shown toxic effects to Daphnia or A549 lung cells when side products were eliminated by additional washing steps.
Tao et al. 2009	0.8, 0.7, 0.6, 0.5, 0.45, 0.4, 0.35, 0.3,0.2, or 0 mg/L	Water	D. magna were maintained in an open 2000 mL flask with 12 hours light, 12 hours dark cycles. Sub-lethal concentrations were determined using 48 h acute toxicity test as described by EPA Standard Procedure 2024. The LOEC of the daughter daphnids was used as the sub-lethal toxic concentration for the mother.	3 physiological phenomena related to reproduction (death of fetuses, ability of mother to reproduce after exposure, and time to first brood) were evaluated. n-C60 accumulation in fetuses was much higher than in the mother, max concentration of 7000 mg/kg.
Gao et al. 2009	1,000 mg/L	Water	200 mg C60 added to 200 mL natural water. Suspensions were gently mixed on a horizontal shaker to mimic waves. They were then filtered and then two toxicity tests were performed--Ceriodaphnia dubia assay and MetPLATE test.	High levels of C60 were stabilized in organic-rich Sr-1 and Sr-2 samples reaching average concentrations of 1.62 mg/L and 3.09 mg/L. Results show that the dispersion and toxicity of nanoparticles vary significantly with solution chemistry. Measured toxicity was not linearly correlated with the concentrations of suspended MNs as revealed by the two tests.

Hancock et al. 2012	2, 1, 0.5, 0.1, and 0.01 mg/L, control also included	Water	Individual S. typhimurium TA 100 colonies were used to inoculate DM media. The growth of bacteria was followed by measuring OD600 for 24 hours. Mutagenicity was determined by the Muta-Chromoplate Analytical test Kit.	Results showed that particles were heavily aggregated. Growth was impacted by C60 at concentrations greater than 0.5 mg/L over the course of 24 hours. C60 concentrations greater than 0.1 mg/L were found to be mutagenic.
Zhu et al. 2006	-	Water	The current study investigates differences in acute toxicity to Daphnia magna between THF-solubilized and water-stirred-nC60 as arrange-find for further assays in adult male fathead minnow (FHM, Pimephales promelas). The daphnia 48-h LC50 for THF-nC60 was at least one order of magnitude less (0.8 ppm) than that for waterstirred-nC60 (>35 ppm). FHM were dosed with either 0.5 ppm of THF- or water-stirred-nC60 for 48 h. There was 100% mortality in the THF-nC60-exposed fish between 6 and 18 h, while the water-stirred-nC60-exposed fish showed no obvious physical effects after 48 h. Water-stirred-nC60 elevated LPO in brain, significantly increased LPO in gill, and significantly increased expression of CYP2 family isozymes in liver as compared to control fish.	The 48 h LC50 for THF-nC60 was considerably lower (more toxic) than the 48 h LC50 for water-stirred-nC60 (0.8 ppm compared to >35 ppm), respectively.
Zhu et al. 2008	100, 50, 25, 10, 5, 1, 0.5 mg/L	Water, Milli-Q	Each of the powders was added to 100 mL of reconstituted water prepared with Milli-Q water, 64.75 mg/L NaHCO3, 5.75 mg/L KCl, 123.25 mg/L MgSO, 7 H2O, and 294 mg/L CaCl2, 2 H2O, in accordance with OECD. The suspensions were shaken vigorously at room temperature to obtain a final concentration of 1,000 mg/L.	The EC50 of immobilization and LC50 of mortality for C60 NPs were calculated as 9.344 mg/L and 10.515 mg/L, respectively.

Baun et al. 2008	5-8 mg/L	Water, prolonged stirring in Milli-Q	-	Addition of C60 increased the toxicity of phenanthrene more than 10 times when results were expressed as water phase concentrations. Uptake of phenanthrene was faster with C60. 1.7 times higher steady state concentrations were found, but due to very fast clearance after transfer to clean water, accumulation of phenanthrene.

Table 3. Literature review of fullerene/toluene extraction methods used to inform methods development for ecotoxicity experiments.

Toluene Extraction Methods from Literature										
Title	**Suspe-nsion color**	**nC60 added**	**Emulsion agent added**	**Toluene Added**	**Mixing**	**Time**	**Settling**	**Toluene Extraction/Analysis**	**Wave-length**	**C60 Concentration**
Quantification of fullerene aggregate nC60 in wastewater by high-performance liquid chromatography with UV-vis spectroscopic and mass spectrometric detection Wang et al.	Yellow /brown	mL, 5	mL, 5 (2% NaCl)	mL, 5	Vigorously agitated	minutes, 30	Settled until complete separation of acqueous and toluene phases	1-cm UV-vis absorbance of C60 measured with UV-vis spectrophotometer	nm, 332	Calculated using calibration curve from a series of known concentrations of C60 in toluene.
Quantification of fullerene aggregate nC60 in wastewater by high-performance liquid chromatography with UV-vis spectroscopic and mass spectrometric detection Wang et al.	Yellow /brown	mL, 40	*amount not mentioned, presence of salt avoided emulsion problem	mL, 4	Shaker	hours, 4	Settled until complete separation of acqueous and toluene phases	1-cm UV-vis absorbance of C60 measured with UV-vis spectrophotometer	nm, 332	Calculated using calibration curve from a series of known concentrations of C60 in toluene.
Quantification of fullerene aggregate nC60 in wastewater by high-performance liquid chromatography with UV-vis spectroscopic and mass spectrometric detection	Yellow /brown	L, 1	N/A	mL, 10	SPE cartridges 5-6 mL/min and dried under vacuum	N/A	Concentrated with nitrogen to 0.5 mL and diluted with toluene to 1 mL.	1-cm UV-vis absorbance of C60 measured with UV-vis spectrophotometer	nm, 332	Calculated using calibration curve from a series of known concentrations of C60 in toluene.

Wang et al.										
Detection of fullerenes (C60 and C70) in commercial cosmetics Benn et al.	N/A	g, 0.5-1.5 (cosmetic)	mL, 11.3 of acetic acid (GAA) used to control emulsion	mL, 5 in addition to mL, 5 nanopure water and mL, 2 of 100 mM Mg(ClO4)2	Shaker, orbital table at 35 RPM	hours, 1	Settled until complete separation of acqueous and toluene phases for about minutes, 20	The toluene phase was sampled and evaporated under nitrogen and 1 mL was sonicated for 3-5 minutes.	N/A	LC-MS and APCI were used for analysis and quantification of fullerenes.
Trace Analysis of fullerenes in biological samples by simplified liquid-liquid extraction and high-performance liquid chromatography Xia et al.	N/A	mL, 2	mL, 4.5 of GAA used for emulsion problem instead of NaCl	mL, 4.5	Shaker, rotary at 500 rpm and centrifuged at 1500g	minutes, 10	After centrifugation, mL 4 of toluene was measured into conical evaporation tube for evaporation.	N/A	N/A	N/A

Aggregation and Deposition Kinetics of Fullerene (C60) Nanoparticles Chen et al.	Clear, dark purple mixtur e	mg, 36	mL, 1.5 of HPLC-grade ethanol	mL, 30 HPLC-grade toluene	Sonicati ng probe used to sonicate	hours, 3 and every minutes, 20 DI water topped off for evapora tion	Filtered under vacuum and clear yellow filtrate stored in the dark at degrees C, 4	TEM images of nanoparticles were captured for further size analysis and DLS after toluene extraction	nm, 532	Nanoparticles measured over a range of NaCl and CaCl2 concentrations at pH 5.2 and degrees C, 25
C60 in Water: Nanocrystal Formation and Microbial Response Fortner et al.	Yellow	volu me, 1 of water with nC60	volume, 2/5 0.1 M Mg(ClO4)2	Volume, 1	Vigorou sly mixed	minutes, 30	Water portion of system was frozen in a dry ice bath to allow for removal of toluene	HPLC analysis performed	4.6 x 250 mm	A gravimetric procedure was used to evaporate 2 mL of a 100 mg/L concentration suspension to determine the weight of the nC60 in water.

Appendix B

Supplemental Data

Contents

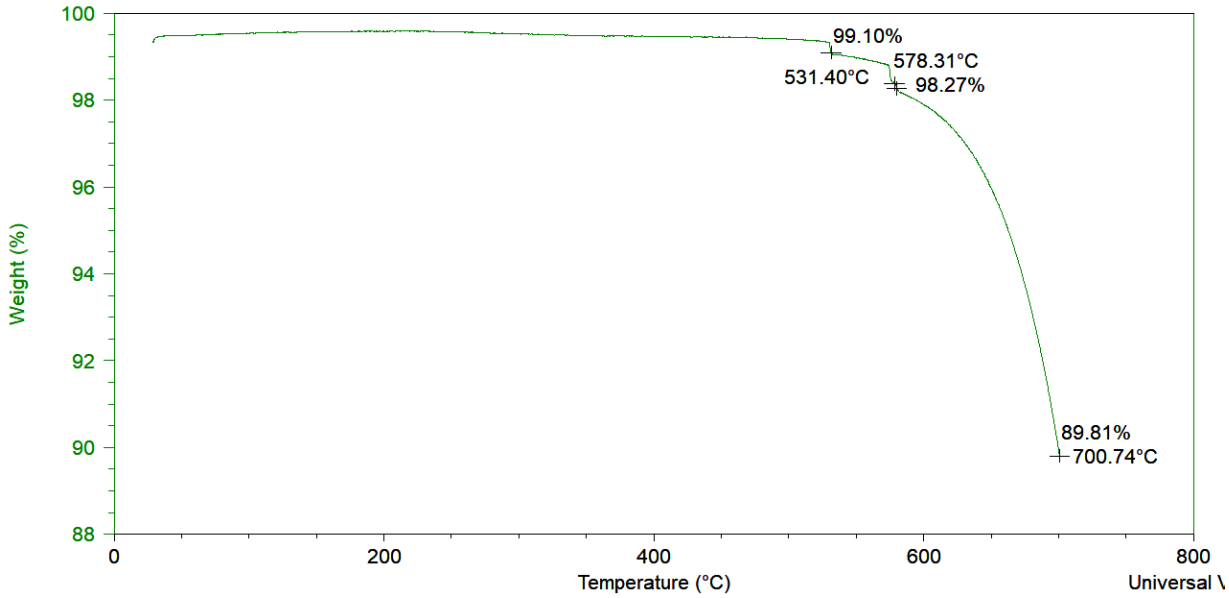

Figure S1. Thermogravimetric analysis of C60 in SFW. C60 has a stepwise degradation, but the weight loss in the initial steps is negligible.

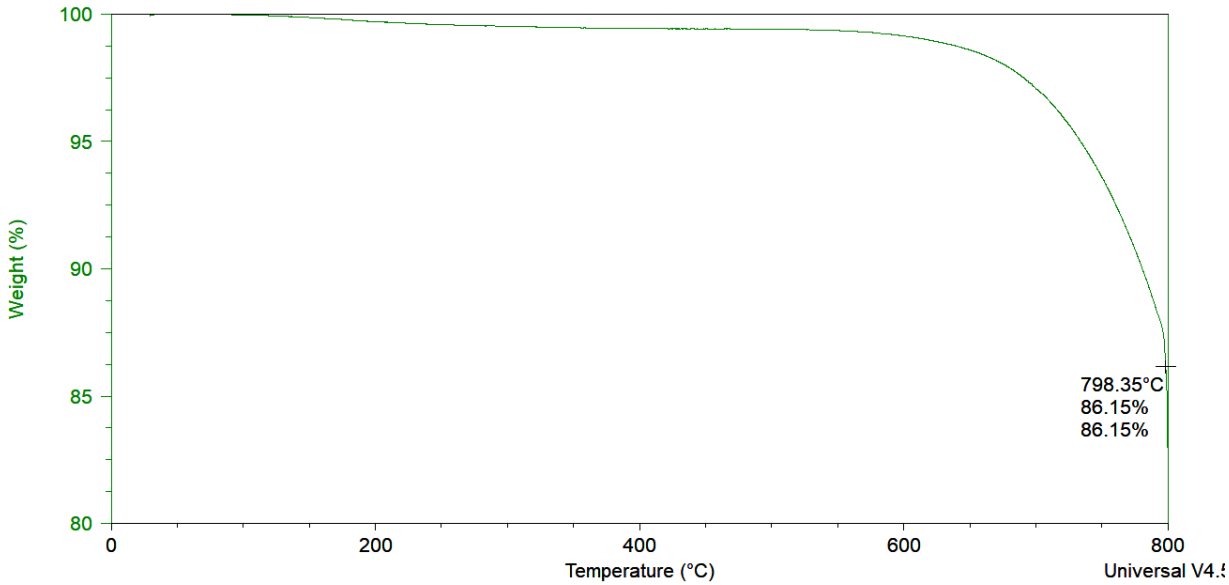

Figure S2. Thermogravimetric analysis of C70 in SFW. C70 degrades in a single step.

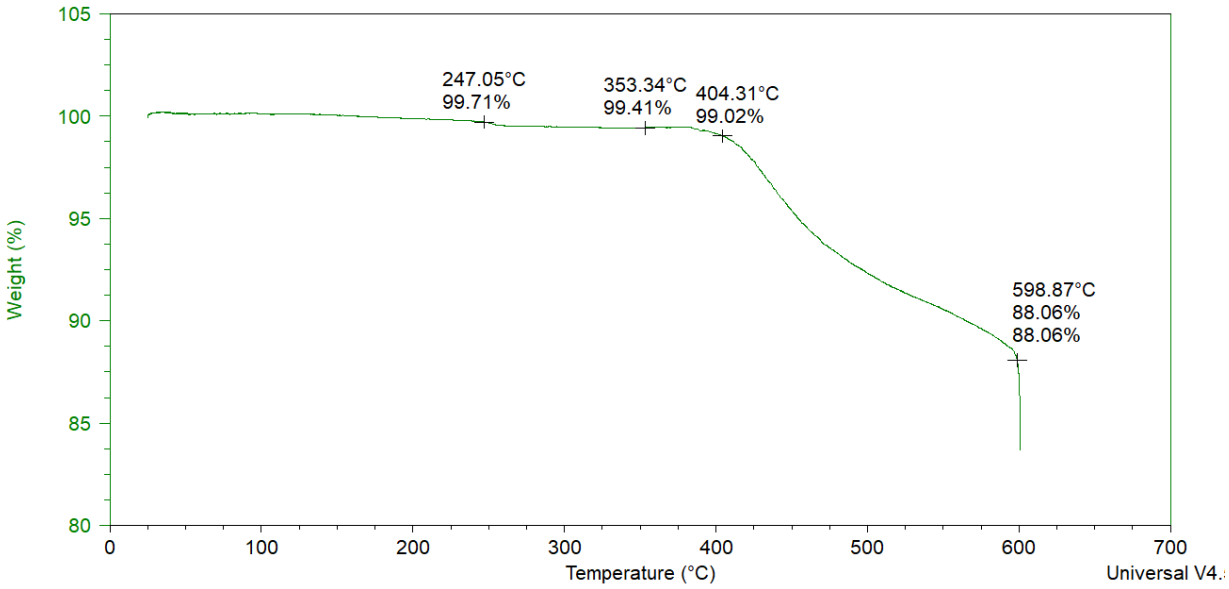

Figure S3. Thermogravimetric analysis of PCBM in SFW. PCBM has a stepwise degradation and the initial weight loss can be attributed to the polymeric nature of the butryic acid methyl ester present in PCBM.

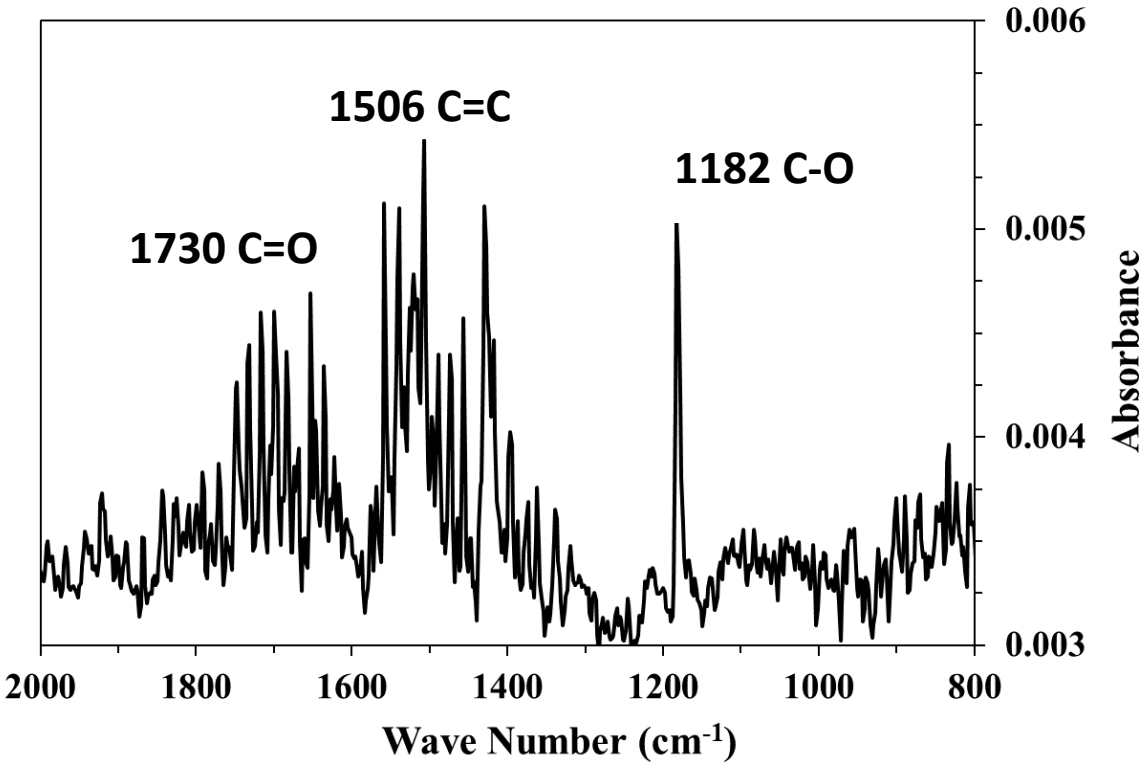

Figure S4. FTIR analysis of C60 in SFW. The light absorbance by the C60 particles as a function of wavelength demonstrate the characteristic peaks of C60.High intensity peaks indicate larger particles in the tested sample.

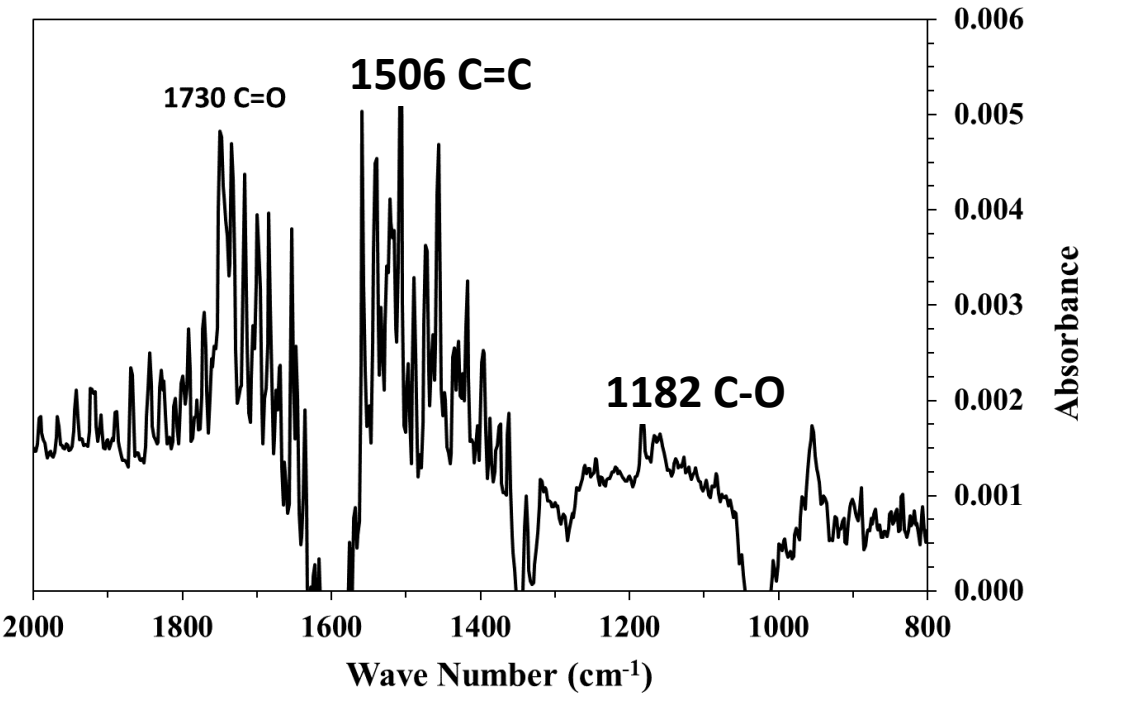

Figure S5. FTIR analysis of C70 in SFW. The light absorbance by the C60 particles as a function of wavelength demonstrate the characteristic peaks of C70. High intensity peaks indicate larger particles in the tested sample.

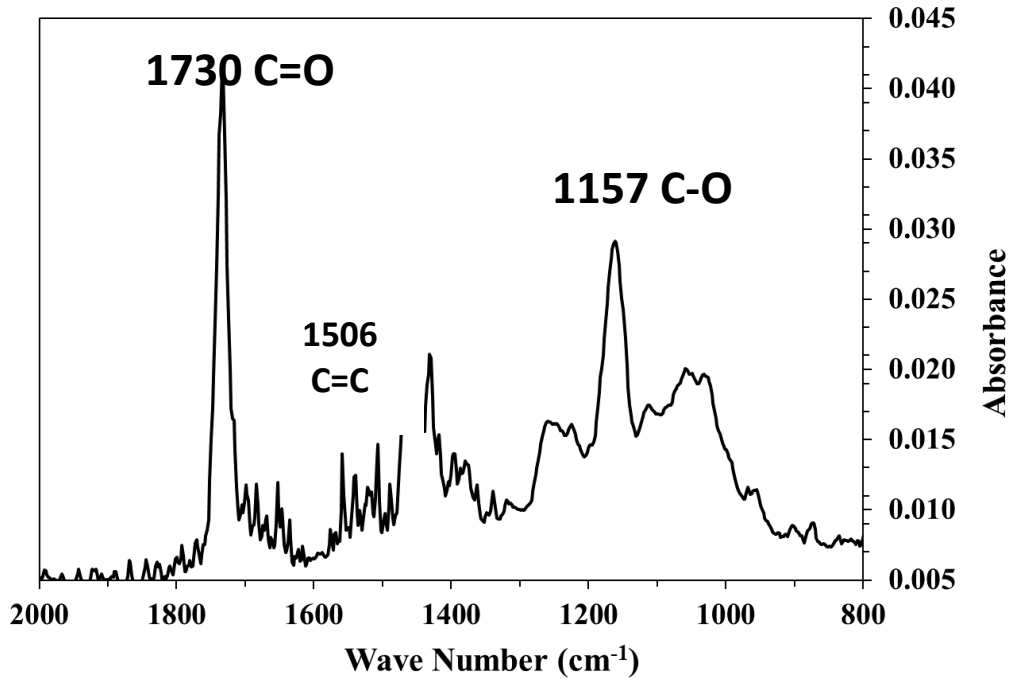

Figure S6. FTIR analysis of PCBM in SFW. The light absorbance by the PCBM particles as a function of wavelength demonstrate the characteristic peaks of PCBM. High intensity peaks indicate larger particles in the tested sample.

Table S1. Comparison of mean heart rates for fullerene treatments relative to the control at all time points.

		Treatment	$\bar{x}^1$	$\bar{x}^2$
Heart rate (0-h)	*D. pulex* (juvenile)	Control	235.1	235.1
		C60	233.8	233.8
		C70	236.7	236.7
		PCBM	231.1	231.1
			$\bar{x}^1$	$\bar{x}^2$
Heart rate (24-h)	*D. pulex* (juvenile)	Control	241.3	241.3
		C60	280.8	280.8
		C70	282.5	282.5
		PCBM	292.0	292.0
			$\bar{x}^1$	$\bar{x}^2$
Heart rate (48-h)	*D. pulex* (juvenile)	Control	220.7	220.7
		C60	285.3	308.4
		C70	266.1	303.2
		PCBM	224.8	294.7

1 Mean heart rates of all individuals

2 Mean heart rates excluding heart rates of the individuals that died within 12-h of the 48-h time point

Calculation and Assumptions for Chronic Concentration:

To determine an environmentally relevant concentration for our chronic studies, values were used from the literature to calculate a worst-case scenario value. The highest estimate for fullerene production in the United States is 80 t/year (Piccinno et al. 2012). We assumed a high estimate for ENM release during manufacturing as 2% as described by Keller et al. (Keller et al. 2012). The concentration was calculated as shown below assuming all the fullerenes in the U.S. were manufactured near Irondequoit Bay in Rochester, NY and 2% were released to the bay during manufacturing.

$$80\frac{t}{year} * 907.185\frac{kg}{t} * 0.02 = 1{,}451.5\frac{kg}{year}$$

Using the Irondequoit Bay surface area of 6,718,460 m^2 and the assumption that the C60 would be released into the top 3 cm of the Bay, the concentration was calculated for our experiments.

$$\frac{1{,}451.5\,\frac{kg}{year}}{6{,}718{,}460\,m^2} * \frac{1}{0.03\,m} = \frac{0.007\,\frac{kg}{m^3}}{year} = \boldsymbol{7\,\frac{mg}{L}}$$

References:

1. Keller AA, McFerran S, Lazareva A, Suh S. Global life cycle releases of engineered nanomaterials. Journal of Nanoparticle Research 2013;15(6):1692.

2. Piccinno F, Gottschalk F, Seeger S, Nowack B. Industrial production quantities and uses of ten engineered nanomaterials in Europe and the world. Journal of Nanoparticle Research 2012;14(9):1109.

Appendix C

Supplemental Information

Contents

Table S1. Scenario (BAU and economic investment) data inputs used in the predictive geospatial model. These metrics describe areas where sites would likely be built in the future or where existing locations would be revitalized.

Siting Metrics	Data Source
Chemical manufacturing facilities	EPA 2016 Toxics Release Inventory (TRI)
Unemployment Areas	U.S. Census Bureau, 2017 American Community Survey 5-Year Estimates: Selected Economic Characteristics

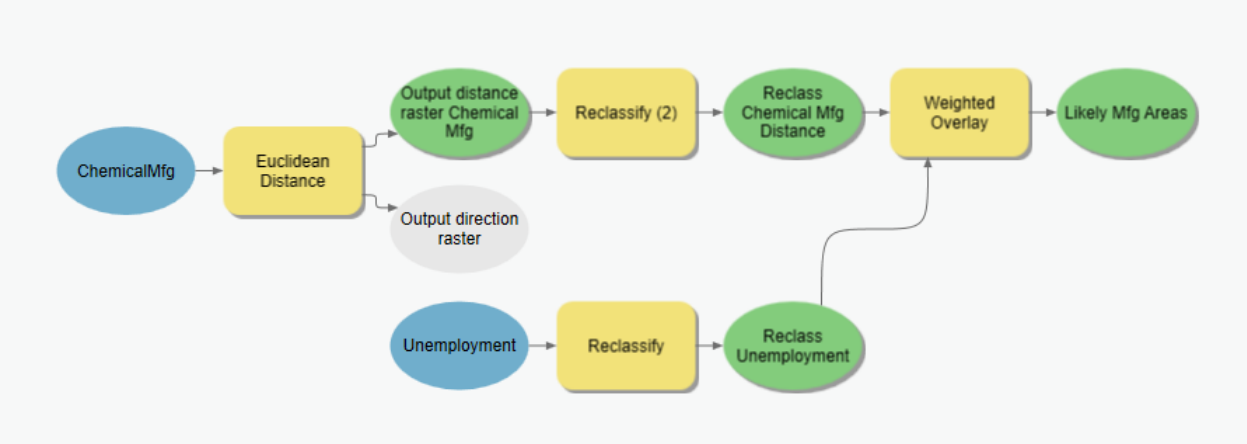

Figure S1. Model builder diagram of the Spatial Analyst tool features used to predict likely manufacturing locations.

Table S2. Spatial data added as layers for the ArcGIS Pro spatial analysis of potential ENM manufacturing release locations and their proximity to vulnerable ecosystems.

Spatial Risk Data	**Description**	**Data Source**
National Hydrography Dataset (NHD)	Upstate NY Lakes, ponds, streams, rivers, springs, and wells	United States Geological Survey (USGS)
Critical Environmental Areas in New York State	Areas designated as critical under 6 NYCRR Part 617: "ecological, geological, or hydrological sensitivity that may be adversely affected by any change" (NY DEC)	New York State Department of Environmental Conservation
National Land Cover Dataset (NLCD)	National Land Cover Database classification schemes based primarily on Landsat data (2011)	United States Geological Survey (USGS)
Elevation Data	Digital Elevation Models (10-meter) for New York, elevation values were derived from USGS contour lines mapped at a scale of 1:24,000.	United States Geological Survey (USGS)
Interstate Highway	Rural and urban highways for New York	Federal Highway Administration's National Transportation Atlas Database

Table S3. Data from the BatPaC model for lithium-ion battery performance and cost for electric-drive vehicles from Argonne National Lab was used to find the mass of the anode of a commonly used electric vehicle battery, NMC333-G. Assuming a 10.6 cell capacity, a negative active material capacity of 360 mAh/g, and an excess negative area of 4.19%, the baseline anode mass that was used for the model was 36.82 g.

Material	**% wt**	**Proportion of Anode (g)**	**Ref.**
Graphene	3	1.1	Luo et al. 2012
SWCNT	10	3.7	Ng et al. 2005
Si/SWCNT	85 to 15	5.5	Lee et al. 2016
C60	50	18.4	Enggar et al. 2018
SiO2	34.49	12.7	Jiang et al. 2018
BatPac NMC333-G	100	36.8	Nelson et al. 2017

Table S4. Calculated mass of ENMs per year using the values from Table S3. We assumed the production of nanomaterial was proportional to the theoretical proportion reported in anodes in the literature.

	Amount in anode		wt% anode	g/yr	metric tons/yr
Graphite	36.8	g	100%	35,200,000,000.00	35,200.00
Graphene	1.104	g	3.00	1,056,000,000.00	1,056.00
Si/SWCNT:					-
Si (bulk)	31.28	g	85	29,920,000,000.00	29,920.00
SWCNT	5.5	g	15	5,280,000,000.00	5,280.00
C60	18.4	g	50	17,600,000,000.00	17,600.00
SiO2 (nano)	12.3	g	34.49	12,140,480,000.00	12,140.48

Table S5. Low and high graphene emissions into various compartments.

Graphene	Low (mg/yr)	High (mg/yr)
Total	1,056,000,000.00	21,120,000,000.00
% air	105,600,000.00	8,448,000,000.00
% WW (preWWTP)	105,600,000.00	8,448,000,000.00
%landfill	844,800,000.00	4,224,000,000.00
% WWTP to effluent	3,168,000.00	2,112,000,000.00
% effluent to sediment	3,168,000.00	2,112,000,000.00

Table S6. Low and high silicon (bulk) emissions into various compartments.

Silicon Bulk	Low (mg/yr)	High (mg/yr)
Total	29,920,000,000.00	598,400,000,000.00
% air	2,992,000,000.00	239,360,000,000.00
% WW (preWWTP)	2,992,000,000.00	239,360,000,000.00
%landfill	23,936,000,000.00	119,680,000,000.00
% WWTP to effluent	89,760,000.00	59,840,000,000.00
% effluent to sediment	89,760,000.00	59,840,000,000.00

Table S7. Low and high SWNT emissions into various compartments.

SWNT	Low (mg/yr)	Low (mg/yr)
Total	5,280,000,000.00	105,600,000,000.00
% air	528,000,000.00	42,240,000,000.00
% WW (preWWTP)	528,000,000.00	42,240,000,000.00
%landfill	4,224,000,000.00	21,120,000,000.00
% WWTP to effluent	15,840,000.00	10,560,000,000.00
% effluent to sediment	15,840,000.00	10,560,000,000.00

Table S8. Low and high C60 emissions into various compartments.

C60	Low (mg/yr)	High (mg/yr)
Total	17,600,000,000.00	352,000,000,000.00
% air	1,760,000,000.00	140,800,000,000.00
% WW (preWWTP)	1,760,000,000.00	140,800,000,000.00
%landfill	14,080,000,000.00	70,400,000,000.00
% WWTP to effluent	52,800,000.00	35,200,000,000.00
% effluent to sediment	52,800,000.00	35,200,000,000.00

Table S9. Low and high SiO2 emissions into various compartments.

SiO2	Low (mg/yr)	High (mg/yr)
Total	12,140,480,000.00	242,809,600,000.00
% air	1,214,048,000.00	97,123,840,000.00
% WW (preWWTP)	1,214,048,000.00	97,123,840,000.00
%landfill	9,712,384,000.00	48,561,920,000.00
% WWTP to effluent	36,421,440.00	24,280,960,000.00
% effluent to sediment	36,421,440.00	24,280,960,000.00

Table S10. ENM LD50 (mg/L) ranges for the water column model organism, *D. magna*. Assumptions were noted if ecotoxicity data were not available.

ENM		***D. magna* LD50 (mg/L)**	**Reference**
Graphene	Low High	0.09 84.3*	Cano et al. 2017 Zhang et al. 2019
SWNT	Low High	2.43 >320	EPA ECOTOX, 2018 Revel et al. 2015
Silicon	Low High	No Data No Data	EPA ECOTOX, 2018 EPA ECOTOX, 2018
PC60**	Low High	>35 >463	Lovern et al. 2007 Blaise et al. 2008
SiO2	Low High	1.73 120	Pourdeljoo et al. 2014 Vidya and Chitra, 2016
Methylmercury		0.02	EPA ECOTOX, 2018

*Value for graphene oxide

**Values for C60: Tetrahydrofuran (THF) prepared C60 studies were not considered in our study since THF has been found to influence the toxicity of C60.

Table S11. ENM LD50 (mg/L) ranges for the sediment dwelling organism, *Hyallela azteca* and no observed effect concentration (NOEC) (mg/kg) value for *Lumbriculus variegatus*. Because SWNT absorbs to sediment and can pass through the gut of sediment dwelling organisms, many studies have not observed direct toxicity for carbon nanotubes (Rhiem 2014).

ENM	***Hyalella azteca* LD50 (mg/L)**	***Lumbriculus variegatus* NOEC (mg/kg)**
SWNT	>40*	0.03**
*Revel et al. 2015 **Petersen et al. 2008		

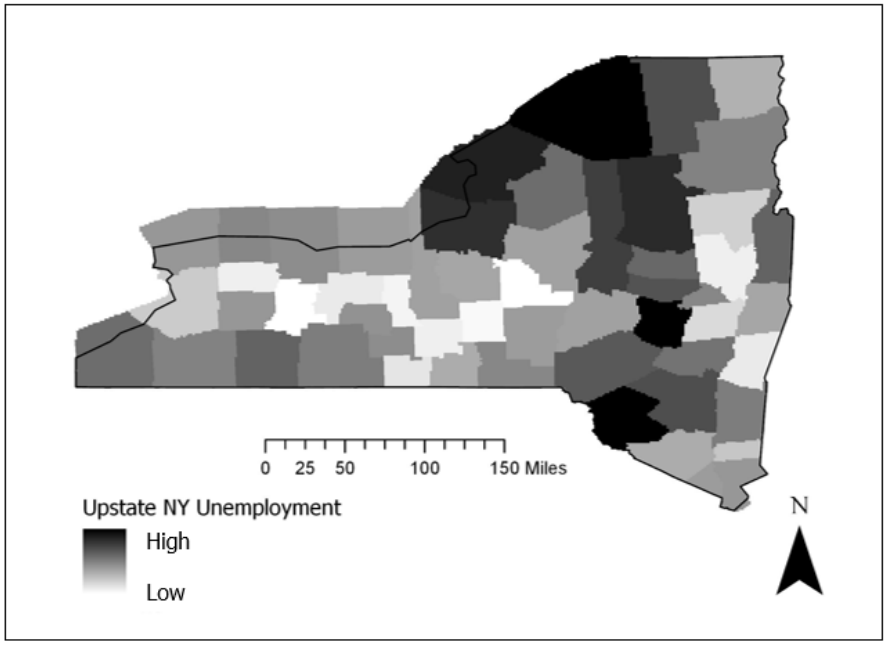

Figure S2. Unemployment data by county for Upstate NY.

Figure S3. Verification that industrial property sites that are for sale are within the boundaries of the likely manufacturing locations under the business as usual scenario.

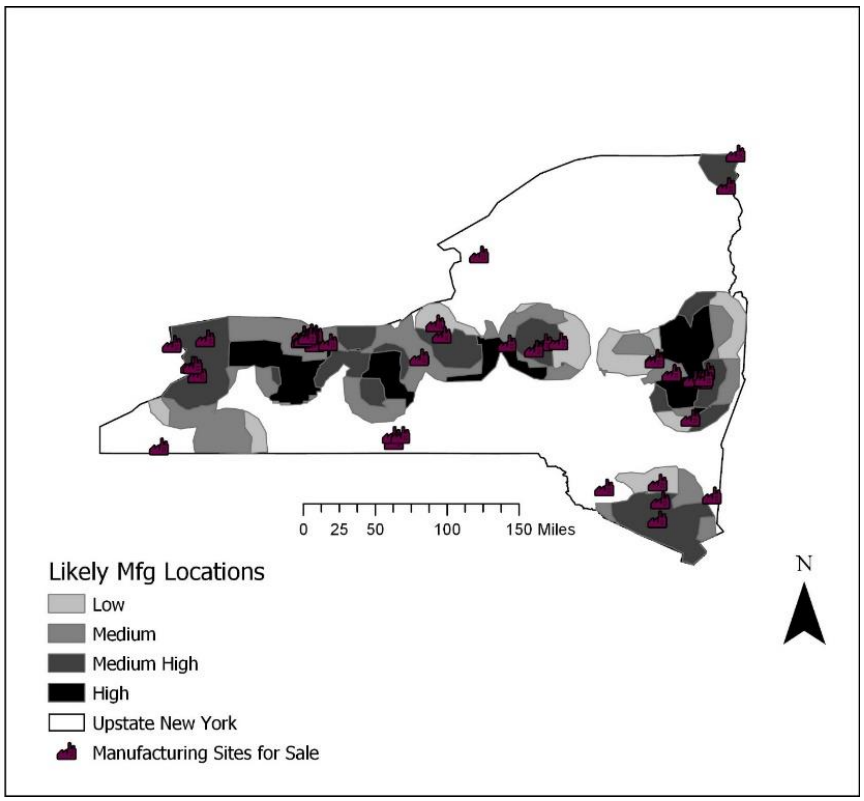

Figure S4. Verification that industrial property sites that are for sale are within the boundaries of the likely manufacturing locations under the economic investment scenario.

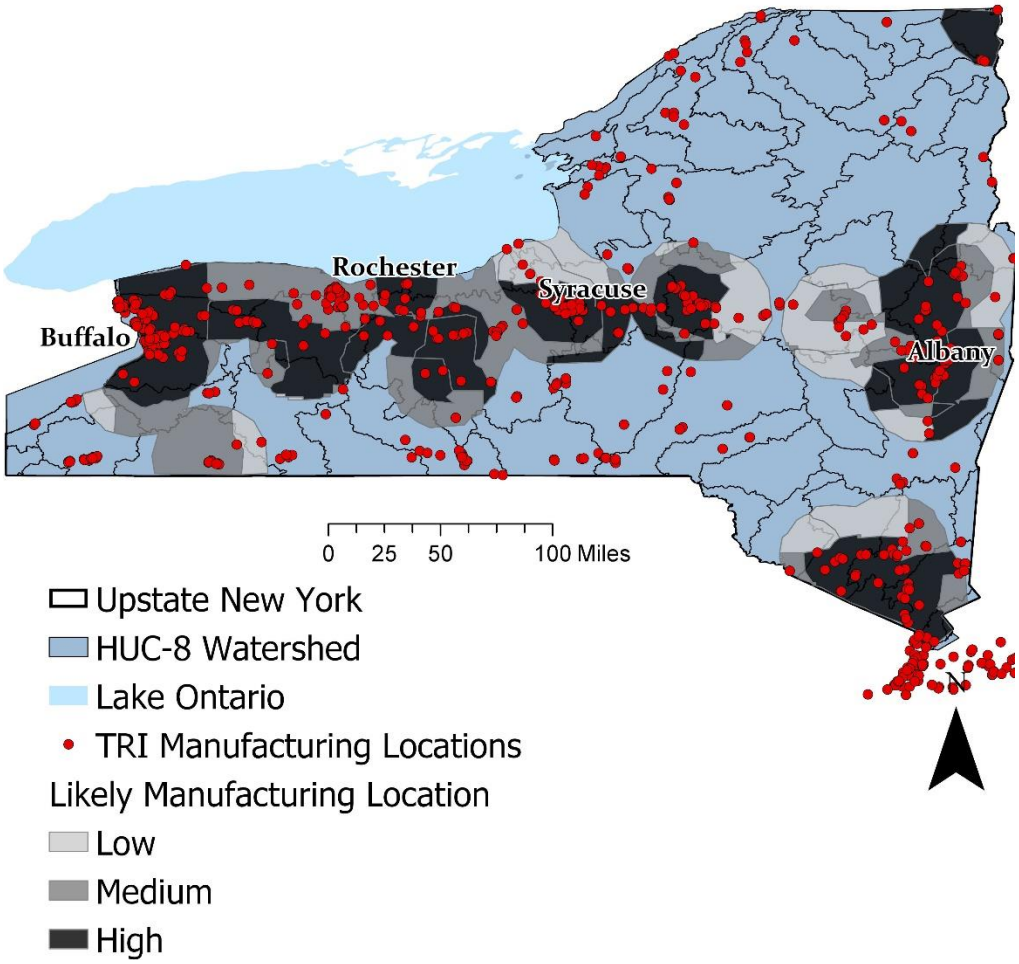

Figure S5. Verification that existing manufacturing sites are within the boundaries of the likely manufacturing locations.

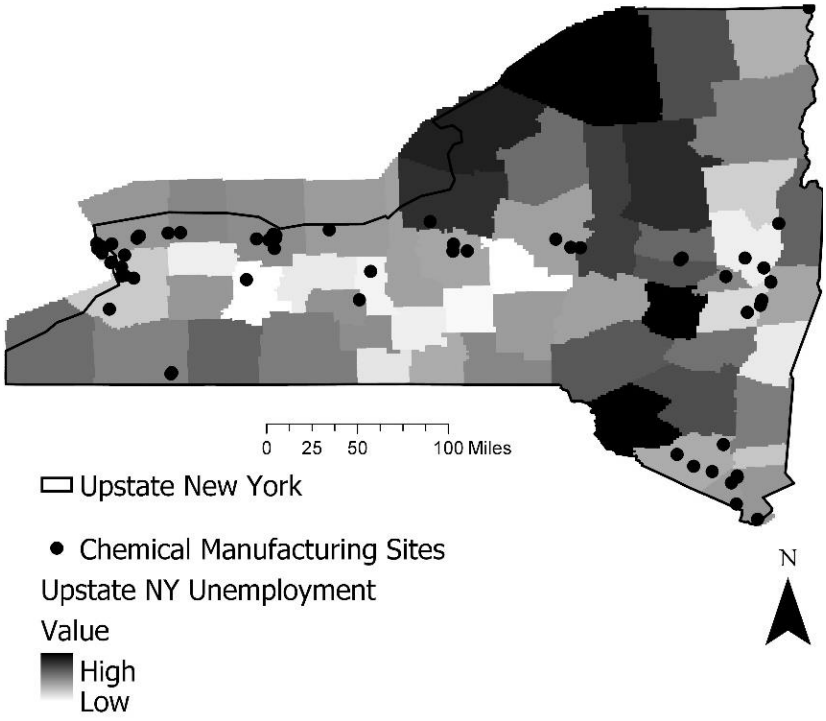

Figure S6. Verification that existing chemical manufacturing sites are near high unemployment areas.

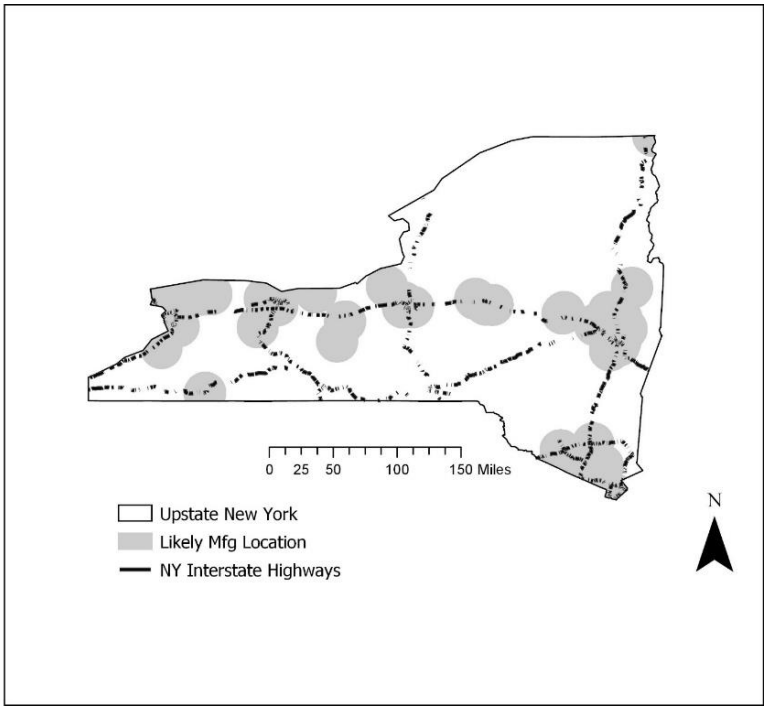

Figure S7. Likely manufacturing locations are located near interstate highways in many cases.

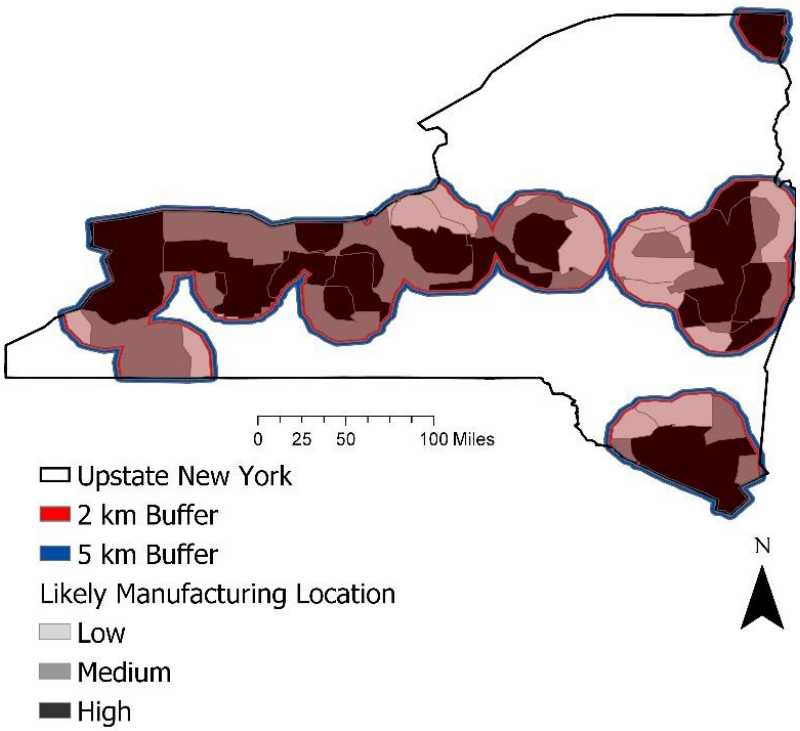

Figure S8. Buffer zones for the economic investment scenario, verifying that the results are comparable to the business as usual scenario.

Table S12. Onondaga Lake parameters used to calculate potential emissions over time.

Onondaga Lake Parameters		Reference
Volume (L)	1.32489E+11	Effler and Hennigan 1996
Surface Area (m2)	1.20E+07	Effler and Hennigan 1996
Sediment dry density (kg sed/m3)	2.60E+03	Parsons and ETS 2014

Table S13. Low and high effluent concentrations for the case study nanomaterials.

Onondaga Lake (1800 ft from mfg site)								
	1	**1**	**10**	**10**	**25**	**25**	**50**	**50**
Material	**Low (mg/L)**	**High (mg/L)**	**Low (mg/L)**	**High (mg/L)**	**Low (mg/L)**	**High (mg/L)**	**Low (mg/L)**	**High (mg/L)**
Graphene	0.00	0.02	0.00	0.20	0.00	0.76	0.01	3.34
Si (bulk)	0.00	0.45	0.01	5.68	0.03	21.56	0.14	94.55
SWNT	0.00	0.08	0.00	1.00	0.01	3.80	0.03	16.69
PC60	0.00	0.27	0.01	3.34	0.02	12.68	0.08	55.62
SiO2	0.00	0.18	0.00	2.31	0.01	8.75	0.06	38.37

Table S14. Low and high sediment concentrations for the case study nanomaterials.

Onondaga Lake (1800 ft from mfg site)								
	1	**1**	**10**	**10**	**25**	**25**	**50**	**50**
Material	**Low (mg/kg)**	**High (mg/kg)**	**Low (mg/kg)**	**High (mg/kg)**	**Low (mg/kg)**	**High (mg/kg)**	**Low (mg/kg)**	**High (mg/kg)**
Graphene	0.00	2.26	0.04	28.38	0.16	107.69	0.71	472.37
Si (bulk)	0.10	63.93	1.21	804.13	4.58	3051.27	20.08	13383.96
SWNT	0.02	11.28	0.21	141.90	0.81	538.46	3.54	2361.87
PC60	0.06	37.61	0.71	473.01	2.69	1794.87	11.81	7872.92
SiO2	0.04	25.94	0.49	326.29	1.86	1238.10	8.15	5430.74

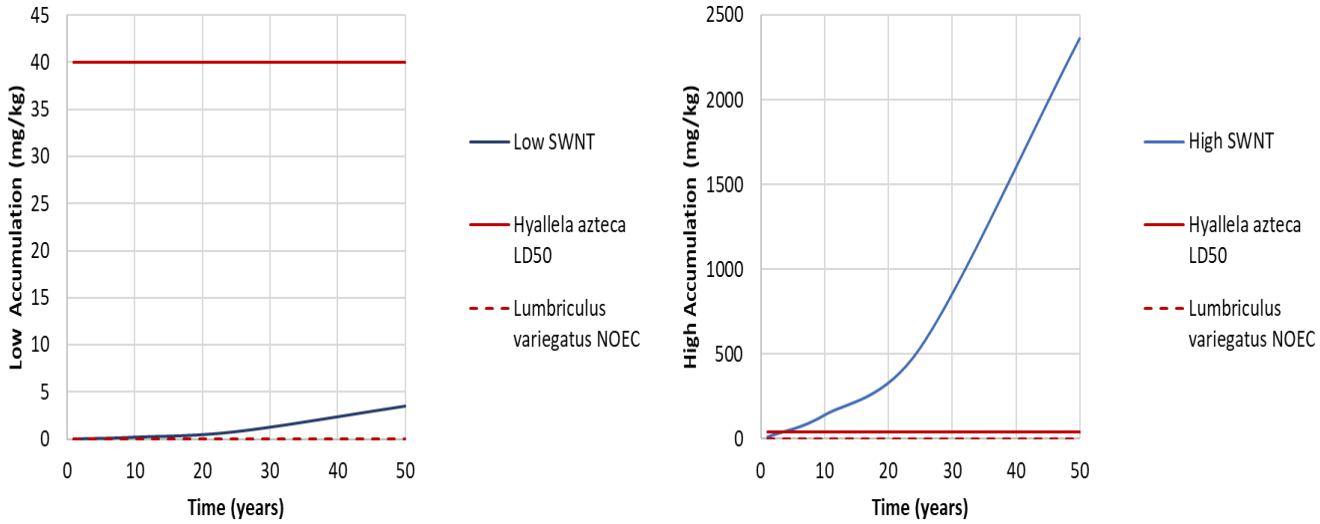

Figure S9. The low and high potential environmental accumulation (mg/kg) in Onondaga Lake for two sediment dwelling organisms, *H. azteca* and *L. variegatus* for SWNT.

Table S15. Seneca Lake parameters used to calculate potential emissions over time.

Seneca Lake Parameters		Reference
Volume (L)	1.59E+13	Halfman 2014
Surface Area (m2)	1.73E+08	Halfman 2014
Sediment dry density (kg sed/m3)	2.65E+03	Halfman 2000

Table S16. Low and high effluent concentrations for the case study nanomaterials.

Seneca Lake								
	1	1	10	10	25	25	50	50
Material	Low (mg/L)	High (mg/L)	Low (mg/L)	High (mg/L)	Low (mg/L)	High (mg/L)	Low (mg/L)	High (mg/L)
Graphene	0.00	0.00	0.00	0.00	0.00	0.01	0.00	0.03
Si (bulk)	0.00	0.00	0.00	0.05	0.00	0.18	0.00	0.79
SWNT	0.00	0.00	0.00	0.01	0.00	0.03	0.00	0.14
PC60	0.00	0.00	0.00	0.03	0.00	0.11	0.00	0.46
SiO2	0.00	0.00	0.00	0.02	0.00	0.07	0.00	0.32

Table S17. Low and high sediment concentrations for the case study nanomaterials.

Seneca Lake								
	1	1	10	10	25	25	50	50
Material	Low (mg/kg)	High (mg/kg)	Low (mg/kg)	High (mg/kg)	Low (mg/kg)	High (mg/kg)	Low (mg/kg)	High (mg/kg)
Graphene	0.00	0.15	0.00	1.93	0.01	7.32	0.05	32.11
Si (bulk)	0.01	4.35	0.08	54.66	0.31	207.42	1.36	909.84
SWNT	0.00	0.77	0.01	9.65	0.05	36.60	0.24	160.56
PC60	0.00	2.56	0.05	32.16	0.18	122.01	0.80	535.20
SiO2	0.00	1.76	0.03	22.18	0.13	84.17	0.55	369.18

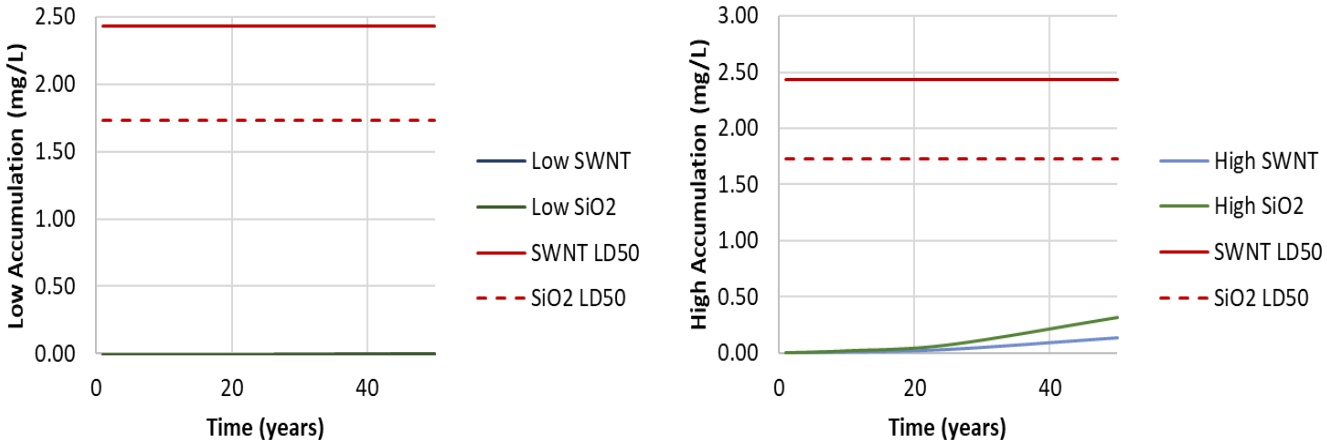

Figure S10. The low and high potential environmental accumulation (mg/L) in Seneca Lake.

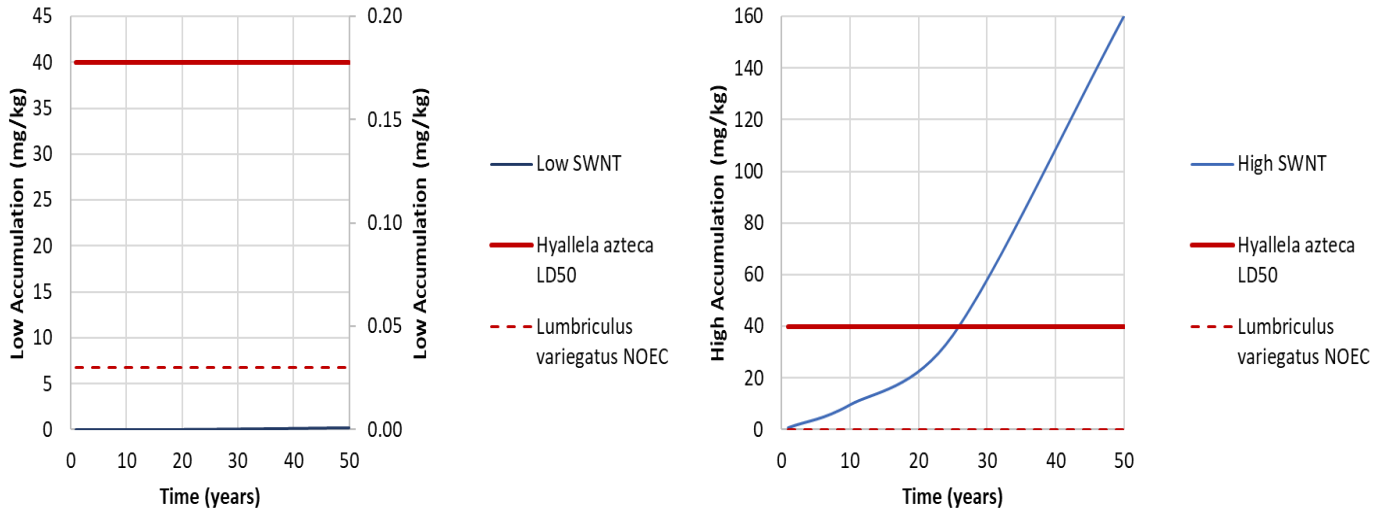

Figure S11. The low and high potential environmental accumulation (mg/kg) in Seneca Lake for two sediment dwelling organisms, *H. azteca* and *L. variegatus* for SWNT.

Table S18. Lake Ontario parameters used to calculate potential emissions over time.

Lake Ontario Parameters		Reference
Volume (L)	1.64018E+15	NOAA - Great Lakes Environmental Research Laboratory
Surface Area (m2)	1.90E+10	NOAA - Great Lakes Environmental Research Laboratory
Sediment dry density (kg sed/m3)	9.00E+02	Tyler et al. 2019 (unpublished data)

Table S19. Low and high effluent concentrations for the case study nanomaterials.

Lake Ontario								
	1	**1**	**10**	**10**	**25**	**25**	**50**	**50**
Material	**Low (mg/L)**	**High (mg/L)**	**Low (mg/L)**	**High (mg/L)**	**Low (mg/L)**	**High (mg/L)**	**Low (mg/L)**	**High (mg/L)**
Graphene	0.00	0.00	0.00	0.00	0.00	0.00	0.00	0.00
Si (bulk)	0.00	0.00	0.00	0.00	0.00	0.00	0.00	0.01
SWNT	0.00	0.00	0.00	0.00	0.00	0.00	0.00	0.00
PC60	0.00	0.00	0.00	0.00	0.00	0.00	0.00	0.00
SiO2	0.00	0.00	0.00	0.00	0.00	0.00	0.00	0.00

Table S20. Low and high sediment concentrations for the case study nanomaterials.

Lake Ontario								
	1	**1**	**10**	**10**	**25**	**25**	**50**	**50**
Material	**Low (mg/kg)**	**High (mg/kg)**	**Low (mg/kg)**	**High (mg/kg)**	**Low (mg/kg)**	**High (mg/kg)**	**Low (mg/kg)**	**High (mg/kg)**
Graphene	0.00	0.00	0.00	0.05	0.00	0.20	0.00	0.86
Si (bulk)	0.00	0.12	0.00	1.47	0.01	5.58	0.04	24.48
SWNT	0.00	0.02	0.00	0.26	0.00	0.99	0.01	4.32
PC60	0.00	0.07	0.00	0.87	0.00	3.28	0.02	14.40
SiO2	0.00	0.05	0.00	0.60	0.00	2.26	0.01	9.93

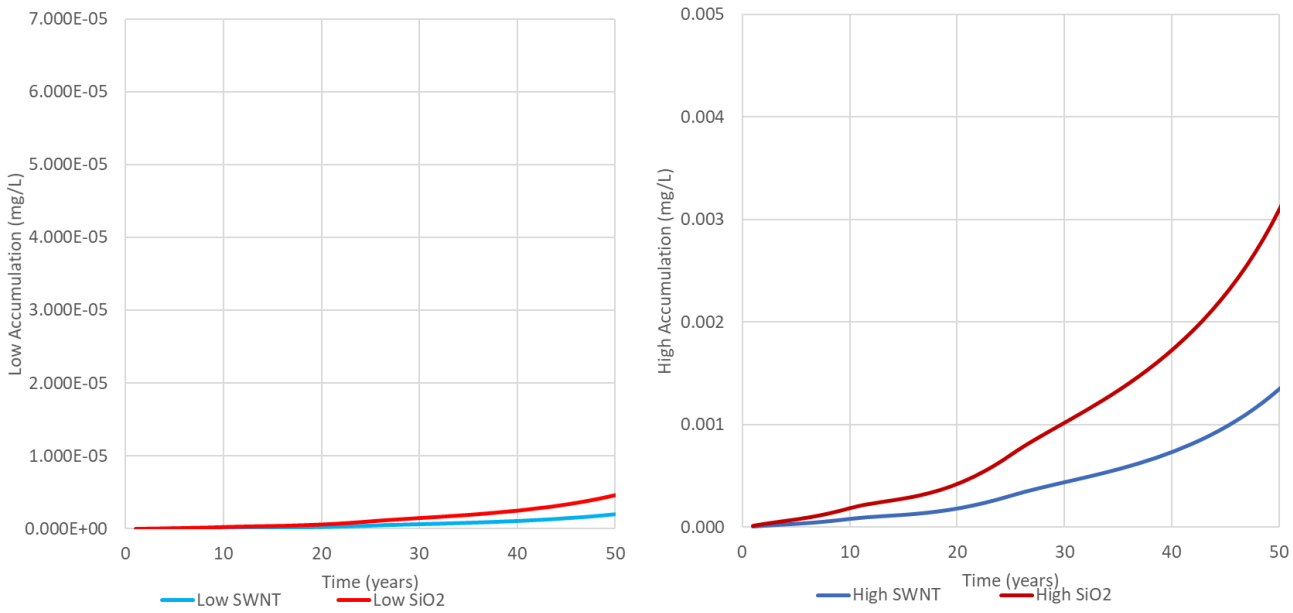

Figure S12. The low and high potential environmental accumulation (mg/L) in Lake Ontario. The LD50 values are not shown because the emissions are not close to the LD50 values, even in the high scenarios after 50 years.

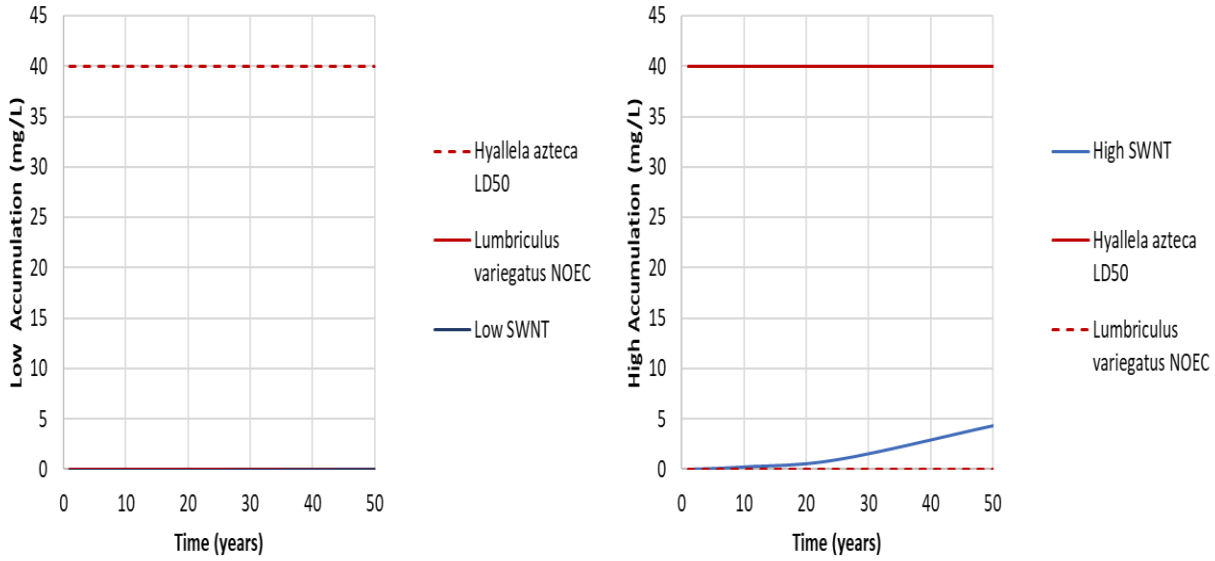

Figure S11. The low and high potential environmental accumulation (mg/kg) in Lake Ontario for two sediment dwelling organisms, *H. azteca* and *L. variegatus* for SWNT.

Onondaga Lake (1800 ft from mfg site)								
	1	1	10	10	25	25	50	50
Material	Low (mg/L)	High (mg/L)	Low (mg/L)	High (mg/L)	Low (mg/L)	High (mg/L)	Low (mg/L)	High (mg/L)
Graphene	0.00	0.16	0.00	2.01	0.01	7.61	0.05	33.37
Si (bulk)	0.01	4.52	0.09	56.81	0.32	215.56	1.42	945.54
SWNT	0.00	0.80	0.02	10.03	0.06	38.04	0.25	166.86
PC60	0.00	2.66	0.05	33.42	0.19	126.80	0.83	556.20
SiO2	0.00	1.83	0.03	23.05	0.13	87.47	0.58	383.67

Table S21. Low and high effluent concentrations under a disruptive innovation scenario for the case study nanomaterials.

Onondaga Lake Sensitivity Analysis: Effluent								
	1	**1**	**10**	**10**	**25**	**25**	**50**	**50**
Material	**Low (mg/L)**	**High (mg/L)**	**Low (mg/L)**	**High (mg/L)**	**Low (mg/L)**	**High (mg/L)**	**Low (mg/L)**	**High (mg/L)**
Graphene	0.00	0.16	0.00	2.01	0.01	7.61	0.05	33.37
Si (bulk)	0.01	4.52	0.09	56.81	0.32	215.56	1.42	945.54
SWNT	0.00	0.80	0.02	10.03	0.06	38.04	0.25	166.86
PC60	0.00	2.66	0.05	33.42	0.19	126.80	0.83	556.20
SiO2	0.00	1.83	0.03	23.05	0.13	87.47	0.58	383.67

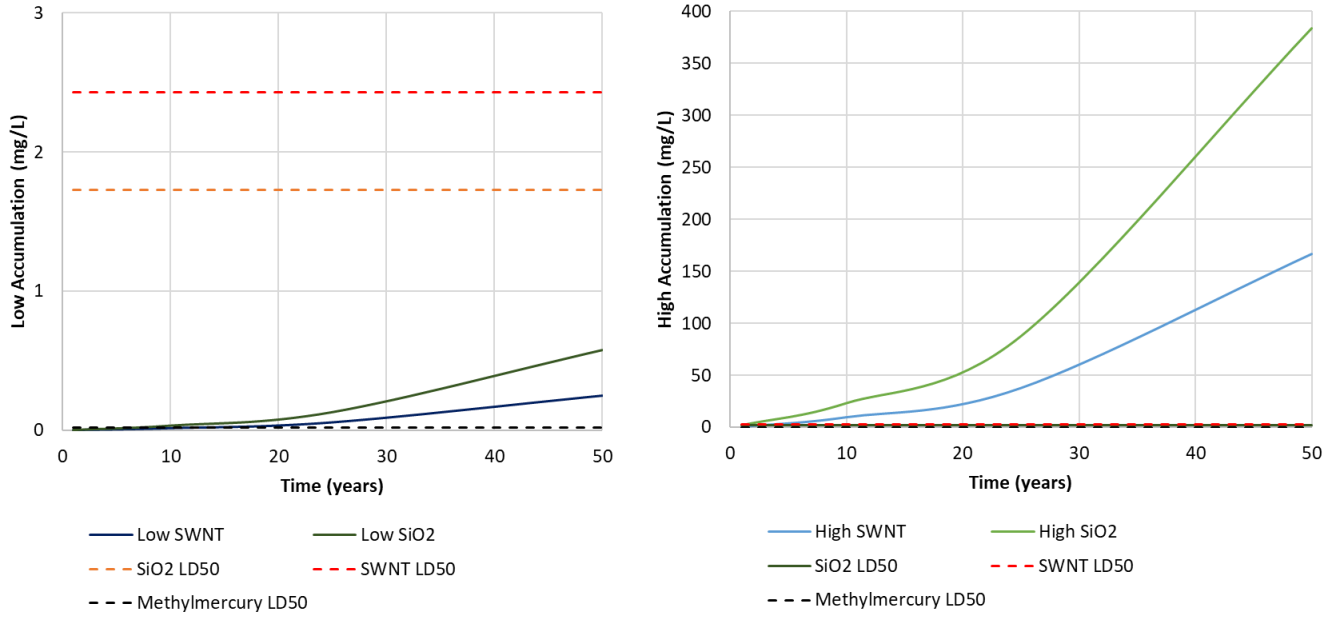

Figure S14. The low and high potential environmental accumulation (mg/L) in Onondaga Lake under the disruptive innovation scenario.

References

1. Ardhi, R. E. A.; Liu, G.; Tran, M. X.; Hudaya, C.; Kim, J. Y.; Yu, H.; Lee, J. K., Self-Relaxant Superelastic Matrix Derived from C60 Incorporated Sn Nanoparticles for Ultra-High-Performance Li-Ion Batteries. *ACS nano* **2018,** *12* (6), 5588-5604.

2. Blaise, C.; Gagné, F.; Ferard, J.; Eullaffroy, P., Ecotoxicity of selected nano-materials to aquatic organisms. *Environmental Toxicology: An International Journal* **2008,** *23* (5), 591-598.

3. Bureau, U., American community survey 5-year estimates. 2017.

4. Cano, A. M.; Maul, J. D.; Saed, M.; Shah, S. A.; Green, M. J.; Cañas-Carrell, J. E., Bioaccumulation, stress, and swimming impairment in Daphnia magna exposed to multiwalled carbon nanotubes, graphene, and graphene oxide. *Environmental toxicology and chemistry* **2017,** *36* (8), 2199-2204.

5. Effler, S.; Hennigan, R., Onondaga lake, New York: legacy of pollution. *Lake and Reservoir Management* **1996,** *12* (1), 1-12.

6. EPA, Toxics Resource Inventory. 2019.

7. EPA, TSCA Chemical Substance Inventory. 2019.

9. Halfman, J., A 2014 UPDATE ON THE CHLORIDE HYDROGEOCHEMISTRY IN SENECA LAKE, NEW YORK.

10. Halfman, J. D.; Woodrow, D. L. In *Stratigraphy, Sedimentology, and Geochemistry of Seneca Lake, New York*, Guide for the... Annual Field Meeting, The Association: 2000; p 27.

11. Jiang, Y.; Chen, S.; Mu, D.; Zhao, Z.; Li, C.; Ding, Z.; Xie, C.; Wu, F., Flexible TiO2/SiO2/C Film Anodes for Lithium-Ion Batteries. *ChemSusChem* **2018,** *11* (13), 2040-2044.

12. Lee, J. H.; Yoon, C. S.; Hwang, J.-Y.; Kim, S.-J.; Maglia, F.; Lamp, P.; Myung, S.-T.; Sun, Y.-K., High-energy-density lithium-ion battery using a carbon-nanotube–Si composite anode and a compositionally graded Li [Ni 0.85 Co 0.05 Mn 0.10] O 2 cathode. *Energy & Environmental Science* **2016,** *9* (6), 2152-2158.

13. Lovern, S. B.; Strickler, J. R.; Klaper, R., Behavioral and physiological changes in Daphnia magna when exposed to nanoparticle suspensions (titanium dioxide, nano-C60, and C60HxC70Hx). *Environmental science & technology* **2007,** *41* (12), 4465-4470.

14. Lowry, G. V.; Gregory, K. B.; Apte, S. C.; Lead, J. R., Transformations of nanomaterials in the environment. ACS Publications: 2012.

15. Luo, B.; Liu, S.; Zhi, L., Chemical approaches toward graphene-based nanomaterials and their applications in energy-related areas. *Small* **2012,** *8* (5), 630-646.

16. Michel, R. L.; Kraemer, T. F., Use of isotopic data to estimate water residence times of the Finger Lakes, New York. *Journal of Hydrology* **1995,** *164* (1-4), 1-18.

17. Nelson, P.; Gallagher, K.; Bloom, I., BatPaC (battery performance and cost) software, Argonne National Lab. 2017.

18. NY DEC Seneca Lake. https://www.dec.ny.gov/outdoor/25574.html.

19. Ng, S.; Wang, J.; Guo, Z.; Chen, J.; Wang, G.; Liu, H., Single wall carbon nanotube paper as anode for lithium-ion battery. *Electrochimica Acta* **2005,** *51* (1), 23-28.

20. Parsons; Systems, E. T., ONONDAGA LAKE SEDIMENT MANAGEMENT UNIT 8 MICROBEAD MARKER PLACEMENT REPORT. 2014.

21. Petersen, E. J.; Huang, Q.; Weber Jr, W. J., Ecological uptake and depuration of carbon nanotubes by Lumbriculus variegatus. *Environmental health perspectives* **2008,** *116* (4), 496-500.

22. Ponte Cabral, S., Effects of fullerenes on a freshwater benthic community: toxicity and implications for ecological functions and services. **2018**.

23. Pourdeljoo, T.; Shariati, F.; Ooshaksaraee, L.; Ramzanpoor, Z., Ecotoxicity of Nano Silica in Daphnia Magna. *Journal of Guilan University of Medical Sciences* **2014,** *22* (88), 11-17.

24. Revel, M.; Fournier, M.; Robidoux, P. Y., Single-Walled Carbon Nanotubes Toxicity to the Freshwater Amphipod Hyalella Azteca: Influence of to the Freshwater Amphipod Sediment and Exposure Duration. *Journal of xenobiotics* **2015,** *5* (1).

25. Tyler, C. Bulk density calculations for Lake Ontario (unpublished data) **2019**.

26. Vidya, P.; Chitra, K., Assessment of acute toxicity (LC 50 96 h) of aluminium oxide, silicon dioxide and titanium dioxide nanoparticles on the freshwater fish, Oreochromis mossambicus (Peters, 1852). *International Journal of Fisheries and Aquatic Studies* **2017,** *5* (1), 327-332.

27. Wiesner, M. R.; Lowry, G. V.; Alvarez, P.; Dionysiou, D.; Biswas, P., Assessing the risks of manufactured nanomaterials. ACS Publications: 2006.

28. Zhang, Y.; Meng, T.; Shi, L.; Guo, X.; Si, X.; Yang, R.; Quan, X., The effects of humic acid on the toxicity of graphene oxide to Scenedesmus obliquus and Daphnia magna. *Science of the total environment* **2019,** *649*, 163-171.

Appendix D

Supplementary Information

Contents

CNM Type	Production (t/year)		Year and Ref.
Fullerene	Worldwide		
	0.15-0.6	Low	2011[1]
	5.5-80	High	2011[1]
	U.S.		
	2	Low	2011 [2]
	80	High	2011 [2]
CNTs	Worldwide		
MWCNT	11-55 (2011, 2012)	Low	2011[1]
SWCNT	550 - >4,065 (2011, 2012)	High	2011[1]
	U.S.		
	55	Low	2011 [2]
	1,101	High	2011 [2]
	Worldwide		
	1,988	Low	2015[3]
	13,738	High	2015[3]
	U.S.		
	60	Low	2015[3]
	1,000	High	2015[3]
	Worldwide		
	26	Low	2015[3]
	359	High	2015[3]
	U.S.		
	0.25	Low	2015[3]
	250	High	2015[3]
Graphene	Worldwide		
	573	Low	2017[4]
	1,321	High	2022[5]
Graphite	Worldwide		2009[6]
	1,143,000		
Silicon	Worldwide		2016[35]
	7,200,000		
Cement	Worldwide		2016[8]
	4,200,000,000,000,000		

Table S1. Data for the production of CNMs in tons per year. If there were a range of values reported for the production amount, a low and high value were reported. U.S. and worldwide data were denoted in the table where data were available. The total CNM production was found to be 12,300 tons per year worldwide. These values will be utilized to establish the material availability constraint and assumptions will be made as to the quantity of CNMs distributed to the energy sector.

Based on the characteristics of each material found in the literature, data were simulated using uniform and normal distributions to mirror the variance of power and capacity output that occurs in the applications of these technologies. To determine the overall portfolio return and variance, the amount of each CNM used in the portfolio was defined for optimization. The Palisade @Risk software was utilized to perform the portfolio optimization and numerical simulation. This tool uses Monte Carlo simulation to show different output probabilities and risks for each scenario analysis performed. @Risk was used to calculate the optimization model outputs by changing the amount of each CNM used in the portfolio to find the optimal return.

Material Type	Material		m2/Wp	g/m2	Distribution	Ref.
Fullerenes	C60	Low High	0.0234 0.179	0.068 3	Uniform	9
	PC60BM	Low High	0.0192 0.0262	0.2 1.44	Uniform	10,11,12
	PC70BM	Low High	0.0136 0.0236	0.203 0.907	Uniform	10,12,13
	BisPCBM	Low High	Mean - 0.027 Stdev - .01	Mean - 0.66 Stdev - .1	Normal	12,13
	ICBA	Low High	Mean - 0.0192 Stdev - .01	Mean - 0.44 Stdev - .1	Normal	13,14,15
Graphene	Graphene	Low High	0.073099 0.595238	10%wt	Uniform	10,11
Carbon Nanotubes (CNTs)	SWCNT	Low High	0.040323 0.173611	0.5%wt	Uniform	10
	MWCNT		Mean - 0.09058 Stdev - .01	2%wt	Normal	15

Table S2. Data for the power output of the CNMs that were incorporated into the model as the return portion of the portfolio optimization. If there was a range of data values for the material, a low and high value were reported. Based on the data available, a normal distribution was assumed where a mean data value existed (with an assumed standard deviation of 0.01) and a uniform distribution was assumed when a minimum and maximum value existed.

Material	% wt	Proportion of Anode (g)	Ref.
Graphene	3	1.1	16
Doped Graphene (N- and B-Doped)	70	25.8	17
SWCNT	10	3.7	18
MWCNT	5	1.8	19
Graphite	67	24.7	20
Si/SWCNT	85 to 15	5.5	21
BatPac NMC333-G	100	36.8	22

Table S3. Data from the BatPaC model for lithium-ion battery performance and cost for electric-drive vehicles from Argonne National Lab was used to find the mass of the anode of a commonly used electric vehicle battery, NMC333-G. Assuming a 10.6 cell capacity, a negative active material capacity of 360 mAh/g, and an excess negative area of 4.19%, the baseline anode mass that was used for the model was 36.82 g.

Material Type	Material		Energy Capacity (mAh/g)	Proportion (g)	Distribution	Ref.
Carbon Nanotubes (CNTs)	SWCNT	Low High	600 1,000	3.7	Uniform	17
	Si/SWCNT	Low High	1,000 2,200	5.5	Uniform	21
	MWCNT		Mean-220 Stdev-73.3	1.8	Normal	17
Graphene	Graphene	Low High	744 1,488	1.1	Uniform	17
	N-doped Graphene		Mean-1,043 Stdev-346.7	25.8	Normal	17
	B-doped Graphene		Mean-1,549 Stdev-516.3	25.8	Normal	17
Alternate Non-Nano Material	Graphite		Mean- 350 Stdev-116.7	24.7	Normal	15

Table S4. Data from several literature sources were used to generate the proportion of CNMs in an anode. The values reported in the literature were on a percent weight basis and therefore the baseline value from BatPaC was used to find the

CNM proportions. Data for the energy capacity of the CNMs as well as the alternate non-nano materials were incorporated into the model as the return portion of the portfolio optimization. Based on the data available, a normal distribution was assumed where a mean data value existed, with an assumed standard deviation that as 1/3 of the mean, and a uniform distribution was assumed when a minimum and maximum value existed.

Model input data were collected for both case studies from the literature and material suppliers (Figure S7). In order to find the producer cost for the economic scenario, a ratio of producer to consumer cost was determined to convert the consumer cost value available. This value was calculated using the Benchmark Input-Output Data tables from the Bureau of Economic Analysis[23,24,25,26] (Table S5). Using the producer cost, the total cost of incorporating CNMs was found using Equation S3 where T is the producer cost ($/g CNM) and M is the amount of CNM (g) added.

$$Total\ Cost = T * M\ \forall_n \quad \text{Equation S1.}$$

The power rating and capacity were maximized while the cost was minimized for each CNM used in the portfolio by dividing the return value by the total cost.

Material Type	Material		Purchaser Cost($)/g	Producer Cost ($)/g	Assumption
Fullerenes	C60	Low High Average	$25[3] $209[1] $92[1,2,3]	$16 $134 $59	Average price of 3 companies, 99.5% pure
	PC60BM	Low High Average	$270[2] $742[1] $506[1,2]	$173 $475 $324	Average price of 2 companies, 99% pure
	PC70BM	Low High Average	$3,250[2] $4,625[1] $3,938[1,2]	$2,080 $2,960 $2,520	Average price of 2 companies, 99% pure
	BisPCBM		$1,750[2]	$1,120	99.5% pure
	ICBA		$1,730[1]	$1,107	99% pure
Graphene	Graphene		$110[1]	$70	4-10% edge oxidized
	N-doped Graphene		$380[4]	$243	
	B-doped Graphene		$380[4]	$243	
Carbon Nanotubes (CNTs)	SWCNT	Low High Average	$120[3] $1,326[1] $582[1,2,3]	$77 $849 $373	Average price of 3 companies, carbon <=95%, >=93%, L-purified, length 5-15 um, avg. i.d. 1.2 nm, 95 wt% 0.7-2.5 nm diam, 0.5-5 um length
	MWCNT	Low High Average	$8.50[3] $117[1] $70[1,2,3]	$5.44 $75 $45	Average price of 3 companies, >98%, l-purified, outer diameter <10nm, 1 gram avg. I.D. 4.5 nm, 95 wt% 5-15 nm diameter, 1010 um length
Non-CNM Materials	Graphite Silicon		$1.60[1] $0.67[1]	$1.02 $0.43	99.9% trace metals basis <150 um ≥98% trace metals basis

1-Sigma Aldrich, 2-SES Research, 3-BuckyUSA, 4-ACS, 5-Molbase

Table S5. Data for the cost of the CNMs as well as the non-nano materials that were incorporated into the model to evaluate the economic risk of utilizing CNMs. The producer costs are calculated using the conversion factor of 0.65 calculated in Figure S2. The assumptions for each material studied are also listed informing the purity of the material and size. These values can be updated with other types of purifications and sizes for further analysis.

Year	IO sector	Description	Producer price	Purchaser Price	Conversion Factor
1992					0.61
	270100	Industrial inorganic and organic chemicals	$ 20.00	$ 33.00	
1997					0.65
	325180	Other basic inorganic chemical manufacturing	$ 20.50	$ 31.70	
2002					0.70
	325188	All other basic inorganic chemical manufacturing	$ 12.90	$ 18.50	
2007					0.64
	325188	All other basic inorganic chemical manufacturing	$ 21.00	$ 33.00	
				Average	**0.65**

Table S6. The producer cost conversion factor was calculated using a conversion value of 0.65, which was found to be the average value in the inorganic chemical manufacturing category. This value was calculated from the Bureau of Economic Analysis benchmark input-output table values[9,18, 20, 22].

To determine the overall portfolio return while considering the environmental cost of the materials in OPVs and LIBs, the power and capacity per cumulative energy demand (CED) (MJ/kg) was calculated for each CNM used in the portfolio. First, the CED value for the CNM was calculated in Equation S4 from literature CED data (Table S7) represented by E (GJ/g CNM) and M, the amount of CNM (g) added. The power rating and capacity were maximized while the CED was minimized for each CNM used in the portfolio by dividing the return value by the CED.

$$CED = E * M \ \forall_n \qquad \text{Equation S2.}$$

Material Type	Material	Cumulative Energy Demand (GJ/kg)
Fullerenes	C60	35.48[27]
	PC61BM	85.74[27]
	PC71BM	122.97[27]
	BisPCBM	87.68[27]
	ICBA	55.73[27]
Graphene	Graphene	500-1,000[28]
	N-doped and B-doped Graphene	500-1,000[28]
Carbon Nanotubes (CNTs)	SWCNT	93-328[29]
	MWCNT	65-295[29]
	Si-SWCNT	15.15-50.40[29,30]
Non-CNM Material	Graphite	0.0426[30]

Table S7. The cumulative energy demand (CED) data were found in several literature sources for the CNMs where it was assumed that the N-doped and B-doped graphene had the same value as graphene due to lack of existing values. For the non-CNMs, the CED values were calculated using SimaPro LCA software. Based on the data available, a normal distribution was assumed where a mean data value existed and a uniform distribution was assumed when a minimum and maximum value existed.

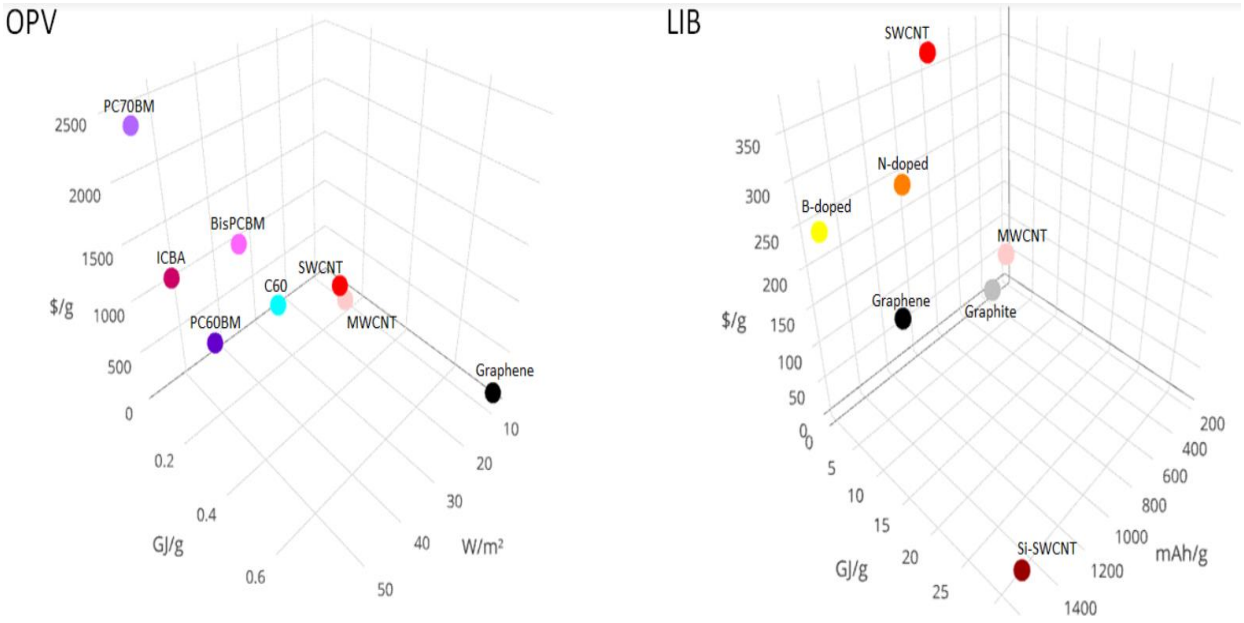

Figure S2. Average sustainability trade-off data collected shown in a 3D plot created in Plotly for CNMs used in OPVs (left) and LIBs (right). These trade-off data include economic ($/g), energy (GJ/g), and performance parameters used in the optimization model. Note the differences in axes and scale for each of the application parameters as well as the stark differences between the same material in different applications (e.g. SWCNT cost in OPVs vs. LIBs).

Financial Portfolio	OPV	LIB
Stocks	Share of CNMs, including: Fullerenes(C_{60}, $PC_{60}BM$, $PC_{70}BM$,BisPCBM,ICBA) Graphene, Carbon Nanotubes (SWCNT, MWCNT)	Share of CNMs, including Fullerene (C60), Graphene (N-doped and B-doped), Carbon Nanotubes (SWCNT, MWCNT), Graphite
Return ($)	Gain in power rating normalized to mass of CNM added (W/g_{CNM})	Gain in capacity normalized to mass of CNM added (Ah/g_{CNM})
Return Variance (σ^2)	Variance in Power rating associated with uncertainty in CNM performance (W/g_{CNM})	Variance in Capacity associated with uncertainty in CNM performance (Ah/g_{CNM})
Risk ($)	Gain in power rating normalized to dollars and energy invested Economic (W/$) Energy (W/GJ)	Gain in capacity normalized to dollars and energy invested Economic (Ah/$) Energy (Ah/GJ)
Constraint: Available funds ($)	Constraint: CNM available worldwide production(g)	Constraint: CNM, graphite available worldwide production (g)

Table S8. Portfolio optimization model parameters in stock market terms that are translated to CNM parameters for both OPVs and LIBs. It is unlikely that just one material will be utilized as an acceptor (OPV) or anode (LIB) and therefore the cumulative risks and benefits are evaluated to determine the optimal materials under various scenarios.

In addition to the supply scenarios mentioned above, a demand scenario was featured for OPVs and LIBs using EIA predictions for future solar power (assuming 1.5% for OPVs[31]) and electric vehicle use, as shown in Tables S8-S10. All sixteen supply and demand scenarios are detailed in Table S12.

Year	Reference Case (GW)	Reference case without CPP (GW)
2010	2.67	
2015	24.95	24.95
2020	56.65	57.01
2030	125.25	104.58
2040	246.34	202.64

Table S9. The power output for solar predicted until 2040 under the Clean Power Plan (CPP) and without the CPP[32].

Year	Type	Reference Case (millions)	Reference case without CPP (millions)
2010	Light-duty vehicle stock: Alternative-fuel cars: 100 mile EV	0.01	
2015	Light-duty vehicle stock: Alternative-fuel cars: 100 mile EV	0.188	0.188
2020	Light-duty vehicle stock: Alternative-fuel cars: 100 mile EV	0.326	0.326
2030	Light-duty vehicle stock: Alternative-fuel cars: 100 mile EV	1.535	1.542
2040	Light-duty vehicle stock: Alternative-fuel cars: 100 mile EV	2.895	2.909

Table S10. The number of light-duty 100-mile electric vehicles predicted until 2040 under the Clean Power Plan (CPP) and without the CPP[33].

Number of Battery Cells/Electric Vehicle	Capacity (Ah) /Battery Cell
5000	2.05
5,900	1.72
6,500	1.86
4,600	2.34
Average: 5500	**1.99**
10,958.75 Ah/Vehicle	

Table S11. The calculation for the capacity per vehicle to understand the 2040 target with and without the CPP. To convert the number of 100-mile vehicles driven to a capacity value (Ah), an average of vehicle battery cell and capacity literature values[34] was taken to calculate the capacity per vehicle. The EIA forecasted value for light duty 100-mile electric vehicles in 2040 is 2.895 million vehicles. Multiplying the target vehicles by the average capacity/vehicle, the target 2040 EIA goal is 3.17E10 vehicles.

Scenario #	Application	Availability	Optimization
1	OPV	Supply: Unconstrained[1]	Max W, Min Variance
2		Supply: Unconstrained[1]	Max W, Min $ and Variance
3		Supply: Unconstrained[1]	Max W, Min CED and Variance
4		Demand: Unconstrained[1]	Meet EIA 1.5% solar projection[3]
5	OPV	Supply: Constrained[2]	Max W, Min Variance
6		Supply: Constrained[2]	Max W, Min $ and Variance
7		Supply: Constrained[2]	Max W, Min CED and Variance
8		Demand: Constrained[2]	Meet EIA 1.5% solar projection[3]
9	LIB	Supply: Unconstrained[1]	Max Ah, Min Variance
10		Supply: Unconstrained[1]	Max Ah, Min $ and Variance
11		Supply: Unconstrained[1]	Max Ah, Min CED and Variance
12		Demand: Unconstrained[1]	Meet EIA electric vehicle projection[4]
13	LIB	Supply: Constrained[2]	Max Ah, Min Variance
14		Supply: Constrained[2]	Max Ah, Min $ and Variance
15		Supply: Constrained[2]	Max Ah, Min CED and Variance
16		Demand: Constrained[2]	Meet EIA electric vehicle projection[4]

1. Worldwide production for cement (USGS)[8]
2. Worldwide production and competing sector limitations[1,2,3, 4,5,6,7,8]
3.EIA Energy Outlook 2016: Renewable Energy: All Sectors: Generating Capacity: Solar[32]
4. EIA Energy Outlook 2016: Light-duty vehicle stock: Alternative-fuel cars: 100-mile EV[33]

Table S12. Description of all sixteen scenarios including the baseline scenario (maximizing performance, minimizing variance), the economic and environmental objective scenarios, the supply scenarios (unconstrained vs. constrained), and the demand scenario (meeting EIA predictions).

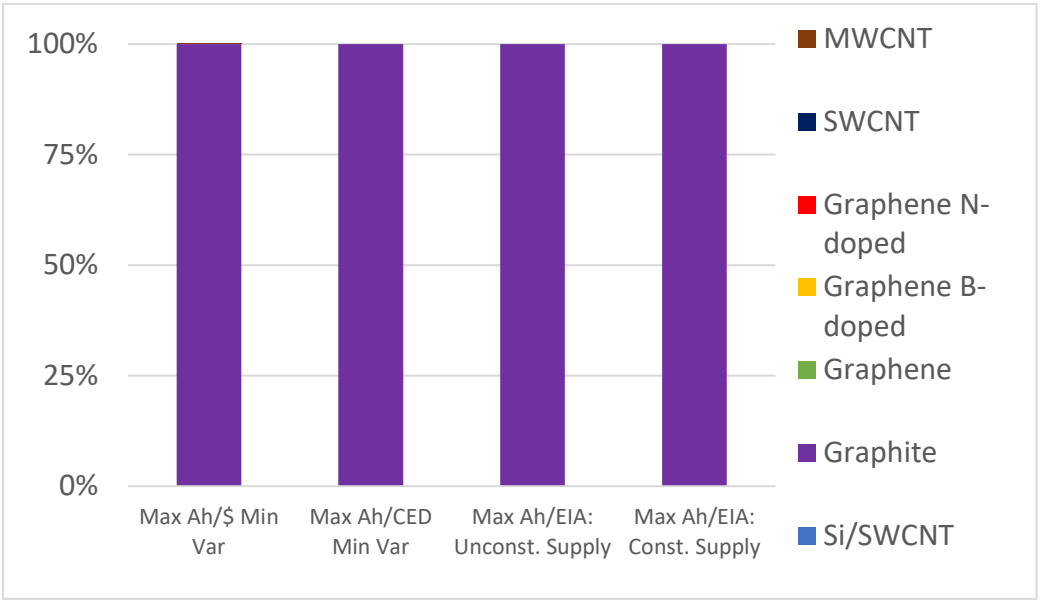

Figure S3. The LIB optimal material portfolios for both the supply scenarios: the economic case (Max Ah/$, Min Var) and environmental case (Ah/CED) given opportunistic demand. Graphite was selected for both supply scenarios when the performance was normalized to the dollars and energy invested because it is the cheapest and least energy intensive material. In the goal-oriented demand case, both unconstrained and constrained supply were evaluated. The model selected graphite for the unconstrained supply as well as the constrained supply to meet the target electric vehicle goal for 2040 while minimizing the variance.

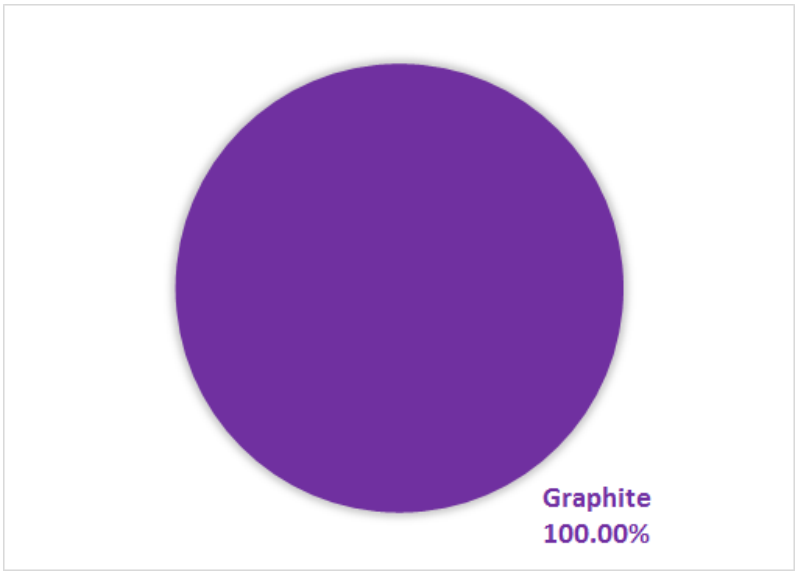

Figure S4. The LIB CNM and incumbent material portfolio for the constrained, 30% reduction supply scenario for the goal-oriented EIA case. Graphite was still chosen as the optimal material even with a drop in its supply because it is still further along the technology spectrum than the other CNMs in the portfolio. However, as supply becomes more constrained, the price of graphite will increase, which could also increase the overall cost of the portfolio.

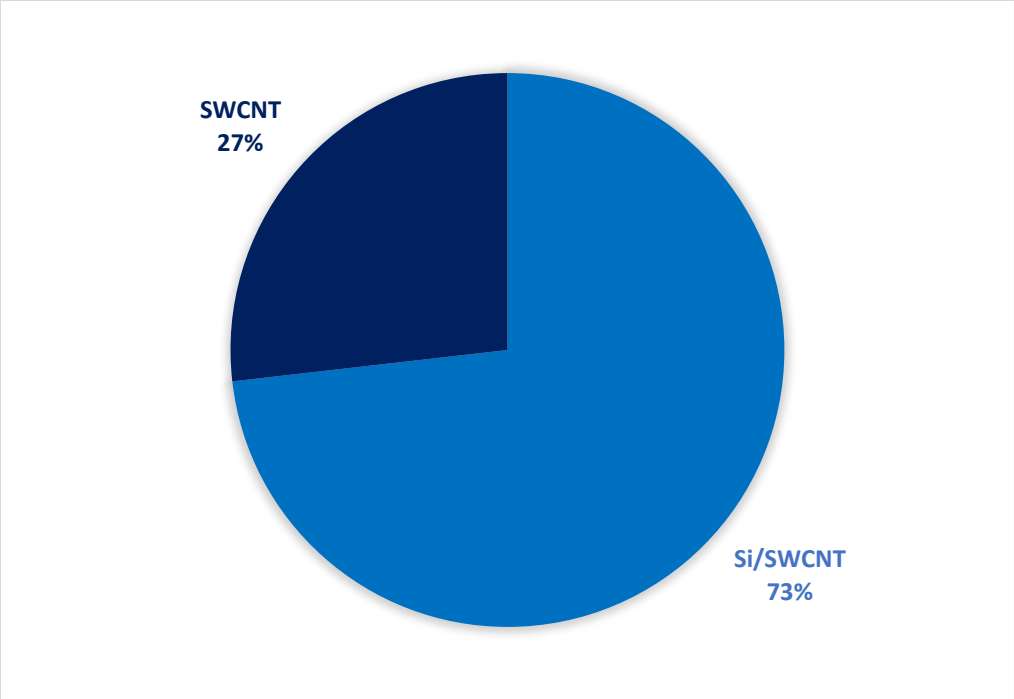

Figure S5. The LIB CNM and incumbent material portfolio for the unconstrained supply scenario for the baseline case: maximizing performance while minimizing variance when graphite is not an option to invest in. Si/SWCNT was selected as the largest portfolio share because it has the highest performance capacity when normalized to the amount of material added to the anode as shown in Figure 1 for the unconstrained supply case with SWCNT as the next largest share due to its relatively high capacity and low variance.

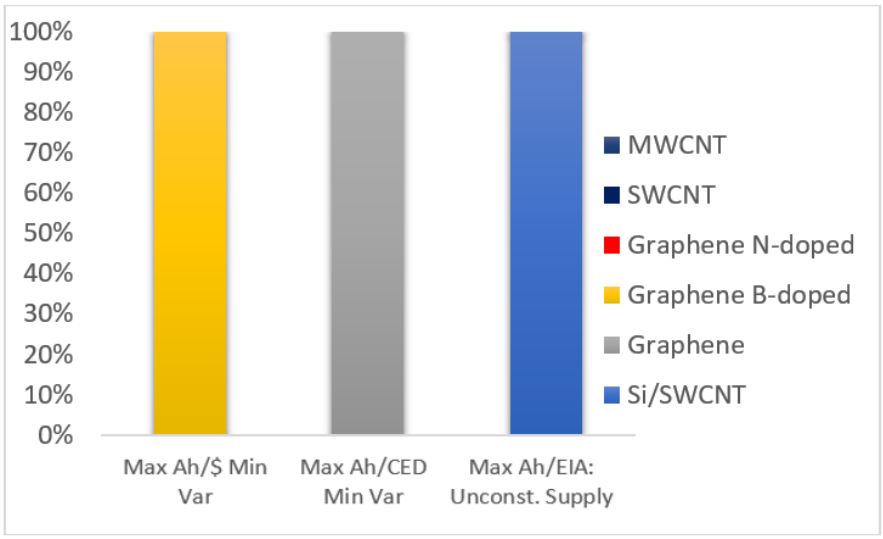

Figure S6. The LIB optimal material portfolios for the unconstrained supply scenario: the economic case (Max Ah/$, Min Var) and environmental case (Max Ah/CED) given opportunistic demand. Graphite was not available to select and therefore Graphene B-doped was selected when the performance was normalized to the dollars and graphene was selected for the energy invested scenario because they are the cheapest and least energy intensive material respectively. In the goal-oriented demand case, the model selected Si/SWCNT for the unconstrained supply to meet the target electric vehicle goal for 2040 while minimizing the variance due to its high capacity value.

	C60	C60 PCBM	C70 PCBM	C60 bisPCBM	C60 ICBA	Graphene	SWCNT	MWCNT
W	3	4	5	6	2	8	7	1
W/GJ	1	4	6	5	2	8	7	3
W/$	2	4	8	7	5	3	6	1

Table S13. Heat map of CNM acceptors in OPVs depicting economic, environmental, and energy trade-offs.

	Si/SWCNT	Graphite	Graphene	Graphene B-doped	Graphene N-doped	SWCNT	MWCNT
Ah	1	6	5	2	3	4	7
Ah/GJ	2	1	7	5	6	3	4
Ah/$	6	1	4	2	5	7	3

Table S14. Heat map of CNM anodes in LIBs depicting economic, environmental, and energy trade-offs.

Scenario	Return	Variance
Unconstrained Supply: Max W, Min Var	1E18	4E5
Constrained Supply: Max W, Min Var	1.8E9	1.2E5
Unconstrained Supply: Max W/$, Min Var	11.8	1.3E5
Constrained Supply: Max W/$, Min Var	10.7	1.6E5
Unconstrained Supply: Max W/CED, Min Var	4.6E3	1.8E4
Constrained Supply: Max W/CED, Min Var	4.6E3	1.7E4
Unconstrained Supply: EIA 1.5% Solar	3.7E9	1.6E4
Constrained Supply: Meet EIA 100% Solar	1.8E9	1.2E5
Unconstrained Supply: Max Ah, Min Var	4.6E16	2.1E7
Constrained Supply: Max Ah, Min Var	1.2E9	2.9E4
Unconstrained Supply: Max Ah/$, Min Var	0.4	2.7E4
Constrained Supply: Max Ah/$, Min Var	0.4	2.7E4
Unconstrained Supply: Max Ah/CED, Min Var	1E4	2.7E4
Constrained Supply: Max Ah/CED, Min Var	4E4	2.7E4
Unconstrained Supply: Meet EIA 100% Electric Vehicle Prediction	8.5E14	3.4E4
Constrained Supply: Meet EIA 100% Electric Vehicle Prediction	3.2E10	3.4E4

Table S15. Summary table detailing the portfolio return and variance values for each portfolio case.

References

1. Piccinno, F.; Gottschalk, F.; Seeger, S.; Nowack, B. Industrial production quantities and uses of ten engineered nanomaterials in Europe and the world. *Journal of Nanoparticle Research* **2012,** *14*, 1109.
2. Hendren, C. O.; Mesnard, X.; Dröge, J.; Wiesner, M. R. Estimating production data for five engineered nanomaterials as a basis for exposure assessment. ACS Publications: **2011**.
3. Saxman, D. Large and Advanced Battery Technology and Marketts. Research, B., Ed. **2015**.
4. Aster, N. The World Market for Graphene to 2017. Publishers, M., Ed.
5. Grand View Research, I. Graphene Market Demand Projected to Reach 1,321.1 tons by 2022. GlobeNewsire, N., Ed.
6. Feytis, A. The bright side of graphite. *Industrial Minerals* **2010,** *7*, 31-39.
7. USGS Silicon. **2016**.
8. USGS Cement. **2017**.
9. Matsuo, Y.; Hatano, J.; Kuwabara, T.; Takahashi, K. Fullerene acceptor for improving open-circuit voltage in inverted organic photovoltaic devices without accompanying decrease in short-circuit current density. *Applied Physics Letters* **2012,** *100*, 37.
10. Dai, L.; Chang, D. W.; Baek, J. B.; Lu, W. Carbon nanomaterials for advanced energy conversion and storage. *small* **2012,** *8*, 1130-1166.
11. Jariwala, D.; Sangwan, V. K.; Lauhon, L. J.; Marks, T. J.; Hersam, M. C. Carbon nanomaterials for electronics, optoelectronics, photovoltaics, and sensing. *Chemical Society Reviews* **2013,** *42*, 2824-2860.
12. Yang, Y.; Li, G. *Progress in high-efficient solution process organic photovoltaic devices*. Springer: **2016**.
13. Anctil, A.; Babbitt, C.; Landi, B.; Raffaelle, R. P. In *Life-cycle assessment of organic solar cell technologies*, Photovoltaic Specialists Conference (PVSC), 2010 35th IEEE, IEEE: **2010**; pp 000742-000747.
14. He, Y.; Li, Y. Fullerene derivative acceptors for high performance polymer solar cells. *Physical chemistry chemical physics* **2011,** *13*, 1970-1983.
15. Wei, J.; Jia, Y.; Shu, Q.; Gu, Z.; Wang, K.; Zhuang, D.; Zhang, G.; Wang, Z.; Luo, J.; Cao, A. Double-walled carbon nanotube solar cells. *Nano letters* **2007,** *7*, 2317-2321.
16. Luo, J.; Zhao, X.; Wu, J.; Jang, H. D.; Kung, H. H.; Huang, J. Crumpled graphene-encapsulated Si nanoparticles for lithium ion battery anodes. *The journal of physical chemistry letters* **2012,** *3*, 1824-1829.
17. Wu, Z.-S.; Ren, W.; Xu, L.; Li, F.; Cheng, H.-M. Doped graphene sheets as anode materials with superhigh rate and large capacity for lithium ion batteries. *ACS nano* **2011,** *5*, 5463-5471.
18. Ng, S.; Wang, J.; Guo, Z.; Chen, J.; Wang, G.; Liu, H. K. Single wall carbon nanotube paper as anode for lithium-ion battery. *Electrochimica Acta* **2005,** *51*, 23-28.
19. Guo, J.; Sun, A.; Chen, X.; Wang, C.; Manivannan, A. Cyclability study of silicon–carbon composite anodes for lithium-ion batteries using electrochemical impedance spectroscopy. *Electrochimica Acta* **2011,** *56*, 3981-3987.
20. Pan, M.; Liu, X.; Liu, H.; Chen, Y. Ultrafine Si/C–graphite composite anode materials with improved cyclic performance. *Materials Letters* **2016,** *178*, 252-255.
21. Lee, J. H.; Yoon, C. S.; Hwang, J.-Y.; Kim, S.-J.; Maglia, F.; Lamp, P.; Myung, S.-T.; Sun, Y.-K. High-energy-density lithium-ion battery using a carbon-nanotube–Si composite anode and a compositionally graded Li [Ni 0.85 Co 0.05 Mn 0.10] O 2 cathode. *Energy & Environmental Science* **2016,** *9*, 2152-2158.

22. Nelson, P.; Gallagher, K.; Bloom, I. BatPaC (Battery Performance and Cost) Software. *Argonne National Laboratory* **2012**.
23. BEA, U. S. 1997 Bridge tables to Other basic inorganic chemical manufacturing. **1997**.
24. BEA, U. S. 2002 Bridge tables to All other basic inorganic chemical manufacturing. **2002**.
25. BEA, U. S. 2007 Bridge tables to All other basic inorganic chemical manufacturing. **2007**.
26. U.S. Department of Commerce, B. o. E. A. 1992 Benchmark I-O bridge tables to PCE and PDE. **1992**.
27. Anctil, A.; Babbitt, C. W.; Raffaelle, R. P.; Landi, B. J. Material and energy intensity of fullerene production. *Environmental science & technology* **2011,** *45*, 2353-2359.
28. Arvidsson, R.; Kushnir, D.; Sandén, B. r. A.; Molander, S. Prospective life cycle assessment of graphene production by ultrasonication and chemical reduction. *Environmental science & technology* **2014,** *48*, 4529-4536.
29. Zhai, P.; Isaacs, J. A.; Eckelman, M. J. Net energy benefits of carbon nanotube applications. *Applied Energy* **2016,** *173*, 624-634.
30. Goedkoop, M.; Oele, M.; de Schryver, A.; Vieira, M.; Hegger, S. SimaPro database manual methods library. *PRé Consultants, The Netherlands* **2008,** 22-25.
31. Zervos, H.; Das, R.; Ghaffarzadeh, K. Organic Photovoltaics (OPV) 2013-2023: Technologies, Markets, Players. IDTechEx, Ed.
32. Administration, U. S. E. I. International Energy Outlook 2016. Reference case projections for electricity capacity and generation by fuel ed.; **2016**.
33. Administration, U. S. E. I. International Energy Outlook 2016. **2016**.
34. Richa, K.; Babbitt, C. W.; Gaustad, G.; Wang, X. A future perspective on lithium-ion battery waste flows from electric vehicles. *Resources, Conservation and Recycling* **2014,** *83*, 63-76.
35. USGS Silicon Statistics and Information: Minerals Information.